Fluorescence spectroscopy and nanomanipulation of individual semiconductor nanocrystals

Thesis submitted in fulfillment of the requirements for the degree of

Doctor rerum naturalium (Dr. rer. nat.)

To the Department of Chemistry of the University of Hamburg

By

Maxime Tchaya Njantio

M. Sc. in Chemistry

May 2010

This thesis was supervised by Prof. Dr. Alf Mews

Gutachter:

1. **Prof. Dr. Alf Mews**

2. **Prof. Dr. Horst Weller**

Date of the public defence: Friday 25th June 2010

For my children

For my wife Adeline

For my parents Berthe and Martin

Abstract

The blinking of single nanocrystals (NCs) is investigated by means of a combined laser scanning confocal microscope and a home built nanopositioner. Artifacts of threshold analysis methods are investigated to understand the origin of the discrepancies of blinking quantification reported by different research groups. It is shown that variations of the distribution of intermediate emitting intensities are the major source of errors. The results strongly suggest that the truncation of the power law is more an artifact than a general feature of NCs. The effect of the material surrounding NCs is investigated by comparing the influence of insulating, hole conducting and electron conducting materials. It is shown that the photoluminescence is quenched in films of hole conducting materials due to the possibility of transfer of the photo-generated hole of NCs. The blinking statistic shows the existence of a correlation between the ON time and the OFF time power law exponents of given NCs and the presence of a memory between consecutive ON event, consecutive OFF events and between ON and OFF events. The necessity of an analysis method independent of the threshold separation between ON and OFF level is suggested to investigate the apparent dependence of the blinking statistic results on the matrix. The nanomanipulation experiments show that electroluminescence of areas as small as 1 μm^2 can be investigated with the home built experimental setup used for this thesis. The nanomanipulation with help of a metallic tip lead to a photoluminescence quenching when charges flow in the proximity of single NCs.

Acknowledgements

I thank all people that helped me and supported me during my PhD life.

I thank Prof. Dr. Alf Mews, for giving me the opportunity to achieve my doctorate work in his group. From the master thesis he introduced me to the conception and development of confocal microscopes and provided me his experience in understanding the problem of single particle optics.

I thank professors and personals of the University of Siegen that played an important role at the beginning of my scientific life. I am particularly grateful to Prof. Dr. W. H. E. Schwarz, Prof. Dr. B. Engelen, Mr. Jochen Eickbusch that particularly helped to solve the immigration difficulties of my wife and my children.

I thank employees of the machine-shop of the Universities of Siegen and Hamburg for their support during the development of the experimental setup. I am grateful to all my former and current colleagues for the nice working atmosphere they contribute to keep in the group. I am particularly grateful to Gregor Schulte for building the Nanopositionner, Dr. Lars Birlenbach for his help in the synthesis of nanocrystals, Jan Flugge for the threshold analysis application, Dr. Herbert Kneppe and Dr. Tobias Kipp for the fruitful discussions, Ma Xuedan for the cyclic-voltammetry experiments, Sandra Flessau and Sebastian Schäfer for reading this thesis, Anton Myalitsin and Jessica Völker for the unforgettable coffee breaks and after work beer, my students Flavie Lavoie-Cardinal, Marcus Janschel, Michael Dreifke, Danniel Jostes, Christian Neuhaus for their contribution through the specialization lab courses.

Thanks to the members of the Cameroonian Community of Siegerland – CCS.eV – for reducing the homesickness always present so far from Cameroon.

Erklärung

Hiermit erkläre ich an Eides Statt, dass ich die vorliegende Arbeit selbstständig verfasst und alle verwendeten Quellen und Hilfsmittel als solche gekennzeichnet habe.

Hiermit erkläre ich, dass vorher keine weiteren Promotionsversuche unternommen worden sind oder an einer anderen Stelle vorgelegt wurden.

Hamburg, den 21. Mai 2010

Maxime Tchaya

Table of Contents

Literature

Introduction

At the time of their discovery in the early ‘80s [1-3], semiconductor nanocrystals appeared already like a scientific and technological breakthrough. The strong confinement of electron-hole pairs in these particles and their high surface to volume ratio offer the possibility to functionalize and manipulate the surface for desired applications without losing the advantages of quantized systems. The elaboration of colloidal synthesis methods where the size, the shape and the solubility of nanocrystals could be controlled played an important role in the interest given to these particles [4-16].

The blinking which is the reversible loss of fluorescence occurring during optical investigations was observed for single nanocrystals in the middle ‘90s [17-19]. This behavior was well known and widely characterized for single molecules and single ions. It was attributed in these systems to quantum jumps and singlet-triplet transitions hindering the absorption and consequently the emission [20, 21]. These pictures have influenced the first models of the blinking of single nanocrystals but it was not possible to imagine the loss of absorption in such particles with high carrier density. Most of the models that were developed account for ionization/re-neutralization processes occurring during the photo-excitation of nanocrystals. In charged nanocrystals the occurrence of internal Auger energy transfer already reported in microcrystals and quantum drops by Efros and coworkers explained the dark events observed [22]. It was however not clear how and why ionization and re-neutralization steps occur.

In 1997, Efros and Rosen proposed a “Radom telegraph model” in which the electron or hole escape occurred via Auger ionization processes [23]. This could however not explain the power law kinetics, the memory between adjacent event durations and the apparent minor dependence of the blinking on experimental conditions reported in further experimental works [24-27]. Although a wealth of experimental and theoretical works have been achieved over the last fourteen years, several controversial reports still unable a common understanding of the blinking of single nanocrystals. Controversy subsist on the existence of a truncation point in the power law behavior at long times. The value of power law exponents is proposed to focus at 1.5 but several reports mention values scattering from 1 to 2 [28-30]. The surface passivation and the experimental efforts made have improved the stability of nanocrystals but no effects on the power law kinetics have been observed. There is no clear certitude on the physical reason behind the blinking however several investigations suggest that it is correlated to a charge trapping happening close or near the surface [31]. The photo-ionization has been demonstrated by electrostatic force microscopy (EFM) [32-36], the interactions of the surface with the environment have shown that electron and hole transporting materials differently influence the photoluminescence [37, 38], recent synthesis methods have successfully produced less or non-blinking nanocrystals [39, 40]. Current theoretical models [28-30] are influenced by the different experimental findings mentioned above. Static models proposing a static distribution of traps have been abandoned because of the non zero probability for the nanocrystals to remain ionized. This would have implied the frequent observation of fluorescence bleaching in nanocrystals. It however does not fit with the reported relative optical satiability of NCs compared to dyes molecules for instance. Two main dynamic models are currently investigated. Diffusion based models which propose a diffusion of both nanocrystal and trap levels. The ionization and neutralization take place via resonant tunneling. The model account Auger detrapping processes and therefore explain the truncation of the power law kinetics and its dependence on external stimulus. It proposes power law exponents of 1.5 for ON and OFF event durations and fails to explain the deviation observed by several other groups. Fluctuating tunneling barrier models account for a distribution of traps and exponential fluctuations of the tunneling barrier width and depth. These models accounts for the different power law exponents and the nearly insensitivity of the blinking to the experimental conditions reported by several groups. None of the models explain the memory and all of them use the charging and blinking picture as hypothesis. Recent findings reported these last two years suggest other pictures that could account emission of charged dots or the necessity to take into account the sign of the charge (electron or hole) and the magnitude of the charging [41, 42].

In order to contribute to the understanding of the blinking this project starts first of all with the investigation of the accuracy of threshold analysis to find the origin of different results reported in the quantification of the blinking. The variation of power law exponents and memory coefficients with the analysis parameter is investigated. Secondly the influence of hole and electron conducting material is addressed. A blinking statistic in insulating and electron conducting materials is performed to investigate the effect of the matrix on the power law kinetics and on the memory. Finally an attempt to physically influence the blinking of single nanocrystals with a charge brought by a metallic tip is achieved.

The work is organized in three main chapters. The first chapter introduces semiconductor nanocrystals and review previous works on the blinking. The second chapter describes the synthesis of semiconductor nanocrystals, the sample preparation and the home built experimental setup. The results are presented and discussed in the last chapter in three sections: the artifacts of threshold analysis, the effect of the matrix and the nanomanipulation experiments.

Chapter I: Theoretical background

This chapter describes the photo-physical properties of II-VI semiconductor nanocrystals. It is a review of previous works with an emphasis on CdSe nanocrystals (NCs). The first part of the chapter introduces the optical and electronic properties of NCs. The second part focuses on the causes of the fluorescence blinking of single NCs. It is a comparison of the different models proposed to explain the blinking.

I. Semiconductor nanocrystals

Semiconductors are materials with properties between those of conductors and insulators. One of their main characteristic is the ability to generate an electron-hole pair (called exciton) using an external stimulus. Depending on the applications thermal, electrical or optical excitation is used to remove an electron from the valence band of the semiconductor and bring it to the conduction band. The hole can be described as the positive vacancy remaining in the valence band when the electron is removed.

The spatial distance between the electron in the conduction band and the hole it leaves in the valence band is called the exciton Bohr radius a_B. It is calculated by the following formula obtained similarly to the electron-nucleus distance in a hydrogen atom:

$$a_B = \frac{4\pi\varepsilon\hbar^2}{\mu e^2}, \text{ with } \begin{cases} \varepsilon: \text{ Dielectric constant} \\ \hbar: \text{ Reduced Planck's constant} \\ \mu: \text{ Reduced mass of the exciton} \\ \dfrac{1}{\mu} = \dfrac{1}{m_e} + \dfrac{1}{m_h} \\ m_e, m_h: \text{ effective mass of the electron and} \\ \qquad\qquad \text{the hole respectively} \\ e: \text{ Elementary charge} \end{cases},$$

In bulk semiconductor, due to the coulomb attraction between the electron and the hole, the exciton behaves like a quasi particle that can propagate in the whole crystal. When the size r of the crystal is reduced, the exciton becomes confined. A strong confinement of the exciton occurs when the size of the crystal becomes smaller than the exciton Bohr radius. This situation is observed in semiconductor nanocrystals. In this case the exciton is better described like an electron-hole pair as the quantization energies of the electron and the hole become dominant compared to the coulomb attraction between them. The electron and the hole are treated each like a particle in a quantum box with high potential walls. Efros and Brus have evaluated the quantization energy of an electron and a hole in confined systems [43-45]. Theoretical models describing the electronic structure of semiconductor NCs are summarized in several reviews [46-48]. Although none of this models give a full description of the electronic structure, they provide a simplified picture of the optical transitions in semiconductor NCs [44] (figure 1).

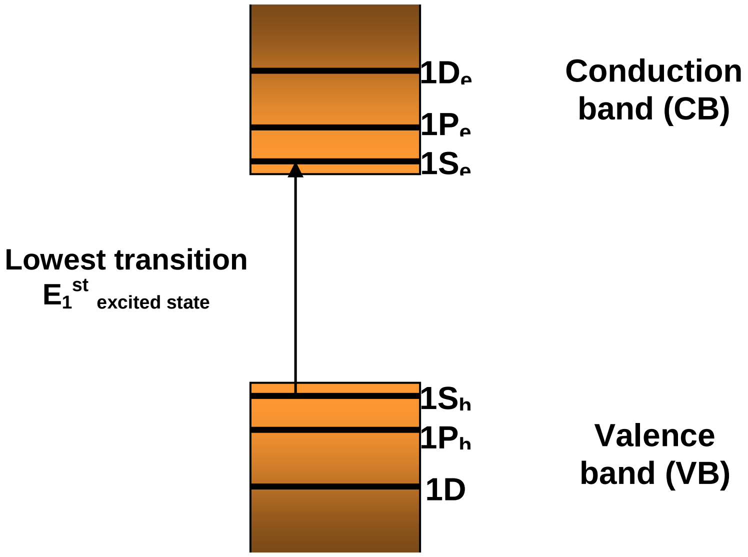

Figure 1: Simplified electronic structure of semiconductor NCs with atomic like energy levels.

The Brus formula obtained using the effective mass approximation is valid for parabolic conduction and valence bands. It gives the energy of the first excited state in semiconductor NCs (transition shown in figure 1). It is given by:

$$E_{1^{st}\text{ excited state}} = \underbrace{E_g}_{\text{Band gap energy}} + \underbrace{\frac{\hbar^2\pi^2}{2r^2}\left(\frac{1}{m_e}+\frac{1}{m_h}\right)}_{\text{Kinetic energy}} - \underbrace{\frac{1{,}8e^2}{\varepsilon r}}_{\text{Coulomb interaction}} .$$

In this formula m_e and m_h represent the effective masses of the electron and the hole respectively, r is the size of the NC. The coulomb interaction term depends on $\frac{1}{r}$ whereas the kinetic energy depends on $\frac{1}{r^2}$. Therefore when the size of NCs is reduced the quantization energy increases. It follows that the absorption energy necessary to excite an electron from the VB to the CB and the fluorescence energy produced when this electron recombines with the hole in the VB depends on the size of the NC.

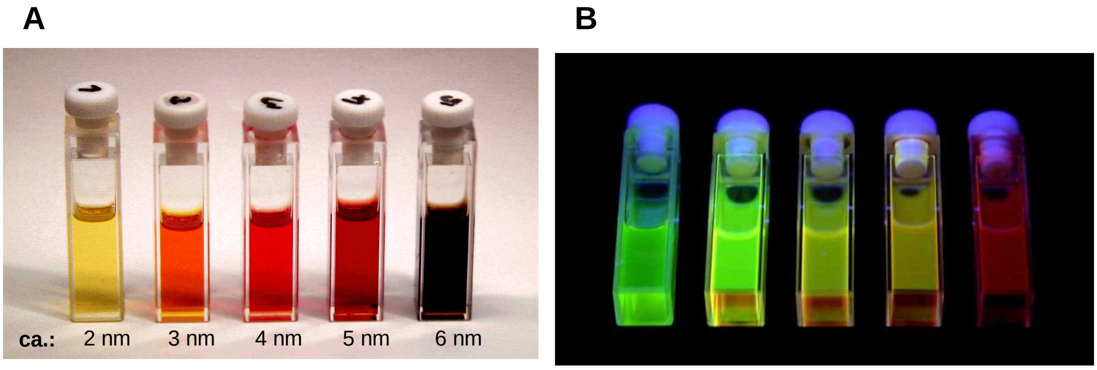

Figure 2: Size tunable optical properties of CdSe NCs ($a_B = 6\ \mathrm{nm}$). A: Absorption, B: Fluorescence

Figure 2 shows the variation of the absorption and the fluorescence of colloidal CdSe NCs with the size. There is a red shift of the absorption and fluorescence wavelength when the size of NCs increases from 2 nm to 6 nm. Most synthesis of NCs as shown in figure 2 are based on a report from Bawendi et al. in 1993 [4]. In their method, dimethylcadmium, phosphine-chalconides or Alkylsilane-chalconides reagents are used in a temperature controlled synthesis to produce CdX (X =S, Se, Te) nanocrystals. This synthesis is simple and produces a high amount of nanocrystals with a narrow size distribution. The colloidal solutions obtained are easily stabilized by attaching appropriate ligands on the surface of the NCs (for instance TOPO). In the first synthesis, a quantum yield of 9,6% for CdSe NCs was achieved but today with improved reaction control a quantum yield of 35% is achievable. The possibility to produce and control the size of NCs in stable colloidal solutions is the fuel of most applications and research works today. The optical stability has been improved by growing shells of higher band gap materials like ZnS and CdS [16]. Elaborate wet chemical techniques allow a control of the composition and the solubility [5-15]. Several works report the incorporation of NCs into biological samples as imaging markers and into optoelectronic devices as luminescent or photon-electron converting material [49, 50].

II. Fluorescence of single nanocrystals

Despite the interesting optical properties and applications of II-VI NCs, the fluorescence intermittency observed in single particle spectroscopy limits their application. Confocal microscopy [51] is generally used to image the fluorescence of single NCs. It is an established experimental method described in several experimental physics textbooks.

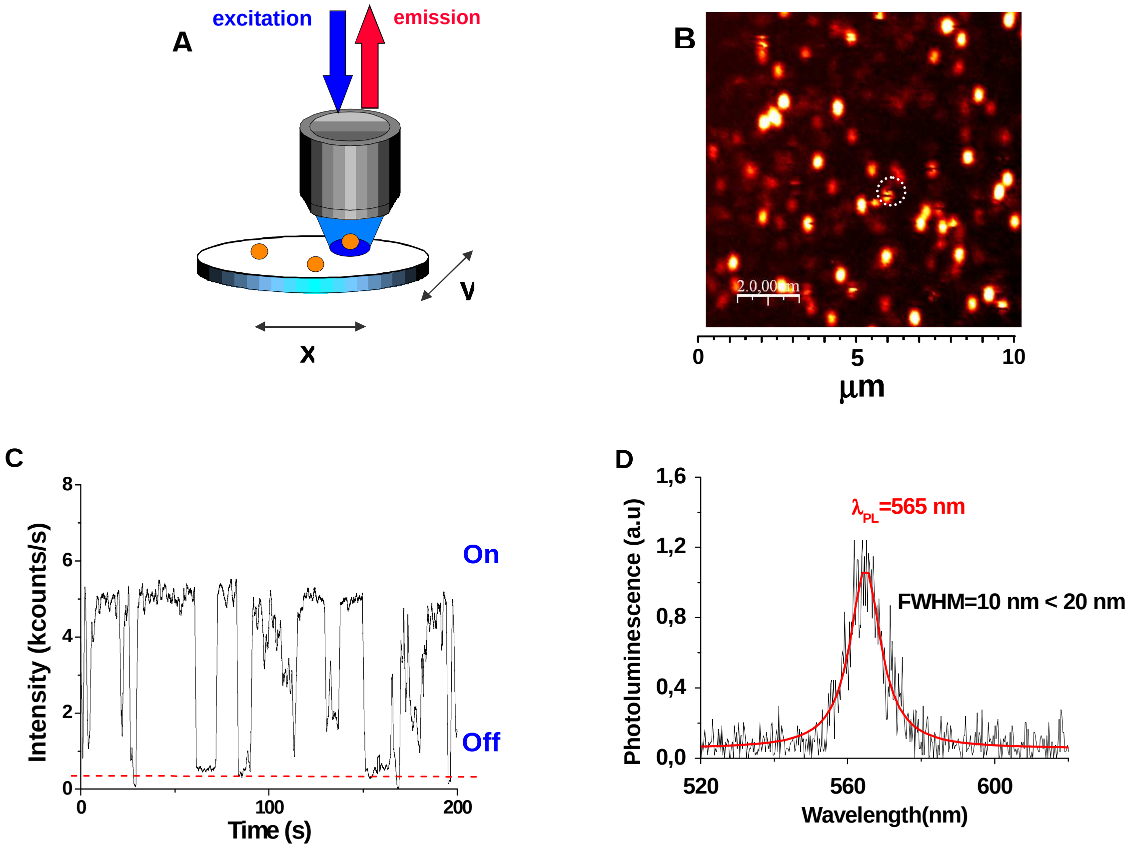

Figure 3: Typical procedure for single NCs detection. A: Diluted solution of NCs dispersed onto a substrate. The sample is scanned over the laser focus. The excitation and the emission go through the same objective. B: Fluorescence image. The bright spots are diffraction limited images of single NCs. C: Variation of the fluorescence of the single NC (circled in B) with time. The fluorescence fluctuates almost digitally from ON to OFF levels. D: Spectrum of the single NC (circled in B). The red curve is a Lorentz fit. A FWHM below 20nm is expected for single NCs at room temperature.

Figure 3 shows an example of a single NC detection experiment. Diluted NC solutions are dispersed onto a glass substrate and excited with diffraction limited focused laser light (Figure 3A). The excitation light and the emitted light go through the same objective and the fluorescence of NCs is recorded using high quantum efficiency detectors (Avalanche photodiode (APD), Photomultipliers, charge coupled device (CCD) cameras, etc.). In the fluorescence image shown in figure 3B, the bright spots show the fluorescence of single NCs. At the position marked by the white circle, a dark line divides the bright spot. This is an indication that during the sample scanning, the NC reversibly switched between emitting and non emitting periods. This behavior is clearly observed in the time trace shown in figure 3C. The single NC circled in figure 3B is kept in the laser focus and the variation of the PL intensity in time is recorded. This graph shows that in 200 s the PL intensity of the NC switched between high ON levels of about 5000 counts/s and OFF levels below 500 counts/s. The red line indicates the background level corresponding to the signal collected by the detector in the absence of NCs. The time trace contains low ON levels originating from different emitting states [52]. Figure 3C shows that the spectral broadening of the emission spectrum of the single NC circled in figure 3B is below 20 nm. The red curve in the figure is a single Lorentzian fit of the spectrum. These spectral properties are characteristic of single NCs emission at room temperature [17]. The reversible switch of the fluorescence between emitting (ON) states and dark (OFF) states is called blinking. It is not observable in highly concentrated samples due to ensemble averaging. It is widely reported for several other single emitters like ions and molecules [29]. Single ions blink because during excitation they jump into an excited state that is not in resonance with the excitation wavelength. In this excited state the ions do not absorb photons and consequently do not emit any light [20]. Single molecules blink because of the possibility of intersystem crossing. The excited molecule can relax to the triplet state instead of relaxing to the ground state. The molecule remain dark until the particle relaxes back to its ground state [21].

The blinking of NCs was first reported in 1996 [17, 18]. Since that first report, several experimental and theoretical works have been achieved to understand its origin. Although up to date the exact mechanism of the blinking is still not understood, much progress has been made over the last fifteen years. Recent reviews summarize the main experimental findings and the current theoretical models on the blinking [28-30, 53]. The different points of controversy on the blinking can be classified into three categories: controversies on the quantification, on the physical reasons and on the theoretical picture.

1. Quantification of the blinking

Threshold analysis of fluorescence time traces is usually used to quantify the blinking of single NCs. Figure 4 describes an example of threshold analysis and shows results that are obtained.

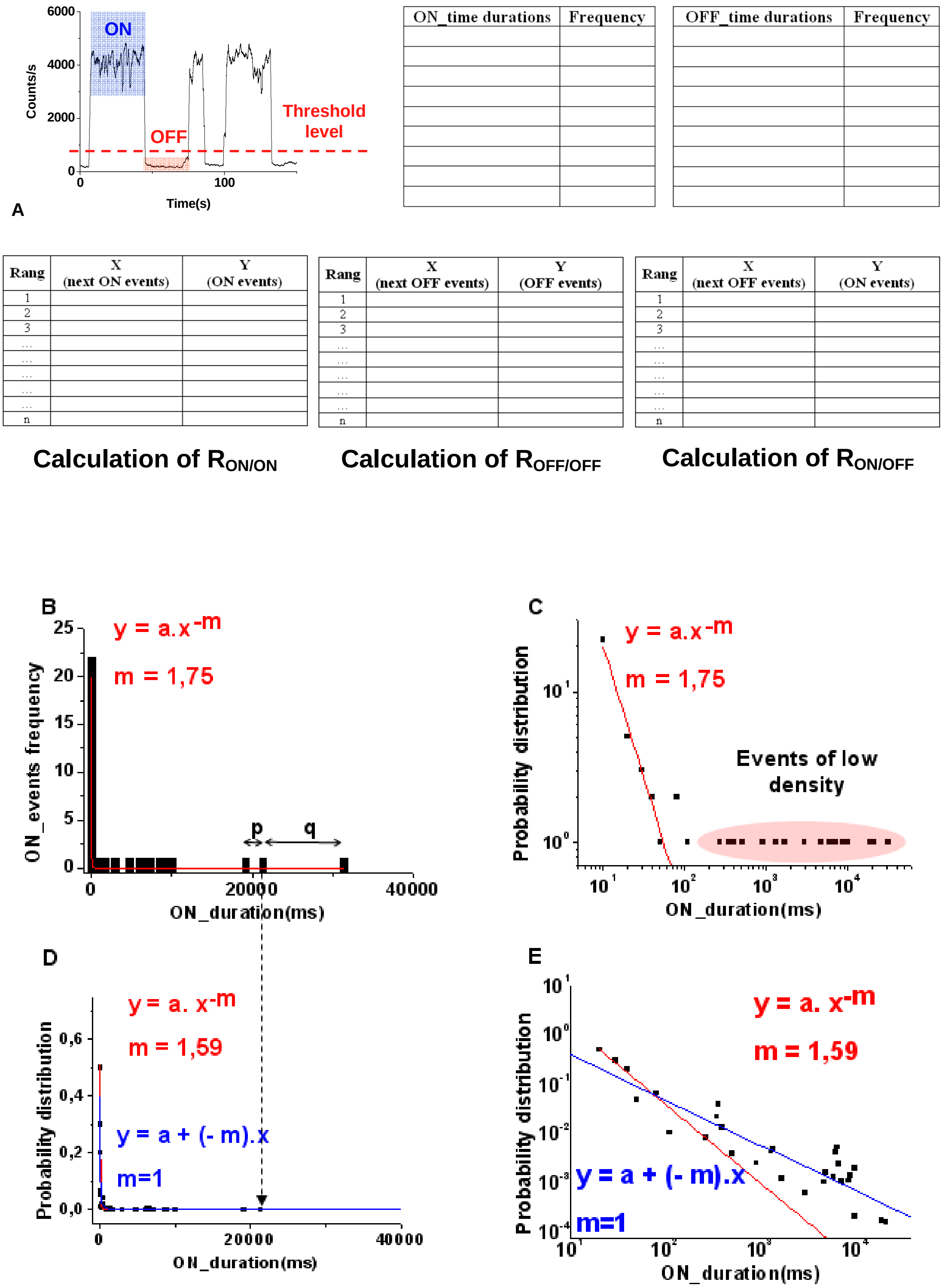

ON_time durations	Frequency

OFF_time durations	Frequency

Rang	X (next ON events)	Y (ON events)
1		
2		
3		
…		
…		
…		
…		
…		
n		

Calculation of $R_{ON/ON}$

Rang	X (next OFF events)	Y (OFF events)
1		
2		
3		
…		
…		
…		
…		
…		
n		

Calculation of $R_{OFF/OFF}$

Rang	X (next OFF events)	Y (ON events)
1		
2		
3		
…		
…		
…		
…		
…		
n		

Calculation of $R_{ON/OFF}$

Figure 4: Description of the threshold analysis. A: example of time trace of single NC. The red line indicates the chosen threshold levels. The table are guide indicate the type of data obtained. B: Example of histogram of the duration of ON events. C: Double logarithmic plots of the histogram in B. D: Histogram obtained by weighing B. E: Double logarithmic plots of the histogram in D.

Figure 4A shows a time trace and the intensity distribution of a single NC. The red dashed line shows the threshold level used to discriminate emitting and dark states. Events below that threshold line are considered OFF and those above are considered ON. With this analysis method it is possible to obtain the frequency of ON and OFF event duration as shown in linear and double logarithmic scale in figure 4B and 4C respectively. The plots of the frequency of event duration represent their probability density. In order to compute events of low density occurring at long time range (see figure 4C), the original probability density is weighed as proposed by Kuno et al. [24]. The data points in figure 4B are weighed by a value corresponding to the average distance to the nearest data points. For the example in figure 4 (B, D) the value $\left(\frac{p+q}{2}\right)$ is the position of the new points. The histogram is then plotted in double logarithmic scale and then fitted either by a power function $y = a.\tau^{-m}$ or by a linear function $y = a + (-m)\tau$, where m is a positive real number representing the slope of the fitting line. Both fitting methods sometimes lead to different results. The first function minimizes the absolute deviation of experimentally obtained probabilities from the power law and overestimates events of high probabilities occurring at short times in a double logarithmic plot. The second function on the contrary, minimizes the deviations of logarithmic probabilities from the power law and therefore finds a line connecting the majority of data points. Differences between the two fitting methods are mentioned in the literature, and the choice of the method depends on each experimentalist [31, 54].

The first blinking statistic using threshold analysis was reported by Kuno et al. in 2000 [24]. Figure 5 shows the results they obtained in 2001

[25]. Their threshold is chosen from two to three standard deviations (σ) above the average detector background. The original probability densities are weighed and the double logarithmic plots are fitted with a linear function as previously described (figure 6 B and C). For both ON and OFF events, the authors obtained a power law dependence of the probability densities with m, the exponent of the power law varying between $m = 1$ and $m = 2$. Similar results are reported by several other experimentalists.

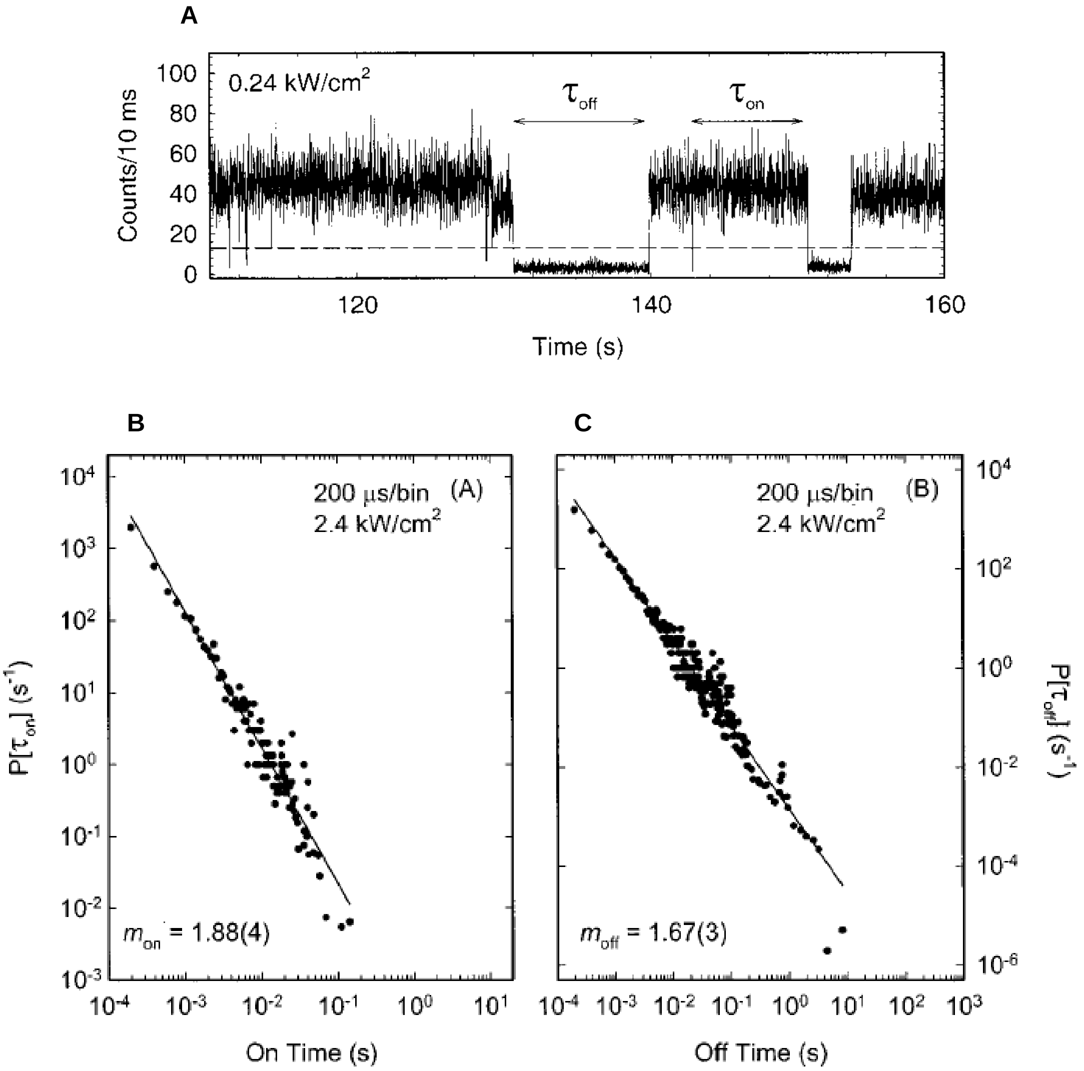

Figure 5: Threshold analysis after Kuno et al. [25]. A: Time trace of a single NC. The dashed line shows the threshold level. τ_{on} and τ_{off} are examples of resulting ON and OFF events respectively. B and C are the ON times and OFF times probability density plots respectively. The line in the graphs shows the linear dependence of the probability densities indicating a non exponential behavior

In 2001 Shimizu et al. [26] reported results of threshold analysis on with some difference to those shown in figure 6. In their analysis shown in figure 6C, the OFF time probability density also follows power law kinetics. The ON time probability density on the contrary follows a truncated power law of the form $P = e^{k\tau}\tau^{-m}$. As shown in figure 6B, at long ON times, the probability density of ON events deviates from the power law. Another important observation of this work is that for all the 300 NCs investigated, the power law exponent remained close to 1.5 with 0.1 standard deviation. The deviations from the pure power law kinetics with experimental conditions shown in figure 6B will be discussed later. Several other experimentalists report results similar to those presented by Shimizu et al. [28, 53]

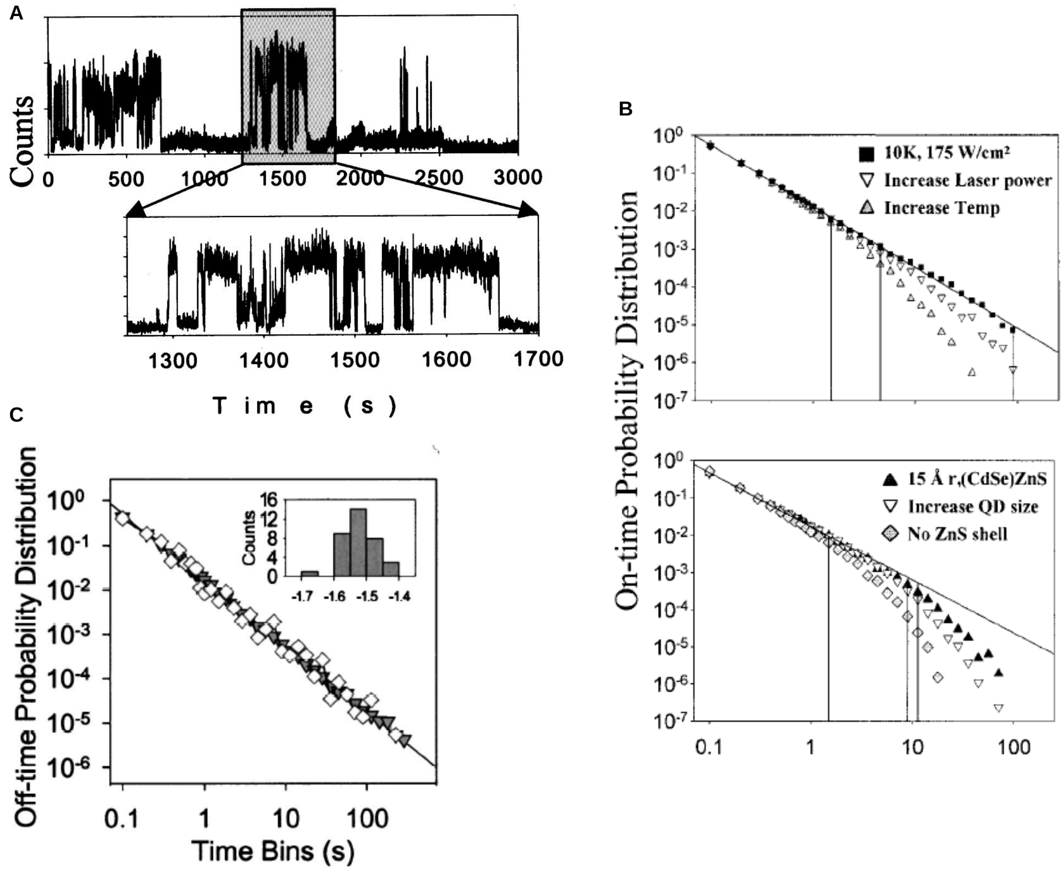

Figure 6: Threshold analysis after Shimizu et al. [26]. A: Time trace of single NCs. B: Probability density of ON times. C: Probability density of OFF times

As shown in the tables in figure 4 the sequence of occurrence of event durations is also obtained from threshold analysis. It is therefore possible to check the correlation between consecutive event durations. A correlation between consecutive events proves a memory in the blinking of single NCs. The first investigation of memory was made by Kuno et al. in 2001 [25]. Their analysis of scatter plots of adjacent events revealed no apparent correlation between consecutive event durations. In 2005 Stefani et al. [27] reported for the first time the existence of a memory in the blinking of single NCs. Instead of visually analyzing scatter plots of consecutive events, they used Pearson correlation coefficients that evaluate the linear dependence between two sets of data points X and Y plotted along the x and y axis respectively. Two types of correlation coefficients R and R_{log} are calculated using the following formula:

$$R = \frac{\sum_n \left(X_n - \bar{X} \right)\left(Y_n - \bar{Y} \right)}{\sqrt{\sum_n \left(X_n - \bar{X} \right)^2} \sqrt{\sum_n \left(Y_n - \bar{Y} \right)^2}}, \quad R_{Log} = \frac{\sum_n \left(Log_{10} X_n - Log_{10} \bar{X} \right)\left(Log_{10} Y_n - Log_{10} \bar{Y} \right)}{\sqrt{\sum_n \left(Log_{10} X_n - Log_{10} \bar{X} \right)^2} \sqrt{\sum_n \left(Log_{10} Y_n - Log_{10} \bar{Y} \right)^2}}$$

X and Y are the event durations to compare. $\bar{X}$ and $\bar{Y}$ are the average values of X column and Y column respectively. R and R_{log} belong to $[-1,1]$ and the closer to zero they are the weaker the correlation is. The closer to $|1|$ they are, the stronger the correlation is. R evaluates the strength of the correlation for long times and R_{log} for short times. Stefani et al. concluded in the existence of a memory for all coefficients higher than 0.1. They showed that consecutive ON times and consecutive OFF times were correlated. They found no correlation between ON times and their adjacent OFF times.

Besides the fact that each experimentalist analyses data from different samples, the differences observed in the quantification of the blinking presented above, can be caused by threshold analysis's artifacts. The power law exponents and the correlation coefficients depend on the chosen threshold value. The choice of this threshold value arbitrary varies between the experimentalists. Recent works particularly investigate the artifacts of threshold analysis on the understanding of the blinking of single NCs [41, 52, 55]. These two reports highlight for the first time the strong dependence of the power law exponents and the truncation times on the chosen threshold value and on the experimental binning time.

Another limit of the threshold analysis is the necessity to describe the fluorescence of single NCs in a nearly binary picture. This binary picture consists of an emitting state producing the maximum intensity and a non-emitting dark state. This scheme was influenced by the attempt to relate the blinking of NCs to the one of single molecules. Two groups suggested in 2002 [56] and 2004 [57] the existence of intermediate emitting states responsible for low ON levels in the blinking trajectories. They pointed out for the first time a correlation between the fluorescence emission intensities and the fluorescence lifetimes of single NCs. In 2006, the first clear evidence of a continuous distribution of emissive states was reported [52]. In this report, the authors exploit an analysis method independent of the threshold analysis to demonstrate that counts of the same intensity levels, originated from different emissive states. Recent reports investigate the existence of power law dynamics on the fluorescence decay of single NCs with the same exponent as those obtained for the fluorescence blinking [58, 59]. This suggests a common mechanism behind the fluorescence decay and the blinking.

Even though the recent investigations [41] suggest a reanalysis and a reinterpretation of old data, the difference in the quantification of the blinking observed by Kuno et al. and Shimizu et al. have influenced the research over the last fifteen years. In order to understand the origin of power law kinetics, the surface of NCs, their environment and the experimental conditions have been tuned in several experiments.

2. Possible physical reasons behind the power law kinetics of the blinking of single NCs

a. Auger relaxation in charged NCs

In their report of 1996, Nirmal et al. [18] attributed the blinking to ionization and re-neutralization processes occurring at the surface of single NCs during the investigation. This picture of the blinking was supported by previous observations made in 1990 by Chepic et al. [22] on semiconductor quantum drops in a glass matrix. It was proposed that a single NC emits until the phot-generated electron (or hole) is trapped near or at the surface of the particle rendering it charged (figure 7). The charged NCs still absorb light but remain dark because of fast internal Auger non radiative relaxation between the second exciton and the unpaired carrier (green lines in figure 7 B and C). Fluorescence is recovered when the NCs re-neutralize. The mechanism of ionization and re-neutralization is still not clear and will be discussed at the end of this chapter. However the efficiency of Auger energy transfer between an electron hole pair and an unpaired charge in quantum confined systems like NCs has been shown in the works of Chepic et al. [22] and of Efros and Rosen [23].

.

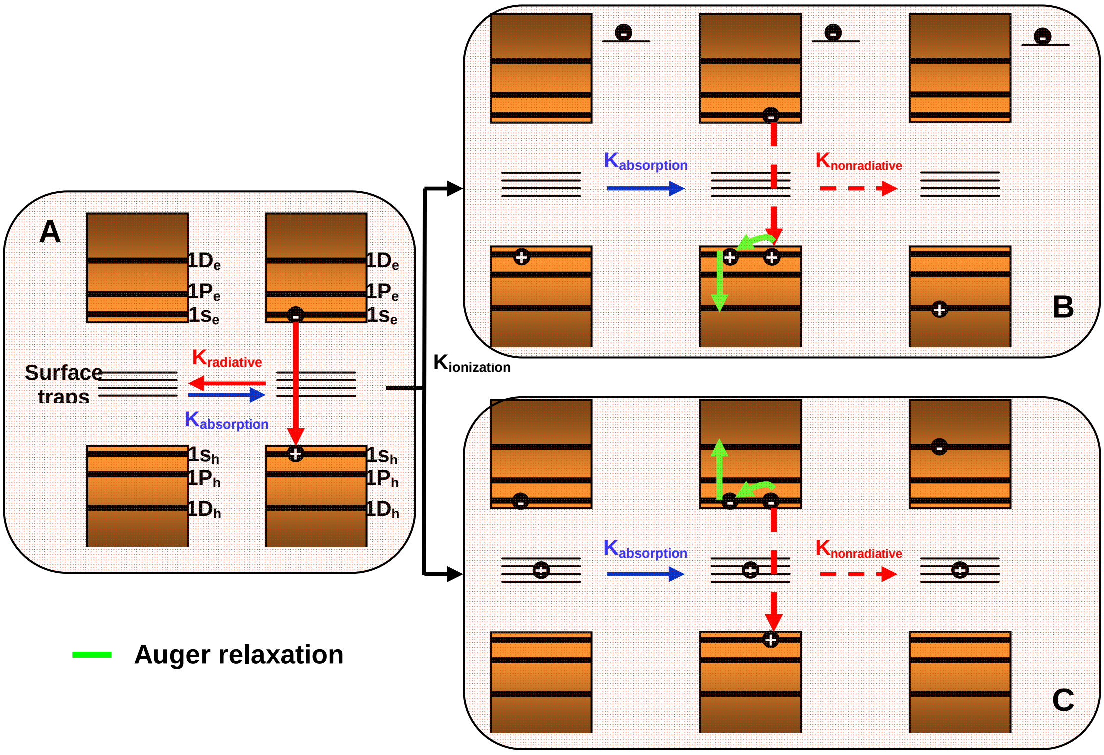

Figure 7: Ionization of single NCs and Auger relaxation. A: Radiative electron-hole pair recombination. B: Positive NC with electron in trap states. Non-radiative electron-hole pair recombination (dashed red line) and Auger excitation of the unpaired hole (green lines). C: Negative NC with hole in trap states. Non-radiative electron-hole pair recombination (dashed red line) and Auger excitation of the unpaired electron.

b. The role of surface states and the evidence of photo-ionization

One important characteristic of semiconductor NCs is the high surface to volume ratio. In these particles about 40 % of atoms reside on the surface [60], therefore the properties and the interactions of their surface with the environment play an important role in their optical properties. The contribution of surface states on the optical properties of NCs is widely reported [31, 60-64]. Although further investigations are still necessary, the surface states could be responsible for the behavior of single NCs under the influence of an external electric [65] or magnetic field [66, 67]. In the picture of darkening of single NCs due to charging, it is proposed that the trap states are close or near the surface. There are no reports directly correlating the charging and the blinking of single NCs. However, there are reports of the photo-ionization of single NCs [33-36]. The authors use EFM to probe the electrostatic charge occurring on single NCs when they are illuminated. Both positive (escape of electron) and negative (escape of hole) charging is observed. This charging depends on the surface states and on the excitation energy [32]. The authors showed that 40% of CdSe/CdS NCs became positively charged whereas only 8% of CdSe/CdS/ZnS NCs could be ionized when illuminated. They proposed that the passivation of the surface by the ZnS shell confined the exciton inside the NCs and prevented the photo-ionization. It is also shown in this study that the magnitude of photo-ionization of NCs increases with the excitation energy. Similar light induced charging is reported on other quantum emitters like nanorods [68]. In the report of Stefani et al. [27] the memory in single NC's blinking is independent of the experimental conditions (excitation power and substrate). This suggests that the blinking is intrinsic to NCs and occurs at their surface or close to it. Recently a similar memory has been observed on single Violamine R (VR) molecules. The fact that these VR molecules show also a power law blinking suggests that a residual memory may be found in other systems with complicated kinetics [69].

In an attempt to diminish the interaction of photo-generated excitons with the surface two groups recently published novel synthesis routes leading to less or none blinking single NCs. They improved the quality and increased the number of CdS shells around the CdSe core [39, 40]. In these particles, due to the small band offset between CdSe and CdS, the hole is confined in the core whereas the electron is delocalized over the CdS shell. Hence the confinement energy is reduced and the probability of Auger relaxation decreases. Furthermore, the high number of shells (typically 19) passivates the surface and strongly reduces the surface traps. Grey levels in the fluorescence time traces attributed to the emission of charged NCs are reported in these samples [70]. Other investigations of such samples suggest that trions (two electrons in the conduction band and one hole in the valence band) are not responsible for the darkening of single NCs [71, 72]. Another group recently reported synthesis of NCs with an alloy core (CdZnSe/ZnSe) [73]. These NCs do not blink but have a broad and inhomogeneous spectrum explained by the emission of charged particles. Several investigations are still needed to understand all the optical properties of these new high quality NCs.

While some researchers attempt to improve and passivate the surface of NCs to reduce the effects of the interactions with the environment on the exciton, some groups investigate the effect of the variation of electron or hole density near the NCs surface on their optical properties. For this purpose semiconductor NCs are investigated in solution or matrix of hole transporting or electron transporting materials. There is a general consensus on the effect of hole transporting materials. At ensemble level, it has been shown that the fluorescence of NCs is quenched in solution containing hole transporting materials [38, 74]. In these studies both static quenching (increase of non radiative centers) and dynamic quenching (transfer of the photo-generated hole to the hole transporting material) are investigated. Opposite observations are reported for electron donating materials. Several single particle investigations report a nearly or complete blinking suppression [37, 75, 76]. The mechanism of this suppression is not clear. It is however proposed that electron donating materials passivate the electron traps at the surface of NCs and therefore reduce or suppress the possibility for the photo-generated electron to escape to the surface. These observations are supported by correlated optical and electrochemical results. Here also the hole injection leads to a fluorescence quenching whereas a photo-brightening occurs when electrons are injected in aerated conditions [61].

c. Effect of structural properties of NCs and experimental conditions on the blinking kinetics

After the first observations of the blinking, the effect of temperature, of NC’s size and composition and of laser power on the blinking kinetics has been investigated. Recently the effect of ligands [77] and the excitation energy [54, 78, 79] have been studied. From all these studies, it follows that NCs always blink following power law kinetics independent of their quality, their composition and the experimental parameters. There is a consensus on the spontaneous kinetics of the process responsible for OFF events. For ON events, some researchers report the breakdown of the power law at long times shown at the beginning of this chapter, suggesting the existence of two processes behind responsible for bright states: A spontaneous process responsible for the power law and a photo-induced process responsible for its breakdown. The kinetics at this breakdown point is sensitive to the size and the composition of the NC and to the experimental conditions [26, 77].

In parallel to the development of analysis methods to quantify the blinking and the experimental investigation presented above, several theoretical models have been developed to explain the blinking of single

NCs. It is generally suggested that the fluorescence intermittency is correlated to ionization and neutralization processes in the NCs or its vicinity. In 1997, Efros and Rosen [23] proposed a random telegraph model to explain how the ionization and the neutralization of the NCs occur. They proposed that the electron (or hole) was ejected near or at the surface of the NC or in the matrix thermally or by Auger autoionization. This model predicted exponential distribution of ON and OFF rates, a strong temperature, size and excitation power dependence of the blinking. It gave a first intuitive picture of the blinking but contrasted with further experimental works [28-30]. The controversy of power law breakdown shown in figure 5 and 6 has fueled two main kind of theoretical models that are constantly adapted to the new experimental observations.

3. Theoretical models of the blinking

a. Diffusion based models

These models are based on the apparent influence of the experimental conditions (temperature, presence of oxygen, excitation power …) on the power law kinetics of NC’s blinking [26, 80]. Both spatial and spectral diffusion is discussed. In the spatial diffusion model, the electron escapes from the NC core by tunneling and diffuse in space. The NC remains dark until the electron diffuses back into the core [81]. The spectral diffusion that was first proposed by Bawendi group [26, 82] is more widely investigated. In this model, the acceptor trap levels diffuse around the NC. Whenever they are in resonance with the NC energy levels, the electron or hole tunnels out of the NC, rendering it dark. Three routes are proposed to explain the fluorescence recovery. In a first picture, the escaping relaxes back into the NC's core; in a second one a charge near the NC's surface recombines with the unpaired carrier in the core; in a third picture a subsequent thermal or Auger ionization of the charged core occurs. This ionization removes the unpaired carrier from the core to trap states near the NC's surface. In this last alternative, since the unpaired charge is localized near the surface, the net charge of the NC's core is null [82]. Recent developments have suggested a photo-induced diffusion controlled electron transfer (DCET) model [53, 83] in which both the energy levels of the NCs and the acceptor levels diffuse. The trapping and de-trapping in this model are governed by the diffusion of the charges at the intersection of NCs' and traps' energy domains. Diffusion models succeed in explaining the relation between the blinking and the spectral diffusion and broadening reported by several groups [82]. Since diffusion is sensitive to experimental conditions, these models predict the sensitivity of the blinking observed by some experimentalists. They explain the truncation of the power law of ON events. The DCET model can also be used to explain the continuous distribution of emissive rates in single NCs [52]. The major limit of these models is that they predict a fix power law exponent of 1.5 although this contrasts with several experimental observations.

b. Fluctuating tunneling barrier models

These models attribute the escape of the charge carrier essentially to tunneling. Verbeck et al. [84] proposed that the electron tunnels into a distribution of traps at the core-shell interface or at the surface of the NC. The trapping and de-trapping probabilities are proportional to

$e^{-\alpha r}$ and $e^{-\beta r}$ respectively. In these expressions r is the distance of the trap and α and ß are the decays lengths giving the depth of the trap. This model predicts the sensitivity of the power law distribution to the dielectric of the matrix [85]. An alternative dynamic tunneling process is proposed by Kuno et al. [24, 25, 86]. They suggested that the electron tunnels on a trap that may be located on the surface or even out of the NC. The fluctuation of the tunneling barrier width and height explains the broad distribution of ON and OFF durations. The tunneling models fail to explain the experimentally observed dependence of the power law deviations on the experimental parameters, the structural properties of the NCs. They explain the fluctuations of the power law exponents.

An important evolution of thoughts can be extracted from all these experimental results and theoretical models. Initially, the discussion was limited to the darkness of charged NCs. Then, Neuhauser et al. [82] suggested that only charged cores were dark and whenever the charge was localized in the shell the fluorescence was possible. Later Verbeck et al. [84] used a similar argument to explain the increase of average ON times and OFF times in capped NCs. These ideas were followed by different theoreticians who took into account the position (core, core-shell interface or surface) and the sign (electron or hole) of this charge in their models. The experimental progress made in the last two years [37, 39, 40, 61, 70-72, 74] confirms the necessity to analyze positive and negative NCs separately. On the other hand, all the authors agree on the non-accuracy of the threshold analysis used to derive the power law kinetics. A recent theoretical advance points this aspect to explain the deviations observed in different research groups [41]. It suggests the existence of conformation changing (active to inactive and vice versa) hole acceptor centers that render single NCs dark. This model explains the strong threshold dependence of the power law exponent and of the breakdown point that could not be explained by previous models. The picture attributing the blinking to a charging of NCs during the excitation is progressively replaced by a one in which the sign and the magnitude of the charge are taken into consideration [41, 42].

Chapter II: Sample preparation and experimental methods

It is shown in the previous chapter that the mechanism behind the optical properties of single NCs is still unexplained. This thesis mainly addresses the correlation between the charging and the blinking of single NCs. It investigates how the increase of electron or hole density influences the blinking. The first section of the chapter describes the synthesis of CdSe/CdS/CdZnS/ZnS NCs used in this thesis. Details of the sample preparation are given in the second section. The third section is a description of the experimental setup and a simple inexpensive method to produce flat aluminized AFM tips.

I. Synthesis of core-shell CdSe/CdS/CdZnS/ZnS nanocrystals

Core shell CdSe/CdS/CdZnS/ZnS NCs used in this work are synthesized following an established method [16]. The following reagents were used:

- For the growth of core CdSe NCs: cadmium oxide powder (CdO, 99.99 %, Aldrich), freshly prepared tetradecylphosphonic acid (TDPA), trioctylphosphine oxide (TOPO, 99 %, Merck), selenium powder (Se, 99.99 %, Alfa), tributylphosphine (TBP, 95 %, Acros), stock solution of Se/TBP (0.5mol/l).
- For the growth of the shells: octadecene (ODE, 90 %, Aldrich), octadecylamine powder (ODA, 99%, Fulka), sulfur powder (S, 99.98 %, Aldrich), CdO powder (99.99 %, Aldrich), zinc oxide powder (ZnO, 99.99%, Aldrich).
- For the purification steps: methanol, acetone, toluene, heptene and hexane.

0.052 g of CdO powder, 0.219 g of TDPA powder and 4.04 g of TOPO powder are loaded in a three necks flask, and evacuated at about 4 mbars for about 45 minutes at room temperature. The flask is then filled with nitrogen and heated to 100°C. After ten minutes a reddish solution appears and the temperature is increased to 150°C. The temperature is increased up to 320°C until complete dissolution of the CdO. Figure 8 summarizes the temperature steps and the color changes observed.

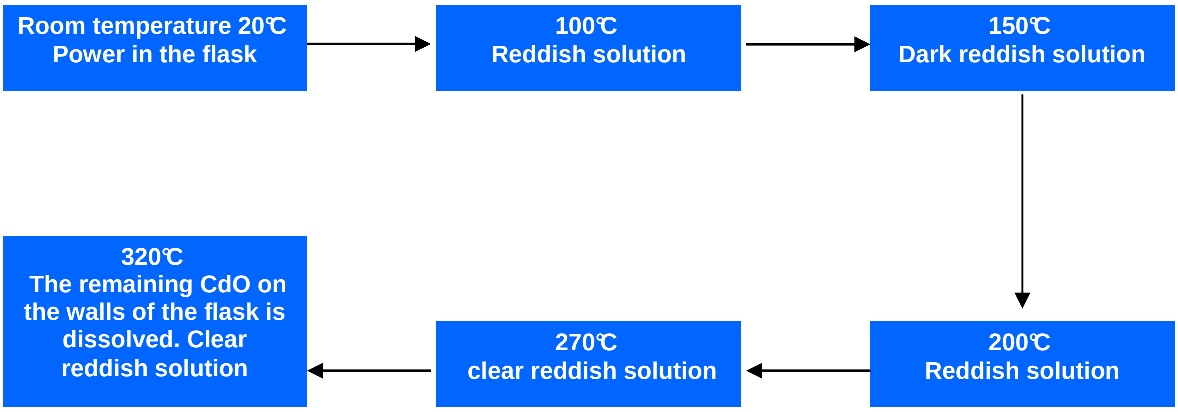

Figure 8: Dissolution of CdO

At 320°C a clear solution is obtained. 1.6ml of freshly prepared Se/TBP solution (0.5 mol/l) is then injected very fast. Then the temperature is rapidly reduced to the growth temperature of 250°C. A previous student in the group [87] showed that a higher quantum yield is obtained when the Se/TBP is injected at high temperatures. After the addition of Se, the color of the solution changes from yellowish to orange and then reddish. After two minutes the system is rapidly cooled down to 50°C. 15 ml of methanol is then injected to obtain an orange precipitate of CdSe NCs. The NCs are purified three times by centrifugation and decantation in the following order:

- Toluene to dissolve the NCs and methanol to precipitate them
- Toluene to dissolve the NCs and acetone to precipitate them
- Heptene to dissolve the NCs and acetone to precipitate them.

After purification the NCs are stored in toluene in a container filled with argon. The shells are grown following the SILAR method [16]. 3 ml of ODE and 1 g of ODA are evacuated in a three necks flask for one hour at 100℃. After cooling to room temperature, nitrogen is filled in the flask and 1 ml of the core NC solution is injected. The mixture is then evacuated for one hour at 50℃. After evacuation, the temperature is raised to 230℃ and the shell growth is processed under nitrogen flow. Several injections steps delayed of 10 minutes are necessary to produce multi-shell NCs. A little amount of the sample is extracted after the growth of each shell for optical measurements. Figure 9 summarizes the growth of the shells and the optical observations. The amount of precursors to be injected and the shell thickness expected are calculated following the literature [16].

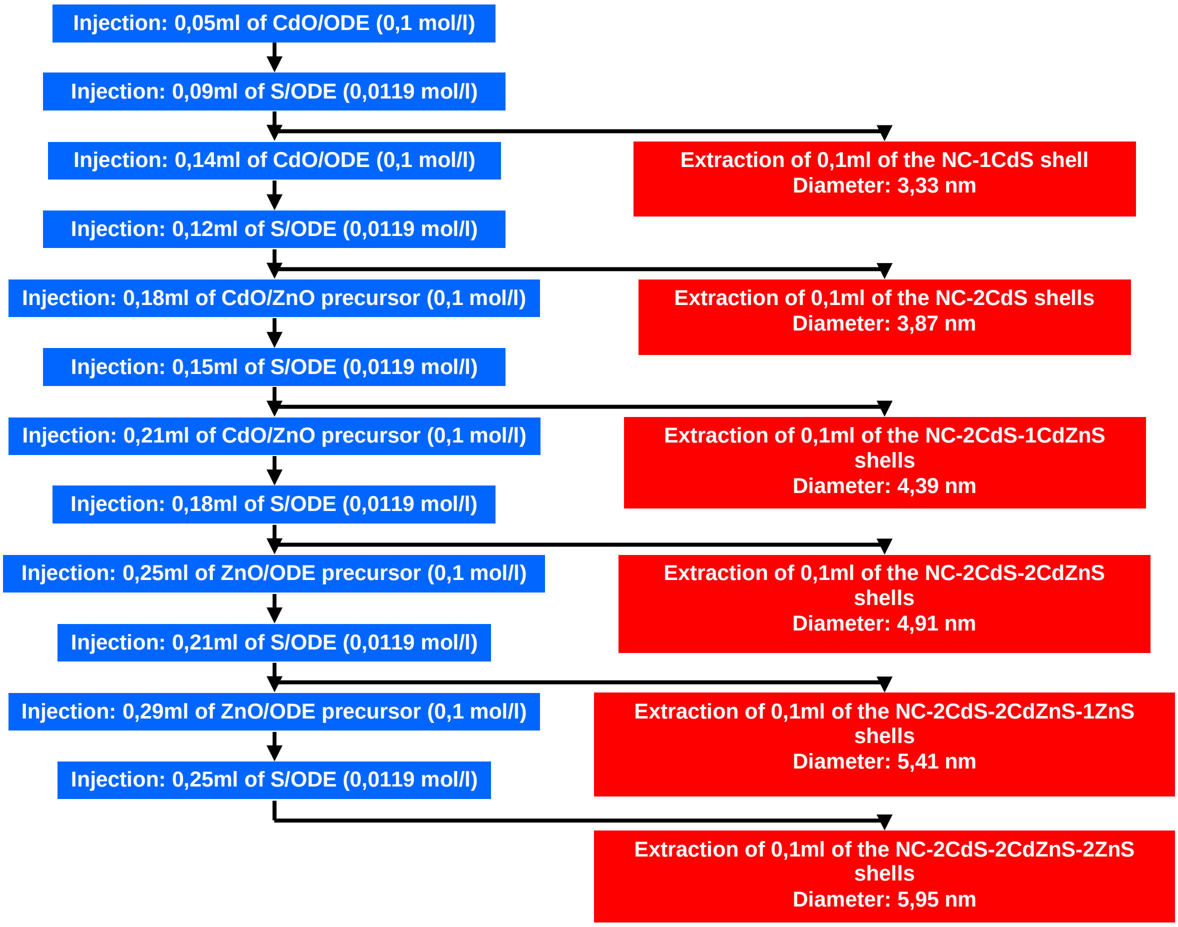

Figure 9: SILAR injection process

After the last injection step the system is kept at 260℃ for 30 minutes to anneal the NCs. The purification is done with hexane, methanol, acetone and toluene similar to the method previously described. Finally the NCs are stored in toluene under argon atmosphere. The quantum yield of the final product, measured relatively to Rhodamine 6G, is 39%. Figure 10 shows the absorption and the fluorescence spectra of the core and the final multi-shell samples. The extension of the electronic wave function in the shell materials causes a red shift of the optical properties of multi-shell samples in respect to core NCs [16].

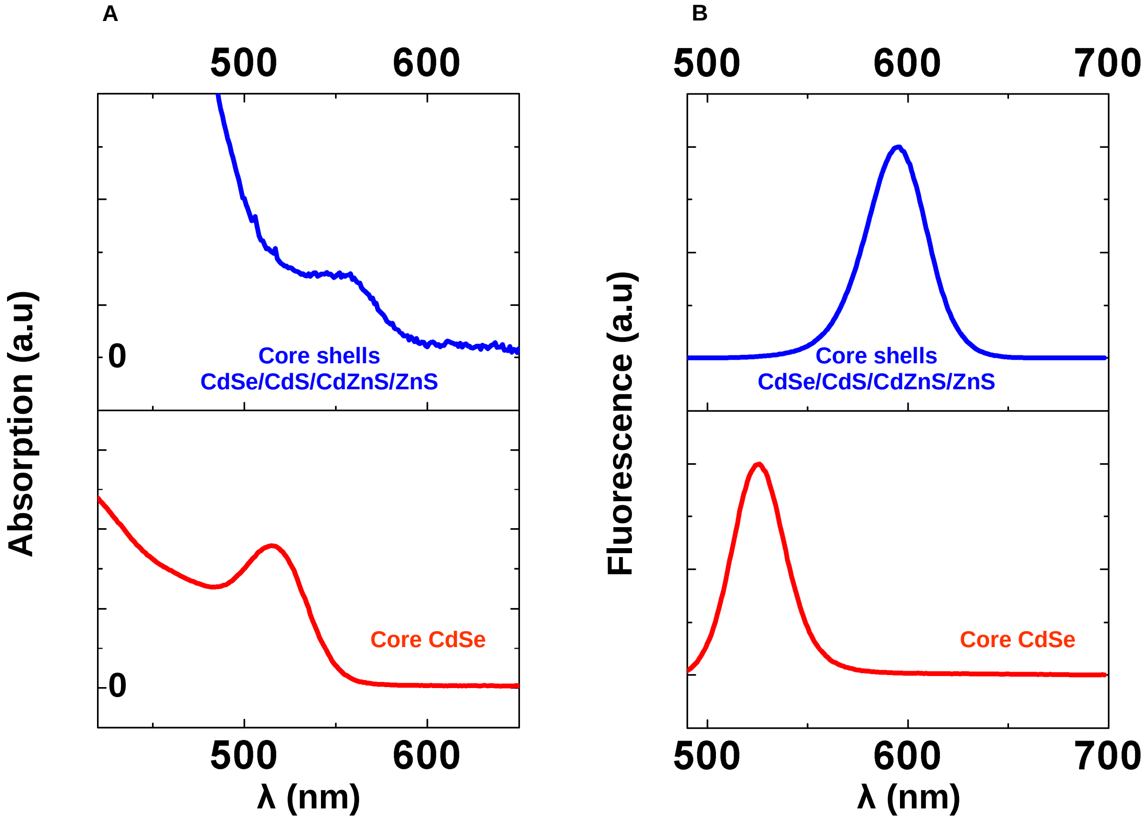

Figure 10: Variation of the optical properties of NCs solutions with the shell growth. A: Absorption. B: Fluorescence

The growth of the shell increases the stability of NC. This is shown by single particle experiments. Figure 11 shows an example of single particle experiments on three of the above synthesized samples. The samples are embedded in zeonex and imaged with the same experimental conditions using the experimental setup described at the end of this chapter. Details of the sample preparation are given in coming paragraphs.

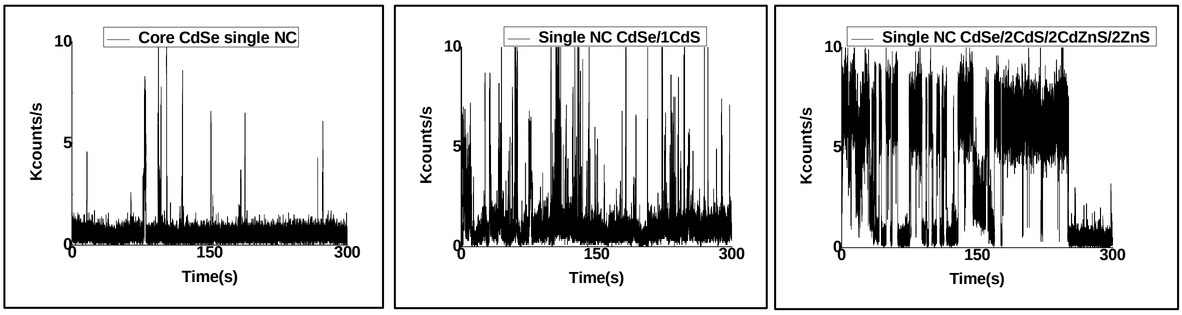

The growth of the shell increase the optical stability of nanocrystals

Figure 11: Effect of the shells on the PL of single NCs. The figure shows time traces of three different NCs. The single NC blinks as expected for single particles and the fraction of time its spend in the emitting ON states increases with the shell thickness..

Figure 11 shows an increase of the quality of NCs after the shell growth. There is an increase of the amount ON intensities from figure 11 A to C. As the number of shells increase, the number of non radiative channels at the surface of NCs decrease [16].

II. Sample preparation

1. Cleaning of glass and indium tin oxide (ITO) substrates

For our experiments, samples are prepared on bare glass or ITO coated glass substrates. Prior to the preparation, the substrates are cleaned. They are successively washed in an ultrasound bath with acetone for 15 minutes, 20 minutes in isopropanol and 20 minutes in distilled water. The cleaned substrates are stored in distilled water and can be used for five days. This cleaning procedure removes polar and unpolar impurities and the substrates are background free for optical measurements. Used ITO glasses are sometimes recycled. The cleaning method is similar but starts with 30 minutes ultrasound bath in toluene. Toluene is chosen here because the embedding materials (PBD or TPD) usually deposited with NCs on ITO substrates are soluble in toluene.

2. Preparation and characterization of nanocrystals/matrix films

The uniformity and the thickness of the matrix film embedding the NCs are important for the reproducibility of fluorescence measurements. In general the solution containing NCs and the matrix is spin coated on the substrate. Two spin coating methods are tested.

Method A: First of all, the substrate is mounted on the spin coater, and then rotated at 3000 rpm. 10 µl of the sample is then deposited on the rotating substrate. The spin coater is stopped 2 minutes after the deposition of the drop.

Method B: The substrate is mounted on the spin coater, a drop of the sample is deposited on the substrate, then the spin coater is first of all rotated at 500 rpm for 10 s and finally the speed is increased to 1500 rpm when the matrix is PBD or TPD and 3000 rpm when it is zeonex. The difference of speed is justified by the higher viscosity of zeonex solutions.

AFM is used to characterize the films produced by the two methods.

Matrix	**Image size**	**RMS Roughness (spin coating method A)**	**RMS Roughness (spin coating method B)**
TPD	1 µm x 1µm	3Å	2 Å
PBD	1 µm x 1µm	4 Å	4 Å
Zeonex	1 µm x 1µm	3 Å	2 Å

Table 1: Comparison of the roughness of the matrix films

Table 1 shows that the two spin coating method leads to atomic roughness (Angstrom scale), with a relatively lower surface roughness for method B.

The thickness of the film is evaluated with AFM. A second glass substrate is used to make scratches on the matrix film. The scratches are localized through the ocular of the confocal microscope and an AFM scan is performed at several positions around the scratch. When the scratch is well made, the height variations at different positions are negligible.

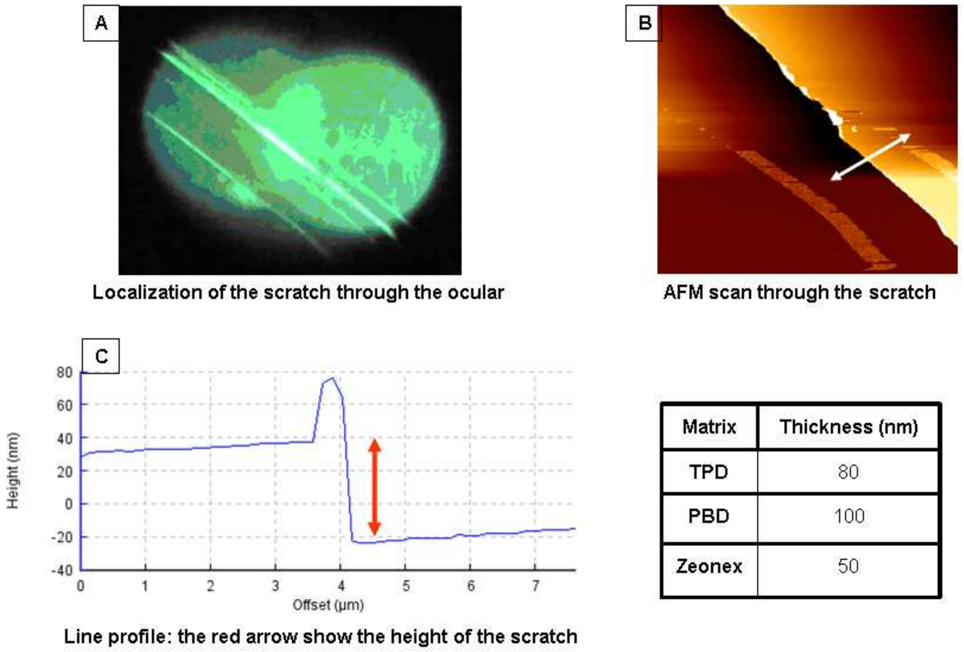

Localization of the scratch through the ocular

AFM scan through the scratch

Line profile: the red arrow show the height of the scratch

Matrix	Thickness (nm)
TPD	80
PBD	100
Zeonex	50

Figure 12: Example of a thickness measurement experiment. A: Photo of the scratch taken with a camera mounted on the ocular. B: AFM scan of the scratch. The white arrow shows the position where the line profile C is taken. C: Line profile at the position indicated on B. The red arrow shows how the height is estimated. The table summarizes the values obtained for different matrices.

The heights reported in figure 12 are obtained with TPD, PBD and zeonex solutions with a concentration of 12 g/l. These solutions are those used to prepare samples for single particle experiments. As it will be shown in the next chapter, the optical properties of single NCs are modified in “sandwiched” samples. These samples are prepared by successively spin coating three NC/matrix solutions on ITO glasses (spin coating method B). The following recipe is used:

- On top of ITO spin coating of 40 µl of the matrix solution (zeonex or PBD).
- After heating the first film 80℃ for 5 min, spin coating of 10 µl of the NC/matrix solution.
- After 5 min of heating at 80℃, spin coating of 20 µl of the matrix solution.

Table 2 shows the analysis of the surface of the sandwiched samples.

Samples	**Zeonex**		**PBD**	
	Thickness	**RMS Roughness**	**Thickness**	**RMS Roughness**
Layer 1: 40 µl of the matrix solution	50 nm	8 Å	80 nm	40 Å
Layer 2: 10 µl of the NCs/matrix solution	90 nm	5 Å	100 nm	50 Å
Layer 3: 20 µl of the matrix solution	170 nm	3 Å	250 nm	70 Å

Table 2: Characterization of sandwiched samples.

The values shown in the table 2 are not comparable to those given in figure 12 and in table 1. These values are relative values and just show that there is a thickness increase due to the multilayer preparation. However, they are measured on ITO which is rougher than glass. Although there is an increase in the thickness and the samples are annealed after each deposition, it is not possible to exclude a local corrosion of the previous layer. This is particularly observed in PBD samples. For zeonex the roughness is low and decreases with increasing layer thickness whereas for PBD samples, the observations are inversed.

III. The experimental setup

The experimental approach consists in combining a confocal microscope for fluorescence detection of single particles with nanomanipulation techniques using nanometer sized metallic tips. The experimental setup is a nanopositioner mounted on the stage of a confocal microscope. The idea is to guide a biased atomic force microscope (AFM) tip on the top of a single NC while recording its fluorescence. To ease the injection of charges into the NCs, the combination of Al (tip) and ITO (substrate) is used and the particles are embedded in the electron conducting material 2-(4-tert-Butylphenyl)-5-(4-biphenylyl)-1,3,4-oxadiazole (PBD) or the hole conducting material N,N‘-Bis(3-methylphenyl)-N,N‘-diphenylbenzidine (TPD) as for organic light emitting diodes (OLED) systems. When a voltage is applied between the tip and the ITO substrate and if the NCs are embedded in only one material, the difference in mobility of electrons and holes influences the sign of the charge approaching the NCs. Figure 13 summarizes the experimental idea and shows the energy offsets between the different materials. The structures of TPD and PBD are shown at the bottom. With this experimental setup it is possible to detect the emission of single NCs under the influence of the charged tip.

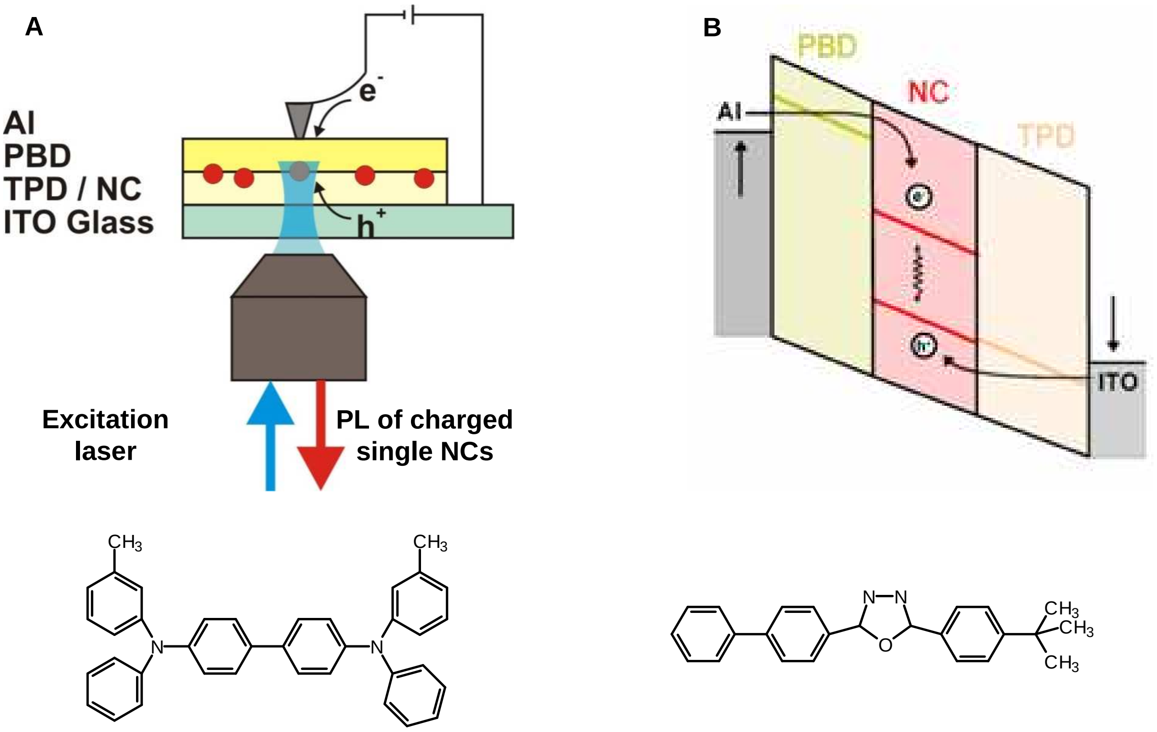

TPD: N,N‘-Bis(3-methylphenyl)-N,N‘-diphenylbenzidine

PBD: 2-(4-*tert*-Butylphenyl)-5-(4-biphenylyl)-1,3,4-oxadiazole

Figure 13: Summary of the experimental approach. A: Setup to correlate the PL and the charging of single NCs. B: Relative energy levels of PBD, NC and TPD. The structure of TPD and PBD is shown.

1. The laser scanning confocal microscope

The confocal microscope (figure 14) used in this work is described in details elsewhere [88]. Light from an Argon ion laser is coupled into a polarization maintaining fiber (*Schäfter + Kirchhoff, model 60SMS*). At the end of the fiber, a collimating lens parallelizes the beam which is then guided to the scanner through a mirror (M1) and a pellicle beam splitter from *Thorlabs* company (R= 8% and T=92%). The scanner consists of motorized mirrors (*Laser Scanner AGERS, open frame scan head*) and a telecentric lens system (L1 and L2). This ensures that only parallel beams enter the microscope's objective, hence optical aberrations are reduced during image scanning. A high numerical aperture (NA= 1,4) oil immersion objective is generally used to ensure maximal resolution of the microscope. Photons emitted by the sample go back through the objective and follow the excitation light path right to the beam splitter. 92 % of these photons enter the detection part of the microscope and are guided either to the APD by the mirror M3 or to the CCD Camera by the tilting mirror M2. Detector lenses are used to focus light on the detectors. The focal length of lens L3 (APD lens) is chosen such that the size of its focus fits the APD chip (50 µm). For L4 (Spectrograph lens) the f-number (f-6 for our spectrograph, $\frac{1}{2NA} = \frac{f}{D}$, where D is the diameter of the entrance pupil of the CCD camera) dictates the numerical aperture of the lens. The details of the conception, optical calculations, the efficiency and the alignment of this microscope are given in the master thesis preceding this doctorate work.

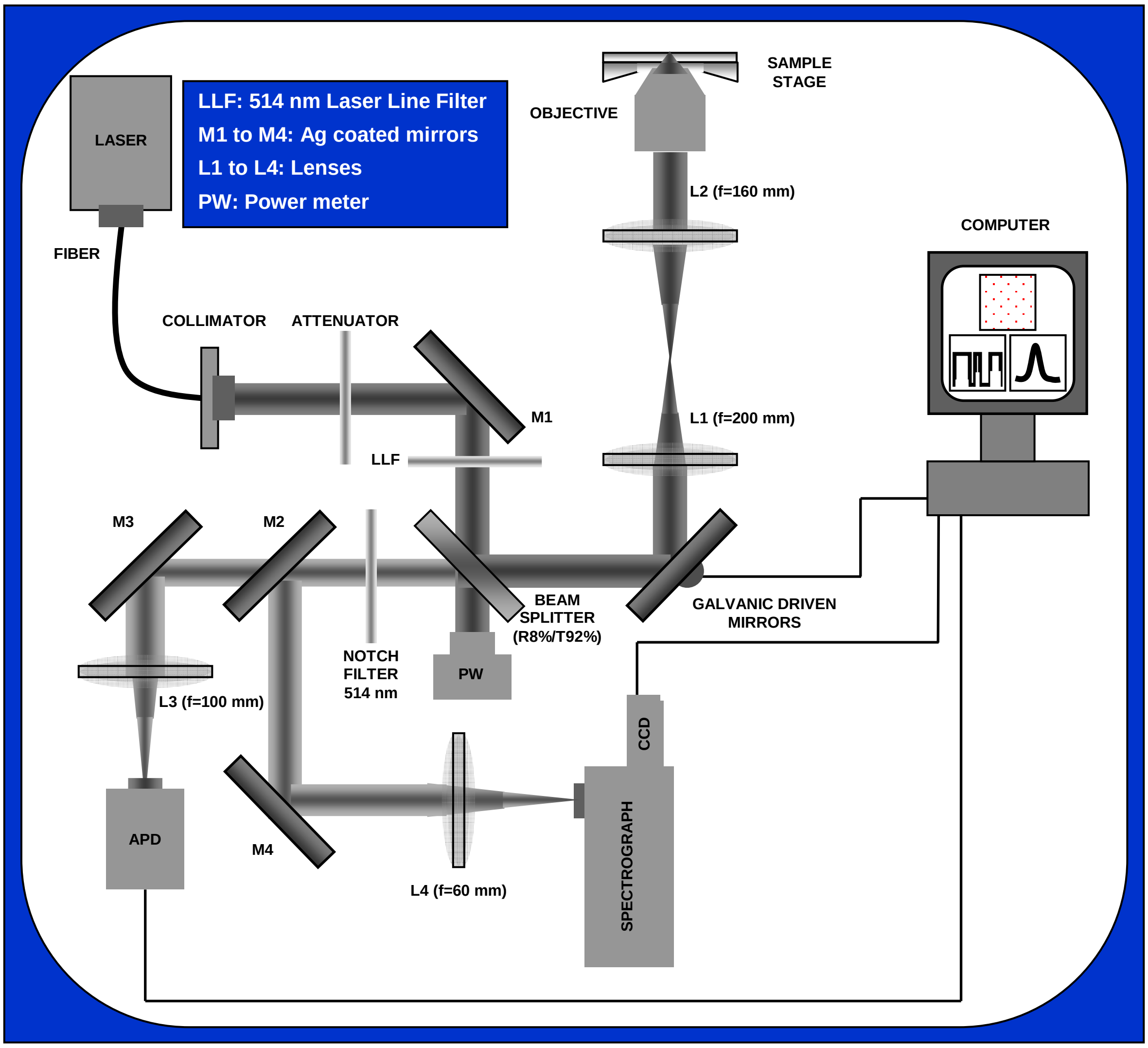

Figure 14: Laser Scanning Confocal microscope.

2. The Atomic Force Microscope and the nanopositioner

On the top of the confocal microscope, an AFM or a nanopositioner is mounted to control the tip. In the course of the project the AFM (*Bioscope, Veeco company*) is replace by a home built nanopositioner because of positioning drift difficulties. The nanopositioner consists of three components A, B and C (see figure 15) made of steel and held together by a strong magnet. Piezo elements surrounding small half ruby spheres placed in the middle and at the bottom of A ensure the motion of the nanopositioner. The up and down motion (z-direction) is performed by B, the tip holder. It is a parallelepiped piece at the bottom of which a copper or gold clamp is mounted to hold and electrically contact the aluminized AFM tip. The left-right and backwards-forwards motions (x-direction and y-direction) are performed by A. It is moved left/right or backward/forward relatively to C by the piezo elements at its bottom. Part C remains fixed during the nanomanipulation. The three steel made spheres at the bottom of C electrically contact the sample. The single steps of the nanopositioner vary between 20 nm and 30 nm. When the tip is moved on the sample and a voltage is applied an electrical circuit is built. Stainless steel and ruby used for the realization of the nanopositioner reduce friction between all the parts and the reproducibility of the step size. A joy stick is used to control all the displacements.

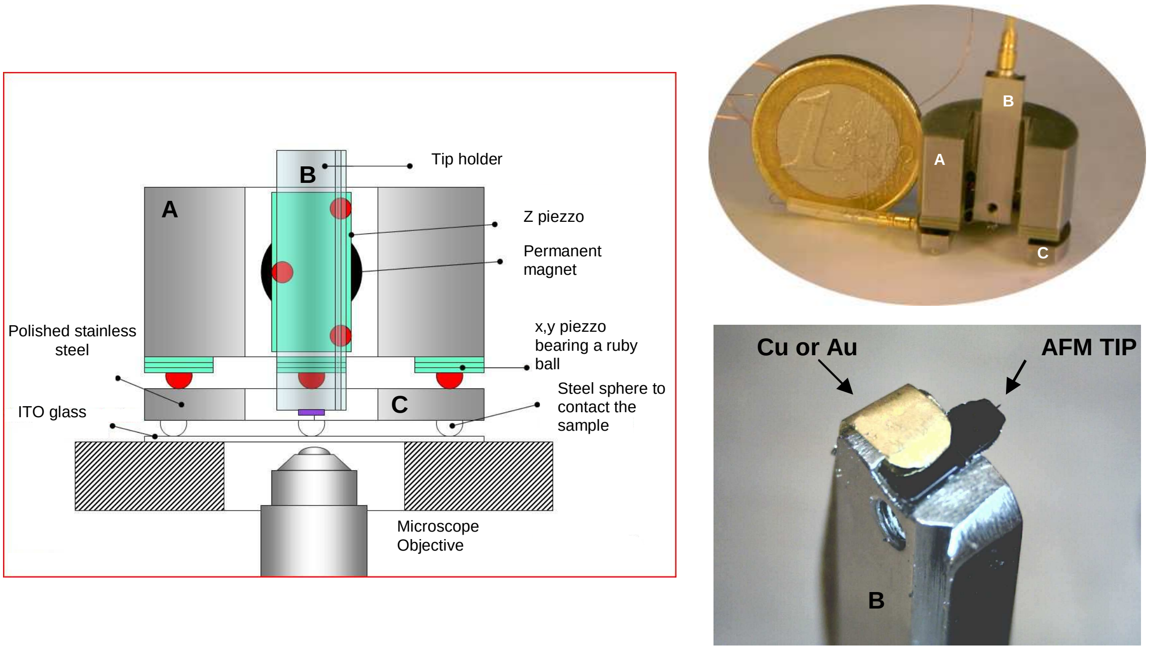

Figure 15: Nanopositioner. On the left picture, the red circles mark the position of the ruby balls. The green parts indicate the piezo elements. The sketch shows a correlation between the bottom of B (tip holder) and the microscope's objective. The photo on the right (top) shows the nanopositioner. The 1 euro coin on the photo gives an idea of its size. The photo at the bottom shows the AFM tip holder (part B).

The copper/gold wires that are seen on the top right photo of figure 15 connect the nanopositioner to a controller. They are also used to electrically connect the tip and the sample. For the charging experiment, the voltage is provided by a function generator (*HP 33120A, Hewlett Packard*). It provides alternative (AC) and direct (DC) tensions with maximal amplitude of 10 V. The frequency and the form (sinusoidal, triangular, square, etc.) of the tensions can be varied. In order to amplify the low current between the tip and the sample, a variable Gain High Speed Current Amplifier (*DLPCA-200, FEMTO*) is added into the circuit. It is also a current - voltage convertor. The voltage applied and the current flowing are first of all read on an oscilloscope (*HM305-2, HAMEG Instruments*) and then stored on a computer. The wires connecting the tip and the sample to the circuit are 20 cm long. This ensures reduces noise in the current signal and allows the detection down to 0.01µA intensities. The tip-sample contact is proved by the flow of a current while a DC voltage is being applied.

3. Processing of flat tips and setup alignment

The use of sharp AFM tips to influence the optical properties of single NCs presents several difficulties. As illustrated in figure 16 A, misalignment between a sharp ~10 nm radius tip and a 10 nm NC cannot be resolved by the 300 nm focus of the microscope. Different observations may result due to the different positions of the NC in the electric field between the tip and the ITO substrate when a voltage is applied. On the other hand, changes of the tip's shape after several landings may produce non uniform electric field lines. Therefore, an easy inexpensive method to produce flat tips is developed to overcome these limitations (figure 16B).

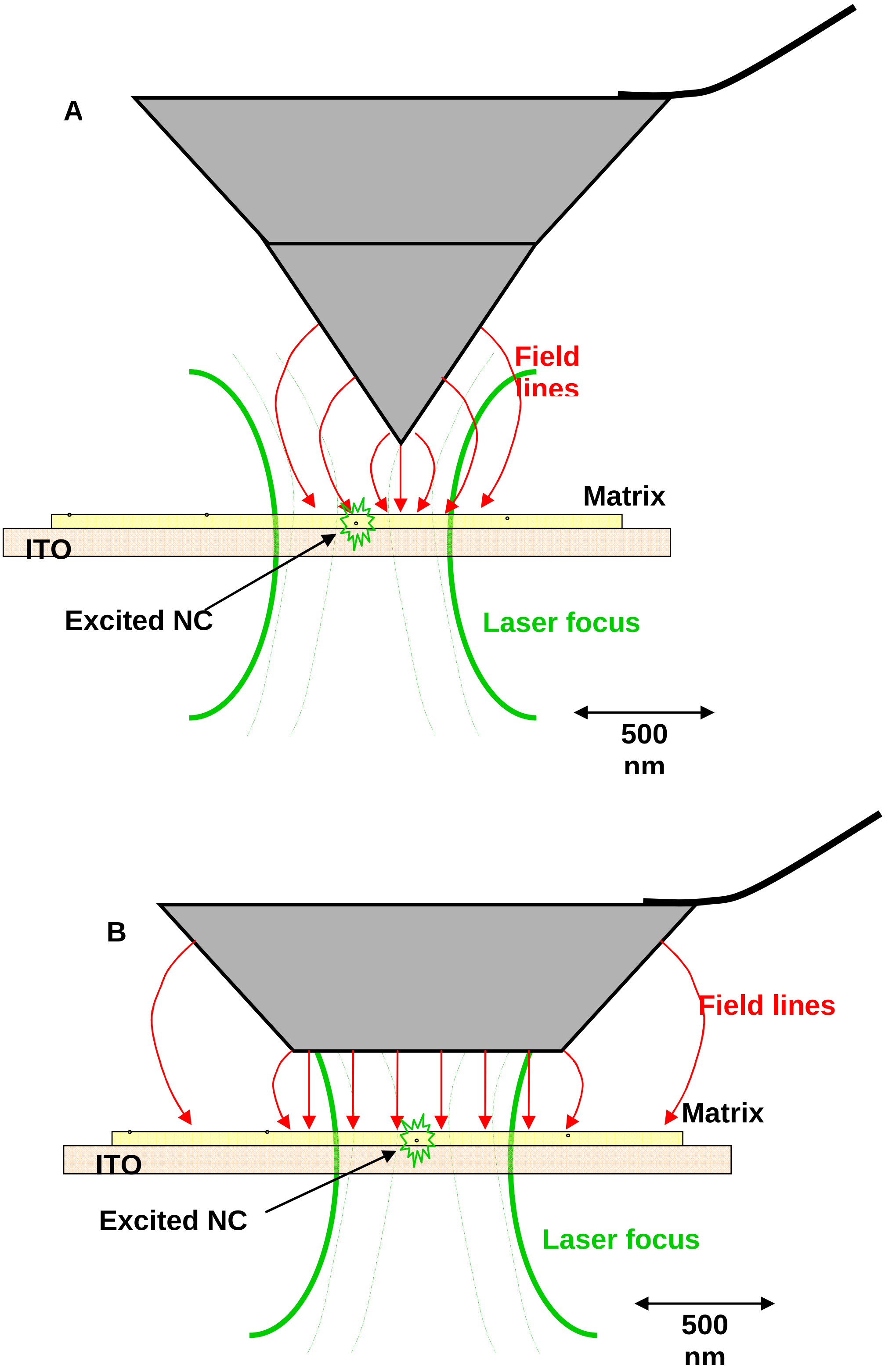

Figure 16: Illustration of the tip – NC - laser focus alignment problems. A: The laser focus is too big to resolve the misalignment of the tip and the single NC particle. This figure shows that the electric field line are not uniform inside the focus. B: Below the flat tip the field line are uniform. The base of the tip is big enough (1µm) and therefore can be clearly resolved with the laser focus.

Old used silicon or silicon nitride AFM tips are first of all coated with 20 to 50 nm aluminum to increase their conductivity. These old used tips are in general thrown away in most labs. SEM pictures of the tips are taken to check their shape before the processing. The tips are mounted on the nanopositioner and an electrical circuit between the tip and the ITO substrate is built. A voltage of 1 V is applied and the tip is slowly brought into contact with the ITO glass. A USB camera mounted in front of the system helps to visualize the last step when the tip is suddenly attracted by the substrate due to Van der Waals forces (see figure 17). There is in general a current flow at this contact point. The magnitude of the current is not constant due to the weak tip-sample contact that is maintained to avoid the complete tip destruction. A current between 0.1 µA and 1 µA is in general observed.

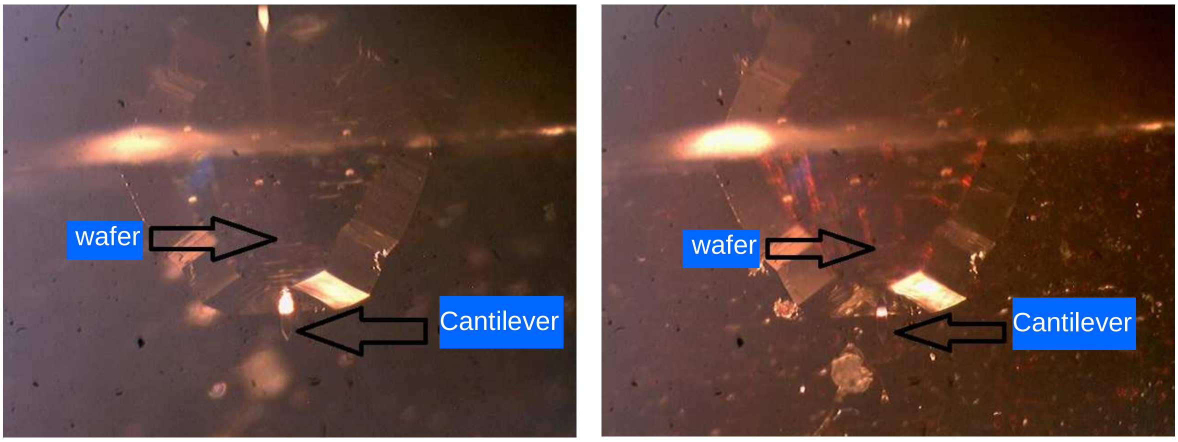

The cantilever starts to bend **The cantilever is strongly bended**

Figure 17: USB camera photo of the tip approach

The tip is then slowly moved left and right or forwards and backwards on the substrate for 5 min. It is kept at this position of weak contact with the substrate, otherwise the whole cantilever can be broken. Figure 18 shows an example of two tips after the processing.

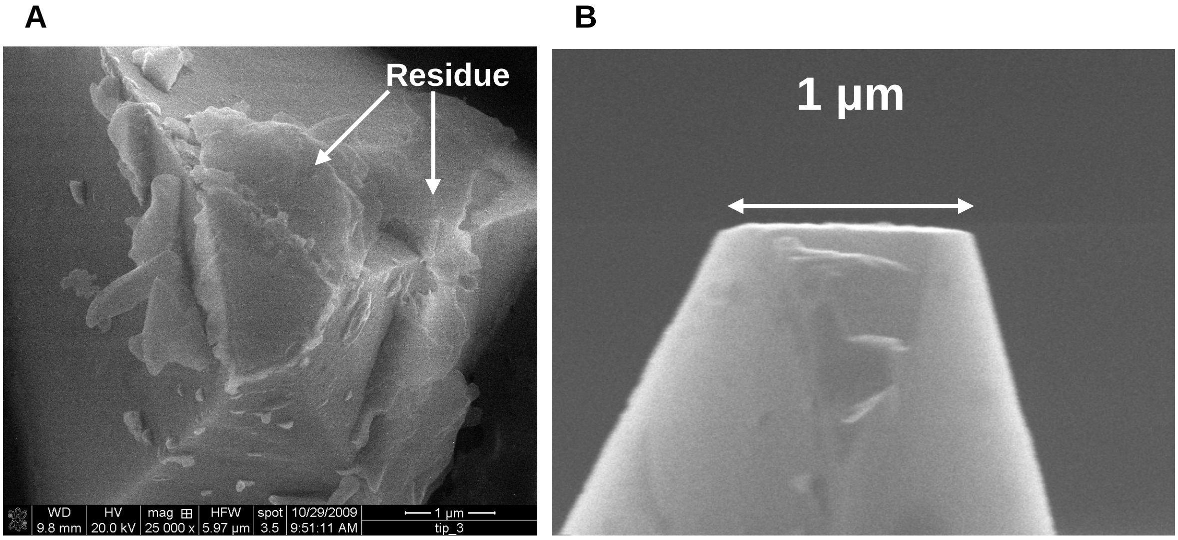

Figure 18: SEM images of flat tips. A: The base of the tip is flat. Residues of molten material remain on the side of the tip. B: A well flattened tip without residual molten parts.

Figure 18B shows that although the tips are successfully flattened, not uniformly distributed materials may surround the tip (figure 18A). It was unfortunately not possible to identify the composition during these experiments. However, from the contrast it is possible to speculate that these residues are molten aluminum. It is intriguing that the tips are not broken during the processing but are instead flatten. To understand the mechanism of this flattening, two control experiments are performed. In the first experiment the tips are moved on the substrate as described above but in the absence of a voltage. This leads to either no modification of the tips or mainly to the destruction of the whole cantilever. No flat tips are obtained with this method. In the second one the tip is brought into the weak contact position and then slowly pressed onto the surface in the presence of a voltage. The electric current usually increases when the pressure increases but disappears after 30 s. After 2 min the tip is pressed again until the current reappears. This procedure is repeated for 5 to 10 min and flat tips are obtained. However, as shown in figure 19, sometimes a part of the broken tip or unknown molten material remains on the flat part of the tip

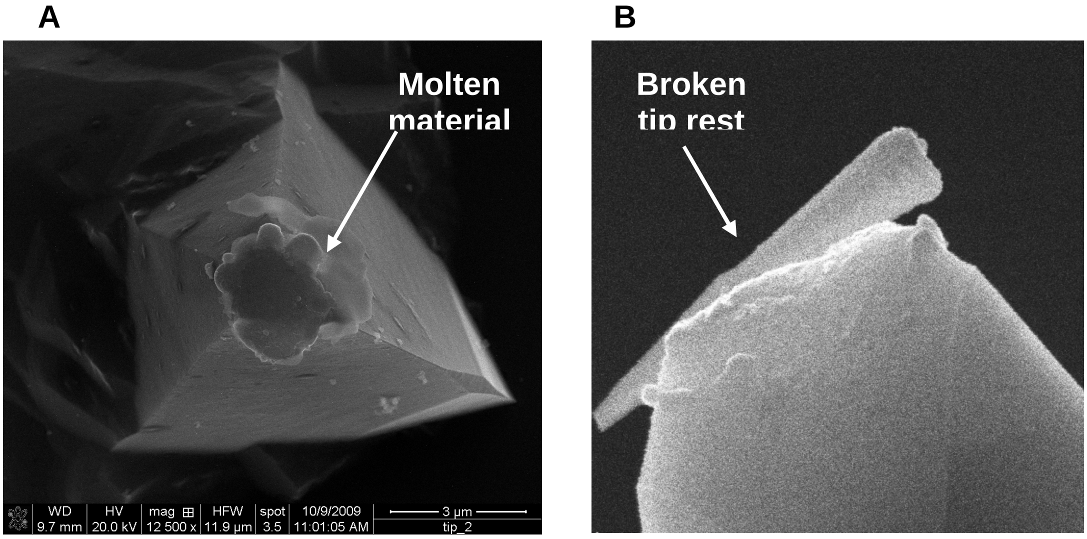

Figure 19: Anomalous flat tip. A: The molten material covers the flat tip. B: The broken part of the tip is glued.

It follows that the voltage is necessary to flatten the tips. 1 V is usually enough to produce good flat tips. 10 V on the contrary produces more anomalous tips independent of the flattening procedure used. The flattened part is in general 800 nm to 1 µm large. This suggests that the flattening takes place at the same position. The first control experiment described above suggests that the flattening is not just the result of a mechanical destruction of the tip. AFM users are familiar with the cantilever destruction when the tip abruptly touches the sample surface. The calculations below estimate the electrical energy produced by the flow of current between the tip and the sample

Electrical energy $= E_{el} = \underbrace{U}_{Voltage} \;.\; \underbrace{I}_{Current\ Intensity} \;.\; \underbrace{t}_{Time}$

For U=1V , I= 0`.1μA the typical electric current when
the tip and the substrate are in contact,
$t = 5$ minutes (the average time neccessary to flatten the tip)
it follows that $E_{elec} = 8.33\times10^{-9}\mathrm{Wh} \cong 3\times10^{-8} KJ$

The heat of fusion of silicon is
$E_F = 50.2\times10^{-20} KJ/mol$
If the tip is approximated to a regular tetrahedron of side length 10 μm,
Its volume is given by: $V = \frac{\sqrt{2}}{12}(10\mu m)^3$ and its mass by: $m = \rho V$
where $\rho = 2.33 g/cm^3$ is the density of silicon. This volume contains
$n = \frac{\rho V}{M} = 2.75\times`10^{-10}$ moles, where M = 28 g/mol is the molar mass of silicon
Therefore to melt the silicon tip
$E = nE_F = 2.75\times`10^{-10}\times50.2.10^{-20} = 1.39\times10^{-22} KJ$ is sufficient
$\frac{E_{elec}}{E_{h(tip)}} \cong 10^{14}$
The calculation for silicon nitride and aluminum coated tip give a relationship of the same order of magnitude between the electrical energy and the fusion energy.

The electrical energy resulting from the current flow is at least 10^{14} times higher than the energy necessary to melt silicon or silicon nitride tips. The same observation is made for the aluminum layer. Although the heat dissipation is high around the tip, the time spent by the tip in contact with the sample is sufficient to melt it. When the tip is moved on the surface, the friction creates additional heating, but the heat dissipation increases. Therefore a temperature assisted breakage probably occurs. On the other hand, the melting induced flattening explains the anomalous tips and the residues observed on flat tips.

The procedure to align the tip with the laser of the confocal microscope is rather simple. The wafer is roughly positioned on the laser focus. Then the tip is brought close to the substrate (a glass cover slide or ITO glass). A USB camera mounted on the ocular helps to place the cantilever on the focus of the objective (figure 20A). The reflection of the tip is then imaged on the APD, and the triangular reflection of the flat tip end is detected (figure 20B).

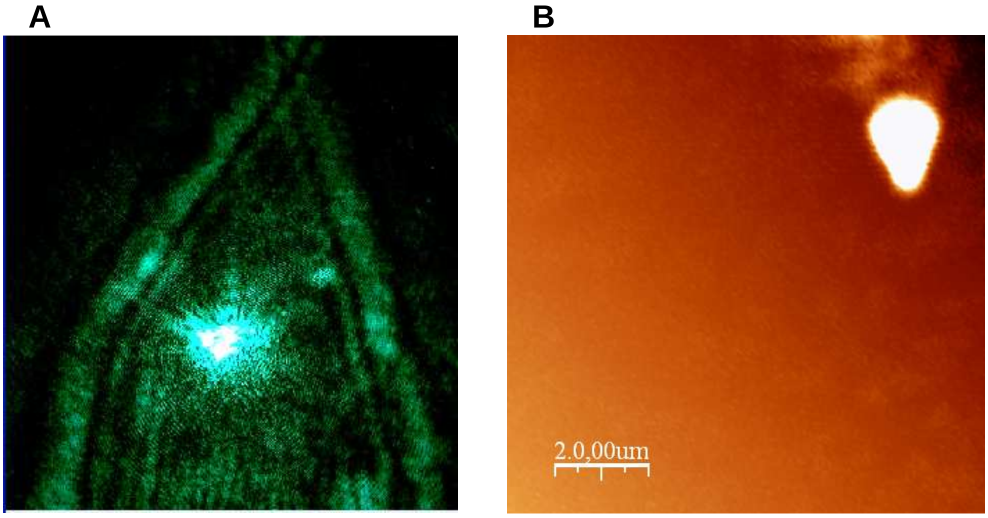

Figure 20: Description of the procedure to align the AFM tip with the laser. A: reflection of the cantilever through the ocular. The green laser light is on the tip. B: reflection of the triangular base of the flat tip taken on the APD.

Chapter III: Results and discussion

The experimental results presented in this chapter are organized in three main parts. In the first part the accuracy of the threshold analysis method is evaluated. The dependence of power law exponents and memory coefficients with threshold values and intermediate emitting states is investigated. In the second part of the chapter, the effect of the embedding matrix on the fluorescence of NCs is shown. Sample of NCs mixed with electron conducting, hole conducting and insulating materials prepared as described in the second chapter are analyzed. The last part of the chapter shows results of the nanomanipulation of the fluorescence of NCs with a biased metalized AFM tip.

I. Artifacts of threshold analysis

Several differences in the quantification of the blinking are presented in the first chapter. There are controversies on the observation of truncated power law kinetics of ON times; on the value of power law exponents that is necessary 1.5 for some researchers and scatters between 1 and 2 for others; on the existence of the memory in the blinking. These differences in the quantification have influenced the theoretical models of the blinking and the interpretation of single NCs experimental results. At the end of the first chapter, two recent reports investigating for the first time artifacts in blinking statistics related to the chosen threshold values and the experimental binning times are mentioned. To further investigate the origin of these artifacts, time traces of single NCs are analyzed with threshold analysis. The histograms of ON and OFF times and the memory coefficients are obtained following the method described in the first chapter. In this part, only the variations of the analysis results with the chosen threshold are addressed. In the second part of this chapter, the physical meaning of the different results will be discussed.

1. Effect of the threshold value

Figure 21 shows an example of a time trace analyzed by threshold analysis. The time trace chosen in figure 21 has well separated average ON intensity and OFF intensity (see the intensity histogram on the right of the time trace). Threshold values are chosen between 500 counts/s and 3000 counts/s (region marked in red in figure 21).

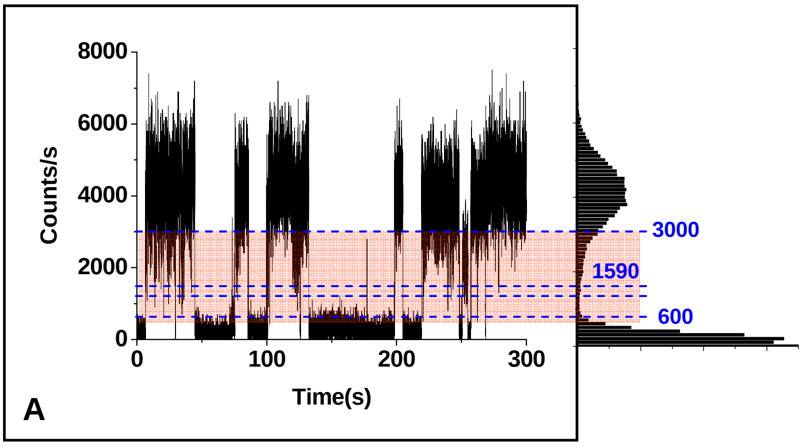

Figure 21: Time trace of single NC analyzed by threshold analysis. The intensity histogram is shown on the right of the time trace. The area marked in red indicates the region where threshold values are chosen.

All graphs corresponding to chosen threshold values are shown in annex 1 of this thesis. For clarity graphs corresponding to threshold values 600 counts/s, 1190 counts/s, 1590 counts/s and 3000 counts/s are shown in figure 22. The threshold value affects both power law exponents and the truncation of the power law. Figure 22 shows that for low for threshold values (600 counts/s for example), the probability density of OFF times follows a truncated power law. And for higher threshold values (3000 counts/s for example), the probability density of ON times follows a truncated power law.

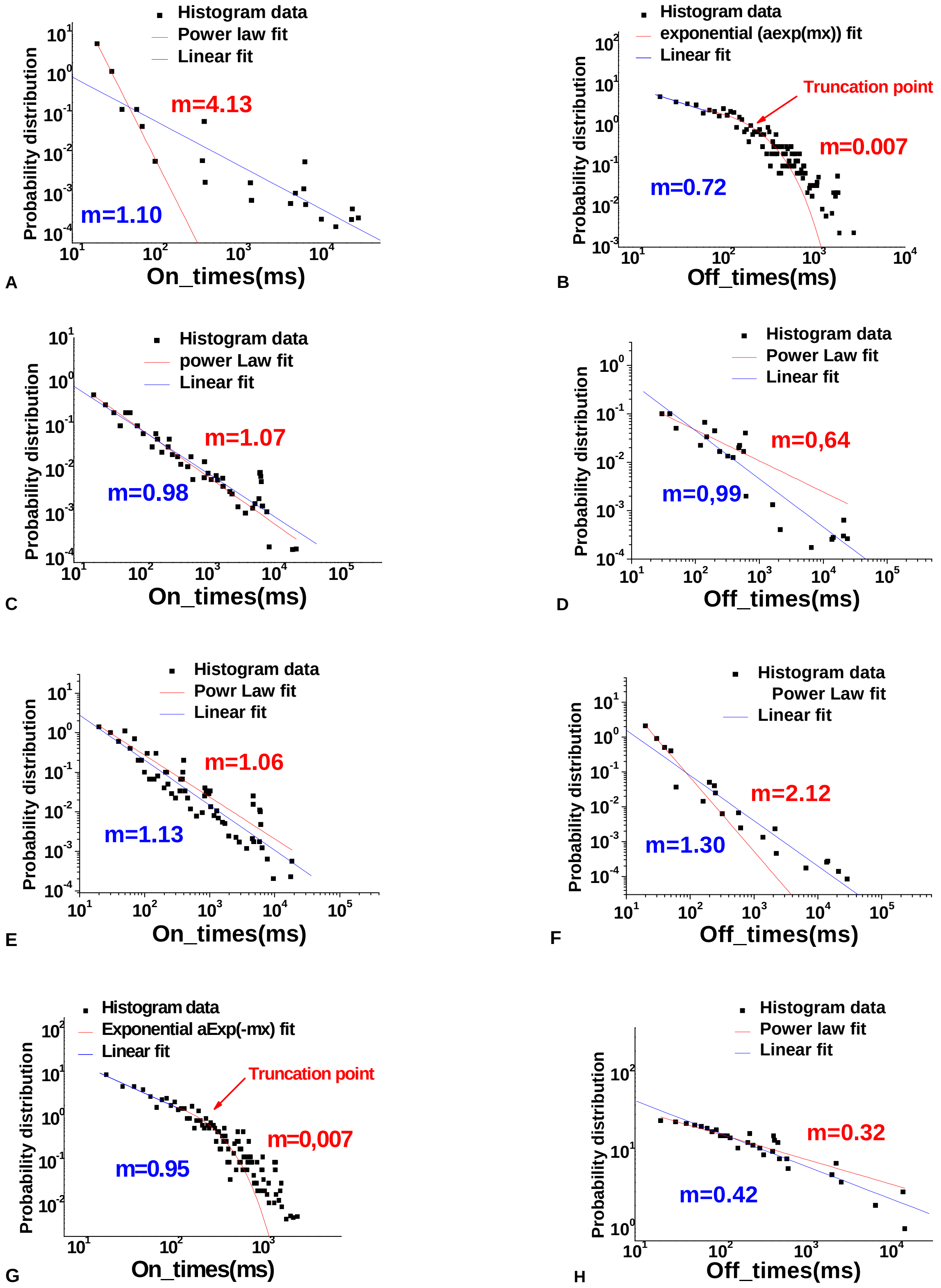

Figure 22: Variation of probability densities of ON times and OFF times with threshold values. (A, B), (C, D), (E, F), (G, H) correspond to threshold values 600 counts/s, 1190 counts/s, 1590 counts/s and 3000 counts/s respectively. In graphs B and G, the red curve shows a single exponential fit of the truncated part. In the other graphs the red curve shows the fit of the data with a power function $y = a.\tau^{-m}$ and the blue curve is linear fit $y = a + (-m)\tau$. The m values are the slopes obtained with the different fitting methods.

The results obtained for all threshold values are summarized table 3. The PW exponents and the LN exponents correspond to the slopes obtained by fitting the histograms with a power function and a linear function respectively (see section II of chapter I). The difference between the two fitting methods is commented in the first chapter.

	ON/ON				**OFF/OFF**				**ON/OFF**	
Threshold	**PW exponent**	**LN exponent**	**R**	**R_{log}**	**PW exponent**	**LN exponent**	**R**	**R_{log}**	**R**	**R_{log}**
500	3.27	1.27	0	0.15	**LN exponent 0.67** **Exponential coef. 0,007**		0.17	0.24	0	-0.1
600	4.13	1.1	0.03	0.24	**LN exponent 0.72** **Exponential coef. 0.007**		0.38	0.40	-0.03	-0.12
790	4.62	0.89	0.20	0.50	0.73	0.99	0.07	0.47	-0.04	-0.24
990	1.59	0.92	0.0,	0.26	0.78	1.05	0.11	0.32	-0.16	-0.25
1190	1.07	0.98	0.06	0.29	0.64	0.99	0.29	0.32	-0.12	-0.15
1390	1.06	1.05	0.06	0.16	2.57	1.21	0.22	0.29	-0.09	-0.14
1590	1.06	1.13	0.01	0.18	2.12	1.30	0.24	0.34	-0.06	-0.09
1790	1.34	1.25	0.03	0.36	1.50	1.35	0.25	0.30	-0.19	-0.11
2000	1.21	1.23	0.31	0.47	2.07	1.40	0.25	0.27	-0.05	-0.05
2300	1.35	1.29	0.07	0.42	2	1.47	0.26	0.26	-0.03	-0.17
2600	1.22	1.35	0.21	0.38	0.31	0.37	0.27	0.31	-0.03	-0.24
3000	**LN exponent 0.95** **Exponential coef. 0,007**		0.37	0.36	0.32	0.42	0	0.23	-0.01	-0.22

Table 3: Variation of analysis results with the threshold values. The red squares highlight thresholds where truncation of the power law is observed.

It can be seen that different power law exponents are obtained from the two fitting methods. The occurrence of power law truncation at threshold values 500 counts/s, 600 counts/s and 3000 counts/s are highlighted red in the table. The correlation coefficients R and R_{log} also depend on threshold values. The results of table 3 are plotted in figure 23 for clarity.

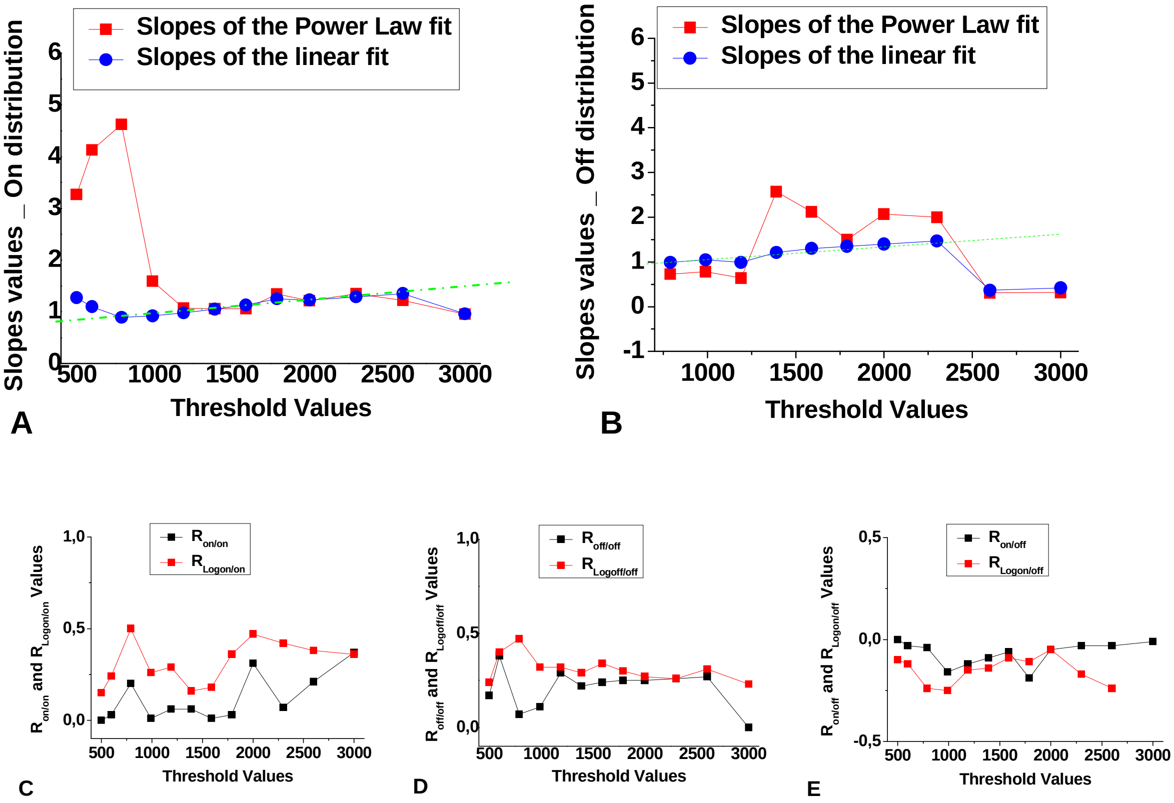

Figure 23: Plots of results shown in table 3. A and B show the variation of ON time and OFF time exponents respectively. The red curves show the variation of PW fit exponents while the blue curves the one of LN fit exponents. The green dashed lines are guide to eye to show the linear variation of the exponents. C, D and E show the variation of the correlation coefficients with the threshold.

For ON time exponents (figure 23 A) the exponents obtained by fitting the histogram with a power function (PW exponents in table 3) are highly varying below 990 counts/s. From 790 counts/s to 2600 counts/s these exponents vary almost linearly and are comparable to exponents obtained by fitting histograms with a line in double logarithmic scale (LN exponents in table 3). On the contrary to PW exponents, LN exponents vary almost linearly in the chosen threshold range (see the green dashed line in the figure). For OFF times exponents (figure 23B) observations similar to those in figure 23A are made. The LN exponents show a linear dependence from 790 counts/s to 2600 counts/s. For the memory coefficients, the threshold dependence also reveals a range of low variation as for the power law exponents. Between 990 counts/s the ON/ON correlation coefficients (figure 23C) show only small variations. A similar range of low variation is found between 990 counts/s and 2600 counts/s for OFF/OFF correlation coefficients (figure 23D) and between 990 counts/s and 1790 counts/s for OFF/ON correlation coefficients (figure 23E).

2. Effect of intermediate ON levels

To understand the threshold effect described above, the contribution of intermediate ON levels is investigated. Changing the threshold value modifies the ratio of such events in both ON time and OFF time distribution. The time trace of figure 21 is smoothed to artificially modify the distribution of intermediate ON level then a threshold analysis is performed at fixed values. The smoothing procedure gives the average value of an arbitrary number of points. Figure 24 shows a ten points smoothed curve (red curve) and the event duration histograms plotted in double logarithmic scale. Only the results obtained at thresholds values 600 counts/s and 3000 counts/s are shown in figure 24. At these values the histograms shown in figure 22 (D, G) showed a truncated power law dependence.

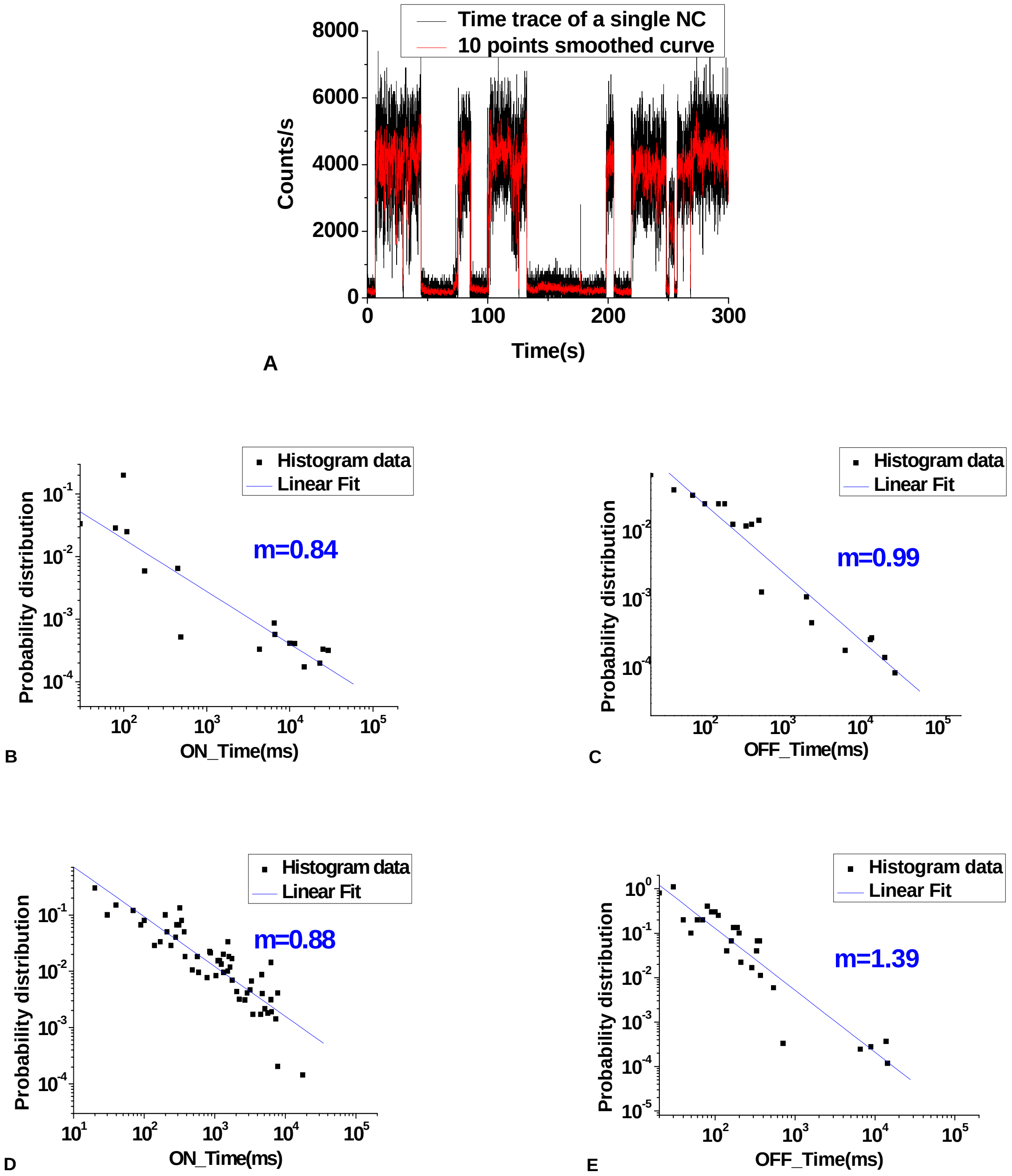

Figure 24: Effect of the low ON intensity levels on the analysis results. A: Time trace of the same particle shown in figure 21. The smoothed curve is shown in red. B and C are the power law distribution obtained with the smoothed data at a threshold value of 600 counts/s. D and E are those obtained at a threshold value of 3000 counts/s. The m values show the exponent of the power law function obtained by LN fit. The tables summarize the new correlation parameters obtained.

Figure 24 shows that changing intermediate ON levels distribution strongly affects the threshold analysis results. The truncation of the power law at threshold values 600 counts/s and 3000 counts/s observed in figure 22 (B, G) disappears in figure 24 (C, D). The variation of the power law exponents and of the memory coefficients is shown in table 4. It follows from results shown in table 4 that all the analysis results are strongly affected by the variation of the fraction of intermediate states at the chosen threshold values.

Threshold (counts/s)	**Data**	**Original**	**Smoothed**
600	m_{ON}	1.10	0.84
	m_{OFF}	0.72	0.99
	$R_{ON/ON}$	0.03	0.17
	$R_{LogON/ON}$	0.24	0.53
	$R_{OFF/OFF}$	0.38	0.15
	$R_{LogOFF/OFF}$	0.40	0.19
	$R_{OFF/ON}$	-0.03	-0.11
	$R_{LogOFF/ON}$	-0.12	0.31
3000	m_{ON}	0.95	0.88
	m_{OFF}	0.42	1.39
	$R_{ON/ON}$	0.37	0.12
	$R_{LogON/ON}$	0.36	0.13
	$R_{OFF/OFF}$	0	0.13
	$R_{LogOFF/OFF}$	0.23	0.24
	$R_{OFF/ON}$	-0.01	0.08
	$R_{LogOFF/ON}$	-0.22	0.14

Table 4: Variation of the analysis results with the intermediate ON levels.

From figures 22 and 23, it follows that although the chosen time trace has well separated ON and OFF average levels, the power law exponents are affected by the variation of the threshold. The PW fit results are more affected than the LN fit results over the chosen threshold range. The two sets of results match between

1000 counts/s and 2600 counts/s for ON times exponents. For further analysis in this thesis the LN fit method is chosen because of the relative low (compared to the PW fit method) effect of the threshold value on the exponents obtained. The strength of the memory also varies with the threshold values. The R coefficients sometimes take the value zero but the sign of the R_{log} coefficients does not change over the chosen threshold range. The breakdown of the power law kinetics observed at long times depends on the threshold value too. At thresholds of 500 counts/s and 600 counts/s, the probability distribution of OFF events deviates from the power law. A similar deviation is observed at 3000 counts/s for the probability distribution of ON events. Figure 24 shows that this deviation from the pure power law also called truncation of the power law is removed by reducing the fraction of low ON levels in the time trace.

It follows from all these observations that the variations of the power law exponents and the correlation coefficients with the threshold values are mainly due to the contribution of low ON levels. This finding is important to understand the mechanism of the blinking. It is usually argued that the power law truncation is the sign of a contribution of a photo-induced mechanism in the blinking. One of the advantages of diffusion-based models is the possibility to explain the dependence of the power law truncation on the structural properties of NCs and the experimental conditions. The results shown in this work suggest that the deviations from the power law are analysis artifacts and not a feature of the blinking of NCs. It is shown that reducing the number of random events crossing the threshold line eliminates the power law deviation. The time traces shown by the two groups of authors in the first blinking statistic reports are qualitatively different. The time trace shown by Kuno et al. [24, 25] contains only a low amount of low ON events like the one analyzed in this work whereas the one shown by Shimizu et al. [26] possesses a high amount of intermediate states. In his recent report, Frantsuzov et al. [41] addresses for the first time the dependence of the truncation time with the threshold, however the chosen time trace has clear intermediate ON levels. In this report the authors do not address the role of these intermediate ON levels in the occurrence of the truncation. Another important conclusion could be derived from the Efros and Rosen random telegraph simulation [23]. It shows that events randomly crossing a given threshold line can be described by an exponential distribution. Since we observe for lower and higher threshold values an exponential distribution at long times, we concluded that the intermediate states in the time trace can be treated like random fluctuations. Therefore the obtained distribution takes the form of a truncated power law when the contribution of these events increases. The existence and the mechanisms of these intermediate states are not necessary correlated to the blinking and need to be further investigated.

The threshold analysis method inaccurately evaluates blinking kinetics when the fraction of low ON intensities increases. The truncation observed in these cases is a measure of the contribution of randomly distributed intermediate levels. Increasing the binning time, the temperature, the excitation power and changing the experimental conditions modify the distribution of these intermediate events. The development of quantification methods independent of the threshold values is necessary. Such methods are proposed by Zhang et al. [52] to analyze time traces in which there is no clear separation between the average ON levels and average OFF levels.

II. Dependence of NC's fluorescence on electron conducting, hole conducting and insulating materials

1. Effect of hole and electron conducting materials on the NC photoluminescence

a. Influence on the quantum yield

The quantum yield of six different solutions of NCs in toluene synthesized following the methods described in chapter II is measured. Then the NCs are mixed with a solution of either TPD or PBD and the new quantum yield is measured. All quantum yields are measured with reference to Rhodamine 6G and the TPD and PBD solutions have the same concentration (0.034 mol/l).

A	**Sample**	**NCs in Toluene**	**NCs + TPD in Toluene**	**NCs + PBD in Toluene**
1	CdSe/Cd_ZnS/ZnS	13%	13%	8%
2	CdSe/2CdS/2Cd_ZnS/2ZnS	32%	32%	20%
3	CdSe/2CdS/2Cd_ZnS/2ZnS	56%	35%	32%
4	CdSe/2CdS/2Cd_ZnS/2ZnS	19%	16%	13%
5	CdSe/Cd_ZnS/ZnS	35%	35%	25%
6	CdSe/2CdS/2Cd_ZnS/2ZnS	45%	43%	36%

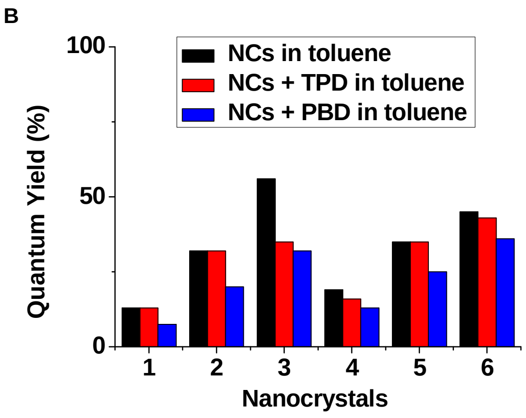

Figure 25: Effect of TPD and PBD on NC solutions. A: Table of the results. B: The influence of TPD and PBD is plotted in a histogram.

The measurements shown in figure 25 are repeated three times to exclude experimental errors. The Rhodamine 6G solutions are freshly prepared to reduce the errors due to aging effects.

The results shown in figure 25 indicate a noticeable reduction of the quantum yield upon addition of PBD for all the six samples (blue bars in the histogram). On the contrary, the effect of TPD is not uniform. Although in sample 3 and 4 the addition of TPD reduces the quantum yield from 56% to 35% and from 19% to 16% respectively, the effect on the other samples is negligible (from 45% to 43% for sample 6) or not observed (sample 1, 2, 5). To explain these contrasting observations made in solution, it is necessary to take into account the effect of toluene (the solvent effects). In a TPD molecule, the electron lone pairs on the nitrogen atoms are delocalized in the conjugated system. This reduces the basicity of TPD and increases its relative (compared to PBD) solubity in unpolar solvents. In PBD, the electron lone pairs are localized in the oxadiazole hetero-atoms cycle. Therefore, this electron rich center will be less solvated by the toluene molecules. It follows that in solution the toluene molecules will hinder the interactions of TPD with the NCs surface and prevent the strong quenching observed in the matrix. The variations of the TPD effect with different NCs samples can be explained by the non homogeneity of the surface and it is discussed in several previous reports [61, 74]. The effect of PBD on the NC’s PL in general will be discussed in coming paragraphs. However, it can be proposed that the quenching of the quantum yield is not due to an electron transfer from the NCs to the PBD or an increase of non-radiative recombination routes. These two mechanisms would be correlated to a strong quenching when NCs are investigated in PBD matrices (opposite observations will shown later). The possibility to observe single NCs in PBD matrices rather suggests that the reduction of the NC’s quantum yield in PBD solution could be due to a reduction of non-radiative rates combined to an increase of the radiative rates. The electron lone pairs localized in the oxadiazole hetero-atoms cycle reduce the non radiative rate by passivation of electron traps and increase the radiative rate by coulomb repulsion with photo-generated electrons in NCs.

b. Quenching of the PL of single NCs by hole conductor

In this experiment, NCs are embedded into films of zeonex, TPD or PBD. The sample preparation is described in chapter II. The spin coating method B is used because it led to more uniform film. The samples are imaged using the confocal microscope as described in the previous chapter. A laser wavelength of 514.5 nm and an excitation power of 40-80 nW entering the microscope objective are used. Fluorescence images, spectra and time traces of NCs are recorded.

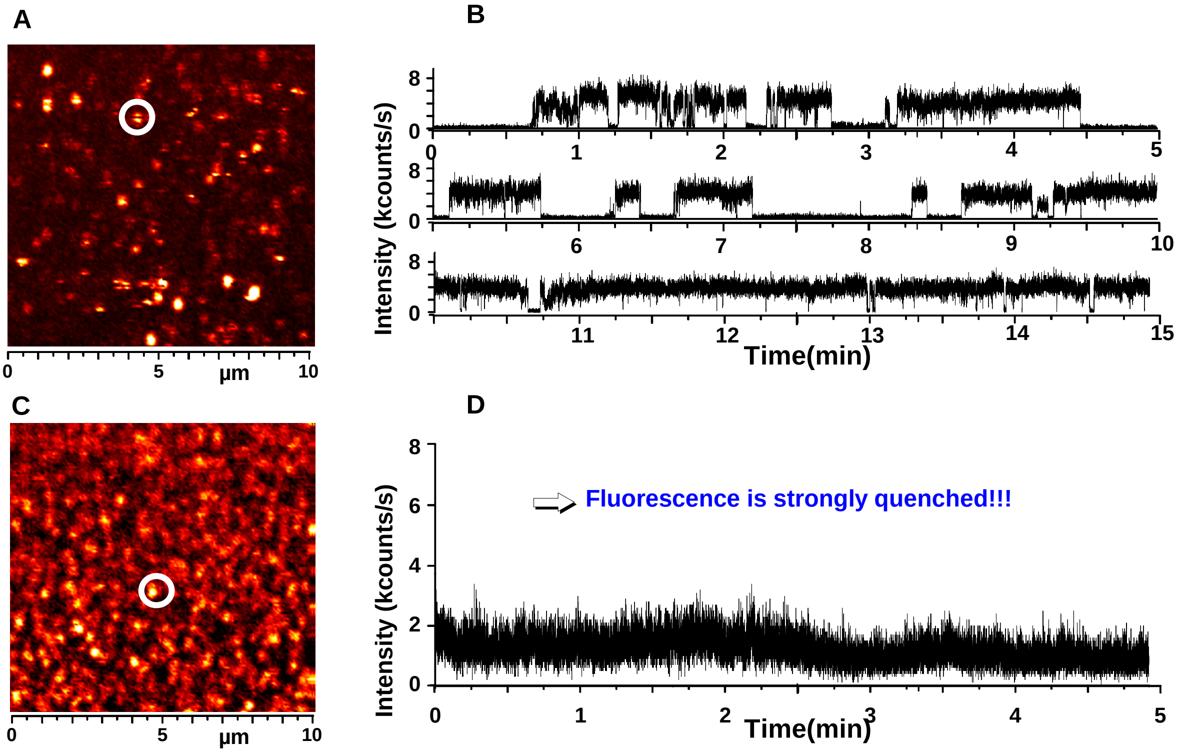

Figure 26: Effect of PBD (top) and TPD (bottom) on the PL of single NCs. A and C are the PL images. The circled areas are where the time traces are taken. B: Time trace of the single NC marked on A. The PL intensity changes between 7000 counts/s and 500 counts/s. D: Time trace of the bright spot circled in C. Although this spot is not a single NC, the PL is lower than in B.

Figure 26 shows the fluorescence of NCs in PBD (A,B) and TPD (C,D). The fluorescence intensity of NCs in PBD changes between emitting levels (7000 counts/s) and dark levels (500 counts/s). In TPD (figure 26C and D), the PL originating from a sample with a high NCs density is strongly quenched to about 1500 counts/s at maximum intensity.

To understand the relative effect of TPD and PBD on NCs, cyclic voltammetry experiments are performed on NCs, TPD and PBD. The measurements are made with a HEKA PG310 potentiostat/galvanostat using a platinum disc as working electrode, a platinum wire as counter electrode and a silver reference electrode. Ferocene [Fc/Fc$^+$ (+0.4 V)] in dry dichloromethane is used as electrolyte.

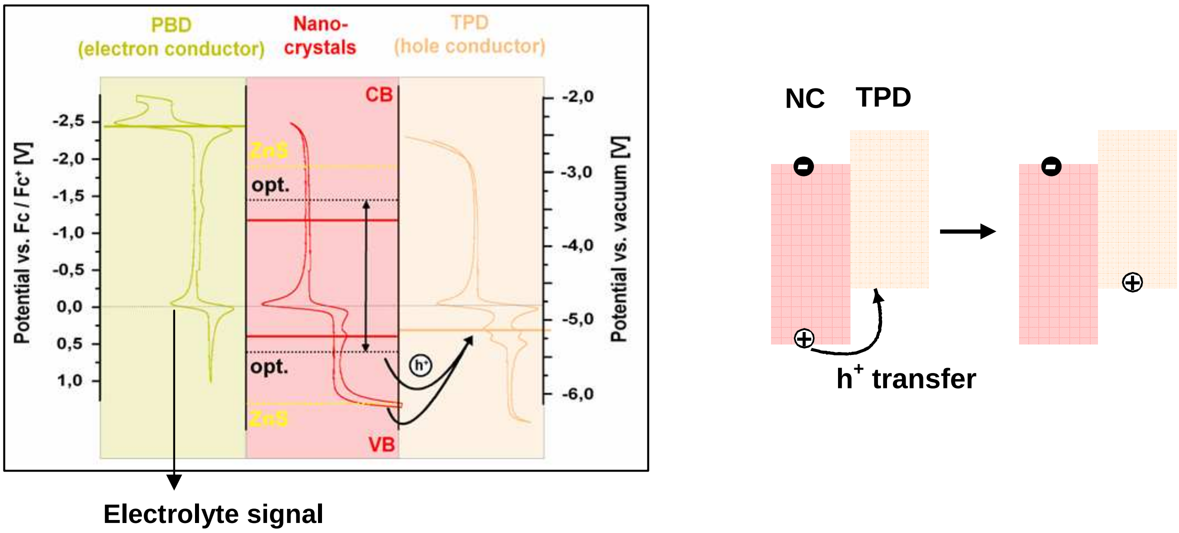

Figure 27: Determination of the energy levels of NCs, TPD and PBD. A: Cyclic voltammograms. The ZnS levels are taken from literature [89]. The optical transition of the NCs is deduced from the absorption line. B: Sketch of the offset between the NCs and the TPD energy levels.

The results shown in figure 26 and 27 are obtained with sample 2 (see paragraph (a)). In the cyclic voltammograms of figure 27A, peaks above the potential of the electrolyte indicate the reduction potential of the sample while those below indicate the oxidation potential. The red cyclic voltammogram shows the measured oxidation potential of NCs, the optical transition (dashed lines labeled opt.) is derived from their absorption spectrum and the ZnS potentials are taken from the literature [89]. For PBD no oxidation potential (loss of electrons) is detected while no reduction potential (gain of electrons) is detected for TPD. The sketch in figure 27B shows that, the photo-generated hole can migrate to the TPD HOMO rendering the NC core negatively charged. The cyclic voltammograms shown in figure 27 are affected by experimental source of errors inherent to CV measurements: the deposition of samples onto electrodes, the concentration, the electrolyte used and the instrument settings [90].

Several pictures could explain the PL quenching observed in the TPD matrix. A possible energy transfer from the NCs to the TPD is excluded because of the mismatch of their optical properties (TPD absorbs and emits below 500 nm and the NCs emission is at 570 nm). The cyclic voltammograms in figure 27 show that a hole transfer from the TPD to the NCs and an electron transfer from the NCs to the TPD are not favorable (see the energy offsets and the absence of reduction potential on the TPD cyclic voltammogram in figure 27). The remaining possibilities are the migration of the photo-generated hole from the NCs to the TPD or an increase of non-radiative recombination routes due to interaction of TPD molecules with the NCs surface. In the absence of lifetime measurements it is not possible to say which of these two pathways is responsible for the PL quenching.

The quenching of the PL of single NCs observed in TPD matrices fits with previous reports discussed in the first chapter. There is a PL quenching when the concentration of hole conducting material is increased in solution [38]. The quenching of the PL by hole injection or by an increase of hole density in the proximity of NCs is discussed in details in several reports [61, 91].

c. Blinking statistic of NCs in insulating and electron conducting matrices

In paragraph (b), it is shown that single NCs's emission is detectable in the electron conducting PBD. To investigate the effect of electron conducting materials on the kinetics of single NC blinking, a threshold analysis of the time traces is performed. The results obtained in PBD are compared to those obtained in the insulating material zeonex. The importance of such a threshold analysis in the understanding of the blinking of single NCs is explained in detail in the first chapter of this thesis.

Prior to the fluorescence time trace the background of the sample is taken by collecting a time trace of a part of the sample containing no NCs this mean only the matrix. To discriminate ON and OFF levels a threshold value of two to three times the standard deviation above the average background is taken. It is shown in section (I) of this chapter that artifacts inherent to threshold analysis are reduced in this threshold range provided the time trace analyzed has well separated average ON and OFF levels. The histograms of ON and OFF events obtained are analyzed as described in chapter I. The probability densities plotted in double logarithmic scale are fitted with a linear function (figure 28 C and D). It is shown in section (I) of this chapter that this fitting method accurately evaluates the power law dependence of probability densities. The memory coefficients are also calculated for each time trace analyzed.

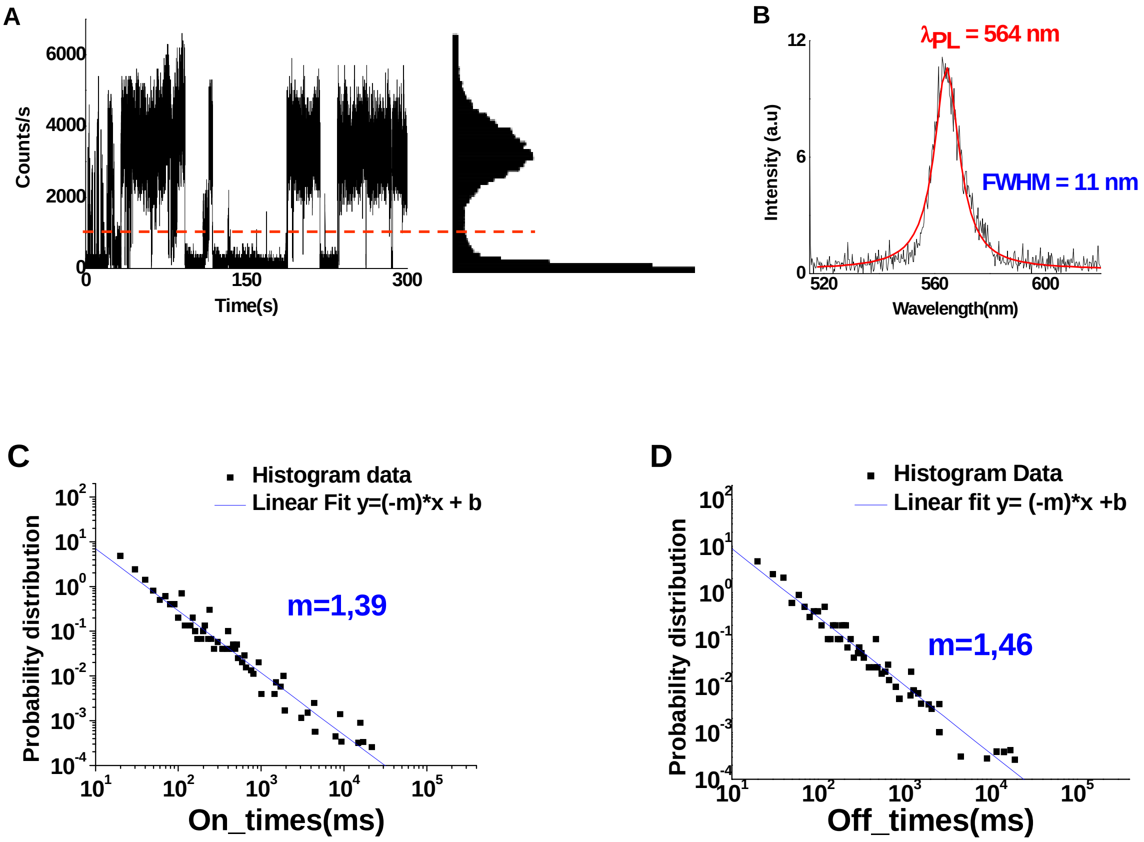

Correlation between consecutive events			
	On / next On	Off / next Off	On / next Off
R	-0.38	0.23	0.08
R_{log}	0.46	0.25	-0.05

Figure 28: Example of results of the time trace analysis. A: Time trace of a single NC. The intensity histogram is shown on the right. The red dashed line is the chosen threshold level. B: Spectrum of the single NC in A. the red curve is a Lorentz fit. C: Probability density of ON times. D: Probability density of OFF times. The blue lines in C and D show the linear fit of the data. The table summarizes the memory coefficients obtained.

Figure 28 shows typical results obtained from the threshold analysis. Only NCs for which the emission spectrum FWHM is below 20 nm and the average ON and OFF levels are well separated are analyzed. In the absence of antibunching data, the spectral broadening is the remaining argument to account that the emitting spot is a single NC. The spectra are fitted with a single Lorentzian line (figure 28 B) to find the emission wavelength and the spectral broadening. 38 times trace of single NCs in zeonex and 42 times traces of single NCs in PBD are analyzed like the one in figure 28.

In order to investigate the relationship between OFF event and ON event kinetics in function of the matrix, scatter plots of OFF times exponents in function of ON time exponents of the same NC are performed.

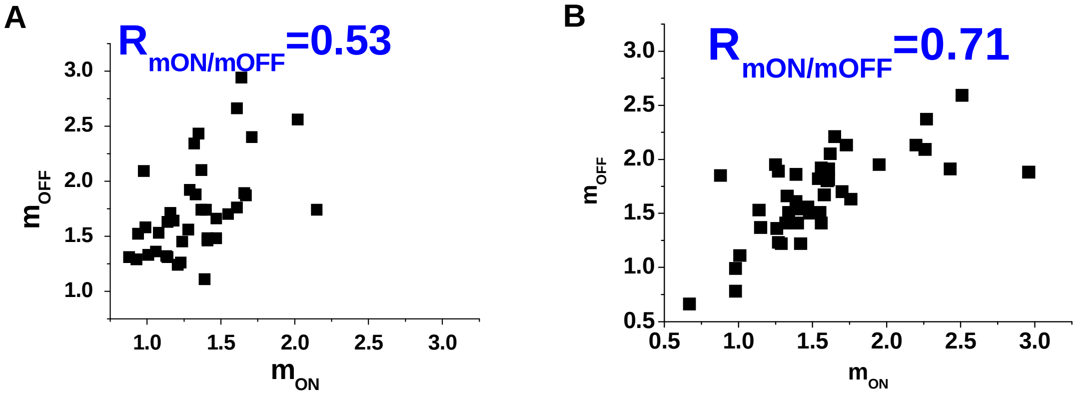

Figure 29: Scatter plots of ON time and OFF time power law exponents. A and B are obtained for zeonex and PBD respectively. The R values indicated are the $R_{mON/mOFF}$ parameters.

In figure 29, the diagonal evolution of the data points show that ON time and OFF time power law exponents of a given NC are correlated. To evaluate the strength of this correlation, a parameter $R_{mON/mOFF}$ is defined and calculated following the linear Pearson correlation coefficient mentioned in the first chapter. The x and y values representing this time the ON time and the OFF time power law exponents of given NCs respectively. $R_{mON/mOFF}$ evaluates the correlation between ON time and OFF time power law exponents of arbitrary chosen NCs.

The results of the threshold analysis obtained for investigated NCs are averaged in function of the matrix and summarized in table 5.

	38 time traces in zeonex		**42 time traces in PBD**	
Parameters	**Mean value/** **Absolute mean value**	**sd**	**Mean value/** **Absolute mean value**	**sd**
m_{ON}	1.34	0.3	1.54	0.5
m_{OFF}	1.74	0.4	1.66	0.4
$R_{ON/ON}$	0.21	0.2	0.17	0.2
$R_{logON/ON}$	0.40	0.1	0.38	0.2
$R_{OFF/OFF}$	0.15/**0.17**	0.2/**0.2**	0.22/**0.22**	0.2/**0.2**
$R_{logOFF/OFF}$	0.33/**0.35**	0.2/**0.2**	0.38/**0.38**	0.2/**0.2**
$R_{ON/OFF}$	0.05/**0.08**	0.2/**0.1**	-0.03/**0.05**	0.1/**0**
$R_{logON/OFF}$	0.06/**0,17**	0.2/**0.1**	-0,18/**0.21**	0.2/**0.1**

Table 5: Summary of the threshold analysis for single NCs in Zeonex and in PBD. m_{ON} and m_{OFF} refer to the ON time and OFF time power law exponents respectively (the exponents used are those obtained by the LN fit method. It will be shown later that they are more accurate than those obtained by the AL fit. The R and R_{log} are the correlation coefficients calculated following formula X. sd is the standard deviation

The memory coefficients can take negative values therefore mean absolute values (in red in table 5) are calculated to avoid misleading average zero values. This is illustrated by the $R_{logON/OFF}$ parameter in zeonex. Because 50% of the NCs show an anti-correlation the memory is hidden during averaging.

The investigations of single NC PL in PBD and zeonex matrices show that the power law exponents are sensitive to the embedding matrix. The ON time exponents are higher in zeonex whereas the OFF time exponents are higher in PBD. The ON time and OFF time exponents of a given NC are correlated independent of the matrix. This suggests that the mechanisms governing the transitions from emitting to dark states and vice versa are similar. In addition, it suggests that these transitions are influenced by the dielectric constant of the matrix. There is a residual memory in the blinking of single NCs. This memory is stronger between adjacent ON events than adjacent OFF events independent of the matrix. The memory between adjacent ON events is stronger in zeonex than in PBD whereas that of adjacent OFF events has an inverse behavior. A few NCs shows an anti-correlation (negative coefficients) between adjacent OFF events in zeonex. Such an anti-correlation is not observed for the NCs in PBD. Between ON and next OFF events, the $R_{ON/OFF}$ parameter is close to zero indicating no correlation between these events at long times independent of the matrix. At short times, the situation is different. Almost 50% of the particles show an anti-correlation in zeonex; therefore the memory is better described by the mean absolute value 0.17. In PBD, most of the NCs investigated show an anti-correlation with a coefficient of -0.18. Finally, in a more general way, the dependence of the memory and power law exponents on the embedding matrix suggests that the blinking kinetics is governed by trapping mechanisms occurring near or close to the surface of the NCs. Any proposed mechanism should therefore account the interactions between the NC's surface and its environment.

The relatively large OFF times exponents observed in PBD compared to zeonex fits with the effect of self trapped charges in dielectric media and the tunneling of the electron to homogeneously distributed traps in the environment of NCs [84, 85]. However this model alone cannot explain the large ON time exponents observed in zeonex. The mechanism should rather introduce the fluctuations of the tunneling barrier as proposed by Kuno et al. [25, 86]. It can be predicted that in the zeonex matrix (polymer film) the conformational changes are higher than in the PBD matrix (small molecules assembly). The faster conformational changes in zeonex increase the rate of the variation of the tunneling barrier. This increases the possibility for a back tunneling of the trapped electron from the trap to the NC. In PBD this back tunneling is slower by the stabilization energy of the dielectric leading to an increase of the OFF time power law exponents. This argument is further supported by the strong correlation between ON time and OFF time power law exponents in PBD and the variation of the memory coefficients with the matrix. The ON to OFF transitions are dominated by the conformational changes (fluctuation of the tunneling barrier) whereas the OFF to ON transitions are affected by the dielectric constant of the environment. In PBD the fluctuation rates of the tunneling barrier are slower whereas the stabilization of the trap charge is higher.

Since the first reports of the blinking, several models summarized in the first chapter have been proposed. Despite the apparent accuracy of the calculations presented, several experimental observations could not be explained. It is not the aim of this discussion to state a model. However, it is the first time that the power law kinetics and the memory of identical particles are investigated in the same studies. Although the exact picture describing the blinking has to be refined, these results account for a model close to the tunneling pictures described in the first chapter. The breakdown of the power law usually presented to rule out these pictures is discussed in the section (I) of this chapter as a result of randomly varying intermediate ON states.

d. Photoluminescence of single NCs in sandwiched PBD samples

Even though the results shown in paragraph (c) indicate a difference of blinking behavior in different matrices, the effect of the surrounding atmosphere is not taken into account [80]. When the NC/matrix samples are deposited on substrates as described in chapter II, there is no possibility to tell with precision the location of the NCs in the film. Some may be on top of the film as reported in the literature [92]. Furthermore for nanomanipulation experiments (see section III of this chapter), a possible physical contact between the metallic tip and single NCs may damage the samples. “Sandwiched” PBD samples are prepared as described in chapter II to ensure the embedment of NCs in the PBD film.

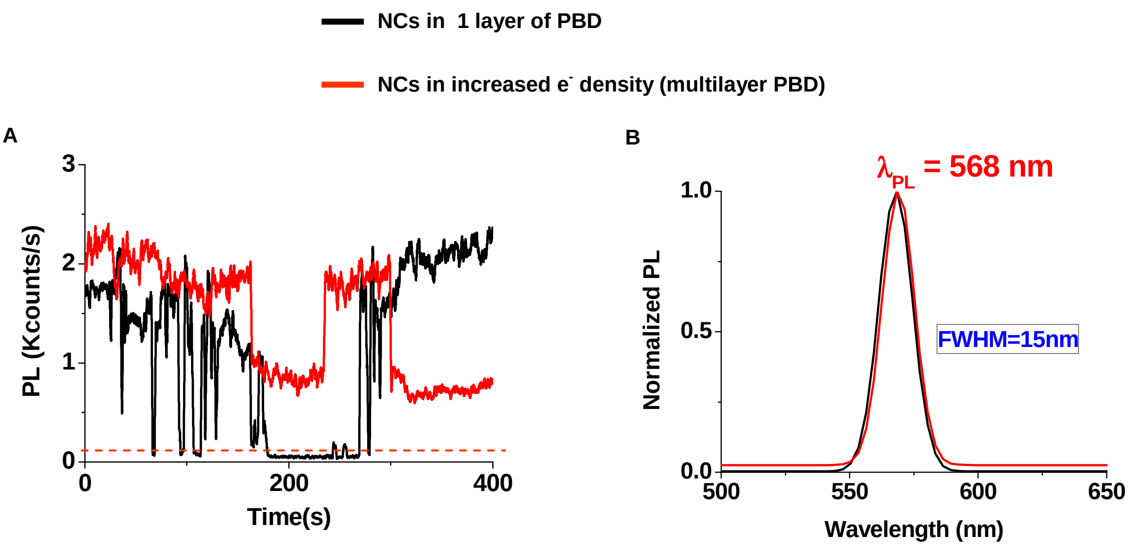

Figure 30: Fluorescence of single NCs in sandwich PBD layers. A: Comparison of the fluorescence of a single NC in one layer of PBD and in sandwich PBD layers. The red dashed line shows the background level. B: Comparison of the spectrum of the NC in A.

Figure 30 shows the flickering of fluorescence of a single NC in sandwiched PBD samples (red curve). The fluorescence time trace (figure 30A) and the spectrum (figure 30B) of this NC are compared with the one of a single NC in one layer (black curves) PBD samples. When NCs are embedded in sandwich PBD layers, the blinking is suppressed. The two samples shown in figure 30 are imaged with the same conditions, their emission intensity is similar (about 2000 counts/s) and their spectra are less than 20 nm FWHM. In the absence of anti-bunching data, these requirements are necessary to account that the signal observed in sandwiched PBD samples does not originate from small aggregates. In one layer of PBD, the PL changes between ON and OFF states whereas the red time trace show that in sandwiched PBD, the PL flickers between high emitting and low emitting states. The same experiment was repeated on 50 NCs in sandwiched PBD, 15 NCs in sandwiched zeonex. In one layer of PBD, one layer of zeonex or sandwiched zeonex samples all investigated NCs blinked. In sandwiched PBD samples, among the 50 investigated NCs only three blinked. The percentage of OFF events for those three NCs is less than 7%.

The absence of blinking suppression in sandwiched zeonex samples suggests that the coverage of the surface is not the main reason explaining these observations. The interactions between the electron conducting PBD and the NCs' surface are probably playing an important role in this blinking suppression. The particular effect of electron conductors on the fluorescence of single NCs is reported in solutions. It is shown that the increased of the concentration of electron donating materials nearly suppress the blinking of single NCs in solution [37, 75]. The mechanism proposed to explain this blinking suppression is the passivation of electron traps at the surface of NCs. A similar mechanism is proposed in this thesis. As already suggested in part (b) of this section, the electron lone pairs localized in the oxadiazole hetero-atoms cycle passivate electron traps at the surface of NCs. The efficiency of this passivation is increased in sandwiched PBD samples. In single PBD samples there is no knowledge of the position of the NCs investigated in the matrix. The particle may be close to the surface of the matrix film and therefore still interacting with the environment. The AFM investigations of the film thickness shown in chapter II show an increase of the layer thickness from single to sandwiched PBD layers. This suggests that NCs are completely covered by the electron conducting PBD in sandwiched samples. Their fluorescence is therefore mainly influenced by the properties of the material.

III. Nanomanipulation of NCs in electron conducting materials

1. Electroluminescence (EL) of NCs/PBD films

In this experiment, NCs are diluted in a solution of PBD and spin coated on clean ITO substrates. The fraction NC/PBD is chosen so that no single NCs are detected and rather a uniform emitting layer is seen on the PL image. The ITO substrate and the flattened aluminized tips are connected as shown in figure 31A. The laser is turned OFF and a voltage ramp is applied between the substrate and the tip. The EL signal is recorded on the APD of the confocal microscope.

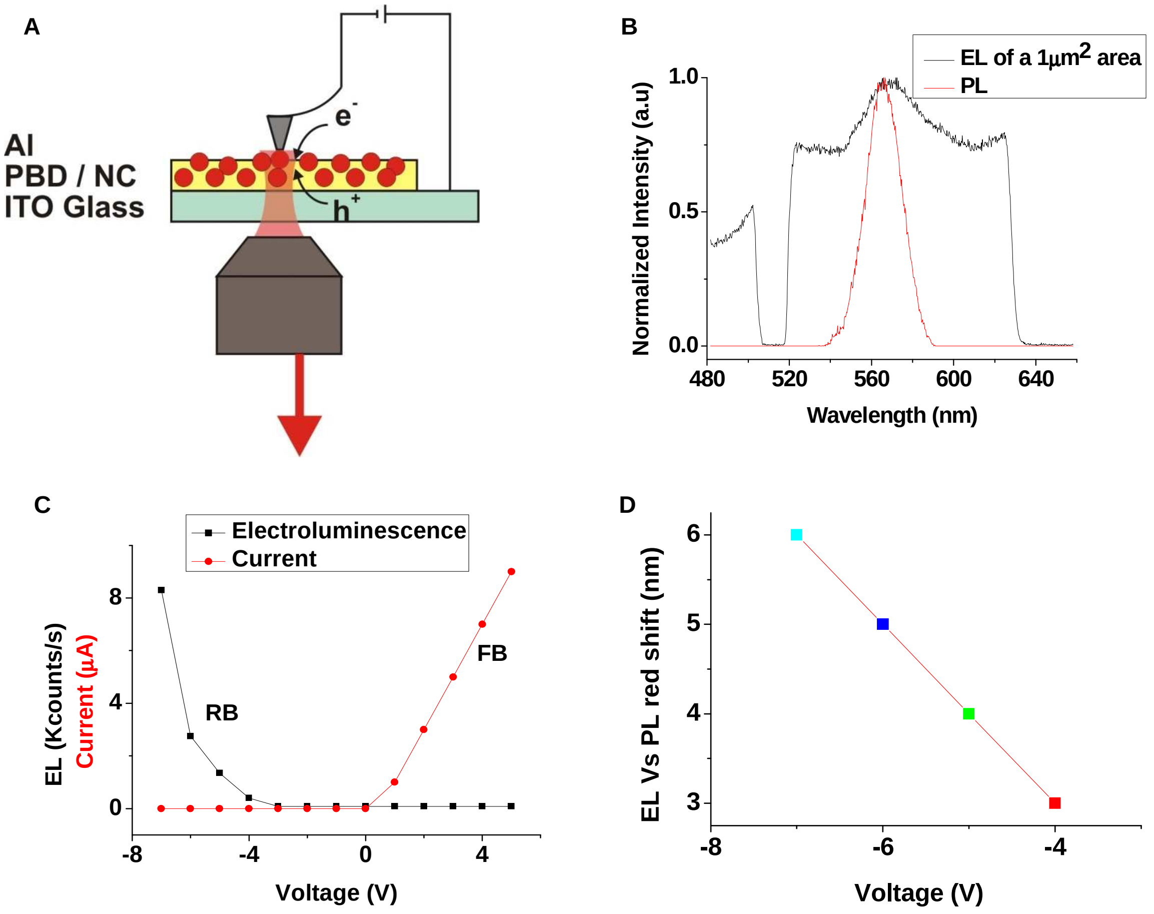

Figure 31: Electroluminescence (EL) of 1 μm^2 areas from NCs/PBD blends. A: Sketch of the setup. B: Comparison of the EL signal and PL signal. C: Variation of the EL and the PL with the applied bias (FB: forward bias, RB: reverse bias). D: Increase of the EL red shifts with the applied bias.

Figure 31 shows an example of EL experiment. The EL and the PL signal are shown in black and red respectively in Figure 31B. A high background originating probably from the PBD is also detected. Figure 31C shows that the EL signal and the current flow occur in opposite directions. There is a red shift of the EL signal increasing with the applied bias as shown in figure 31D. In similar experiments with only PBD or NCs films no electroluminescence could be detected. Figure 32 is proposed to explain the electroluminescence results shown in figure 31.

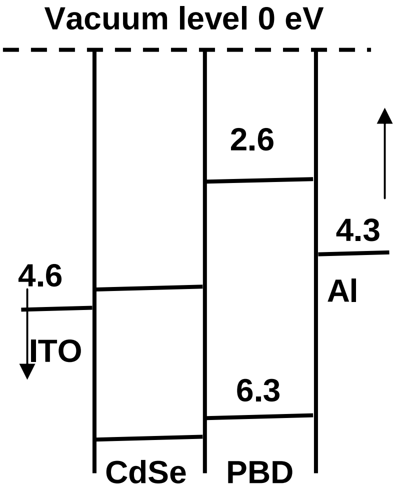

Figure 32: Relative band offset of NCs and PBD. The arrows indicate the forward bias.

The relative band offsets of PBD shown in figure 32 are taken from the CV results shown in figure 27 and from the literature [89]. There is no knowledge of the relative spatial arrangement of PBD and NCs in our structures. The NCs/PBD films prepared are uniformly fluorescing. Therefore both NCs and PBD are in contact with the ITO substrate and the Al tip.

When the ITO substrate is positively biased compared to the Al tip (forward bias), electrons are injected in the PBD and holes in the NCs. PBD is known to be a good electron conductor and a poor hole transporter therefore the hole injected into NC are trapped inside the PBD. The absence of an electroluminescence signal suggests that the recombination of the electron hole pair occur close to the Al tip where the quenching happens. A similar situation is discussed in the literature [93-95]. It is difficult to explain the electroluminescence observed at reverse bias when the ITO substrate is negatively biased compared to ITO substrate. A possible mechanism could account that at 4 V, electrons tunnel in NCs and holes in PBD. Most of the holes are trapped inside the PBD layer and electrons build up a negative charge at the interface between NCs and PBD due to the band offset shown in figure 32. The EL signal shown in figure 31B suggests that electrons and holes recombine at this interface. Several mechanisms are discussed in the literature to explain the dependence of the red shift of the EL compared to the PL shown in figure 31 (B, D). One of the most plausible is the increase of local heating due to the poor conductivity at the NCs/PBD interface [89].

Although more investigations are needed to understand the exact mechanism of the electroluminescence observed, this experiment is a proof of principle that the experimental setup used in this project can be used to study electroluminescence of area as small as 1 μm^2. Further investigations on diluted samples could allow the detection of electroluminescence of single NCs.

2. Charging of isolated CdSe NC embedded in PBD matrix

For charging experiment, NCs are embedded in PBD matrices prepared as described in chapter II. Experiments are made with one layer and sandwiched PBD samples. Flattened aluminized tips are used to ease the tip-NC alignement as explained in the second chapter.

The experiment starts with the localization of the tip by the confocal microscope (figure 33 B). Then a fluorescence image of an area in the proximity of the tip is acquired (figure 33 C). When this area contains single NCs, they are characterized (spectrum and time traces are acquired) in the absence of the tip influence. The tip is then moved to a desired NC while a new fluorescence time trace is being acquired (figure 33 E and F).

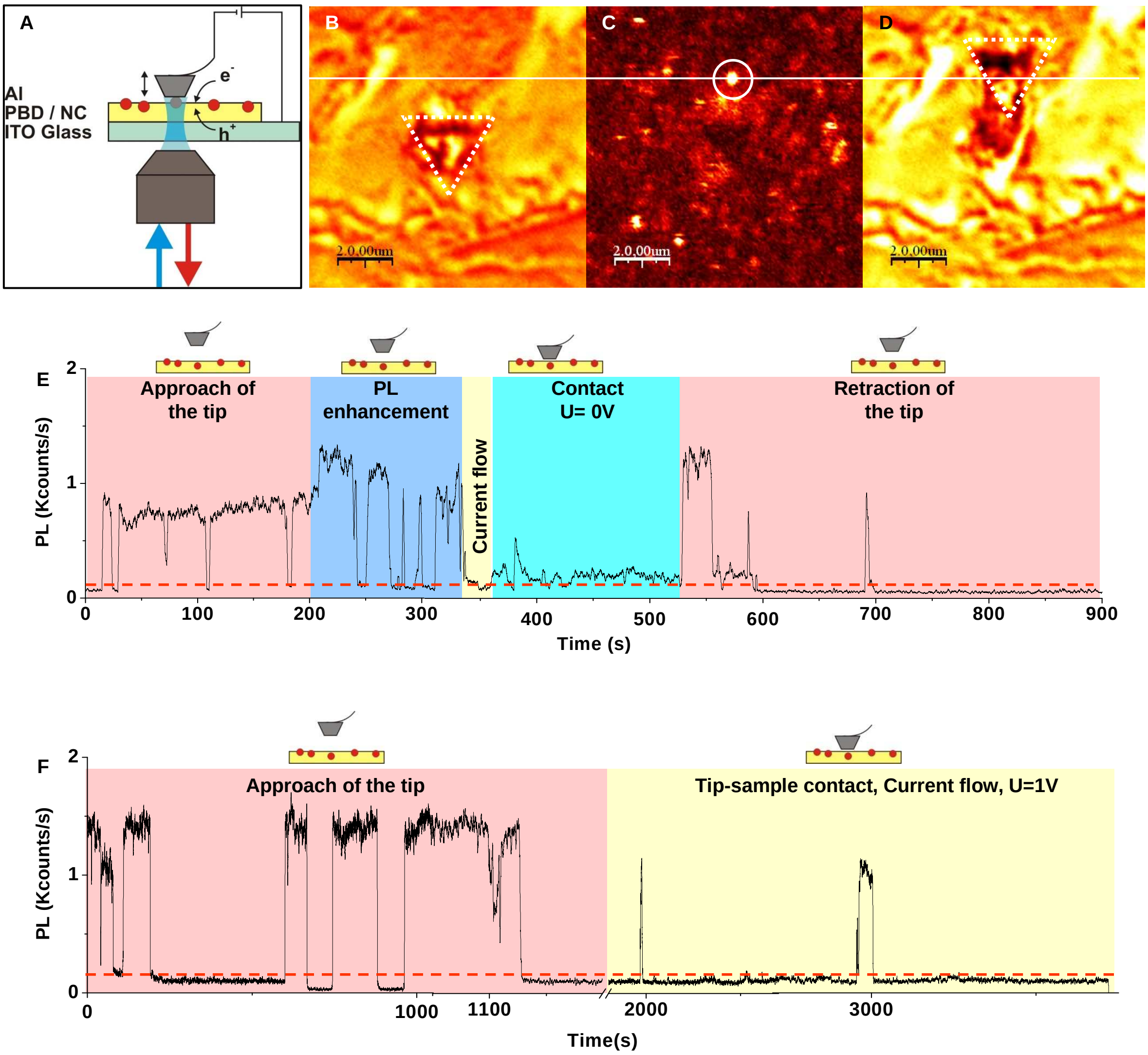

Figure 33: Description of the single NCs charging experiment. A: Sketch of the setup. B: Reflection of the tip marked in the white triangle. C: Fluorescence image. The circled point is where the time trace is collected. D: Reflection of the tip after the manipulation. E and F: Examples of time trace acquired during the nanomanipulation. Sketches of the tip-sample relative position are given as guide to eye. The red dashed lines in the time traces indicate the background level.

Different colors codes are used in the time traces shown in figure 33 to highlight the different effect observed. The dashed red line in the time traces shows the background level. The time traces shown are from to different NCs. Before the influence of the tip, the NCs emit intermittently (marked pink) as expected with properties described at the beginning of this chapter. While the tip is approaching the NCs, there is a PL enhancement of 40% the maximal intensity (marked blue). When the tip approach is performed in presence of a 1 V DC voltage no current is observed indicating the absence of contact between the tip and the sample. When the tip enters in contact with the sample (marked yellow), a current flow starts and the PL is quenched. The magnitude of the quenching and of the current depends on the strength of the tip-sample contact. In the time trace of figure 33E, the PL clearly goes below the background level. A longer observation on another NC shown in figure 33F, shows that the NC is not bleached but still emits with a lower maximal intensity and a noticeable reduction of emitting times during the current flow. When the voltage is stopped a low PL recovery is observed (marked green). The magnitude of the recovery increases when the tip is completely removed from the proximity of the NC. The reduction of ON intensities shown in the last part of the time trace of figure 33E indicates that although the tip is removed the quality of the NC was affected during the nanomanipulation experiment. The majority of NCs investigated did not survive the tip approach. The reason is the lack of control of the z-direction of the nanopositioner. The physical destruction of NCs during the approach is illustrated in figure 34

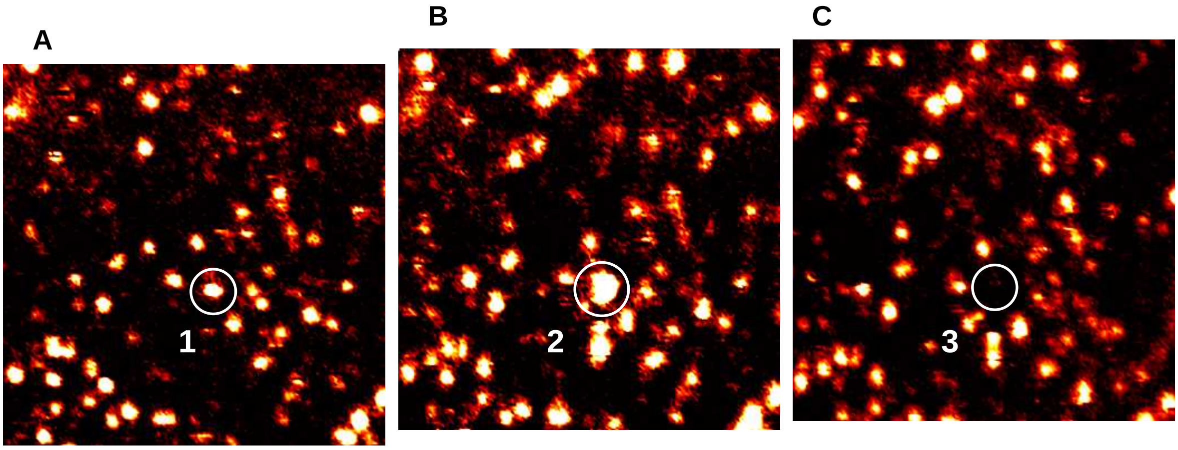

Figure 34: Enhancement and bleaching of the PL of single NCs by a metallic tip. A, B and C are consecutive images of the same area. The images are shifted for clarity. The circled part show the NC on which the tip is landed.

The three pictures in figure 34 are consecutive PL images of the same area. The images are shifted to correct experimental drifts that occurred during these measurements. The emission of the NCs circled in figure 34 A is enhanced due to the presence of the tip in figure 34 B. The NC is completely bleached by further approaching the tip in figure 34 C. It has been mentioned in the second chapter that the steps of the nanopositioner are 30 nm and the film thickness is 50 nm. Therefore when the tip is close to the surface a single step is sufficient to dig into the matrix film resulting in a possible physical alteration of NCs. The evidence of the matrix digging is seen on the images of figure 33 (C, D). The first position of the tip (figure 33B) can be seen on the following images (figure 33 C and D).

The sandwiched PBD samples (figure 35 A and B) are prepared to reduce the risk of physical contact between the tip and NCs. It has been shown in section (II) of this chapter that the fluorescence behavior of single NCs in these sandwiched samples is modified. The majority of NCs flickers without blinking.

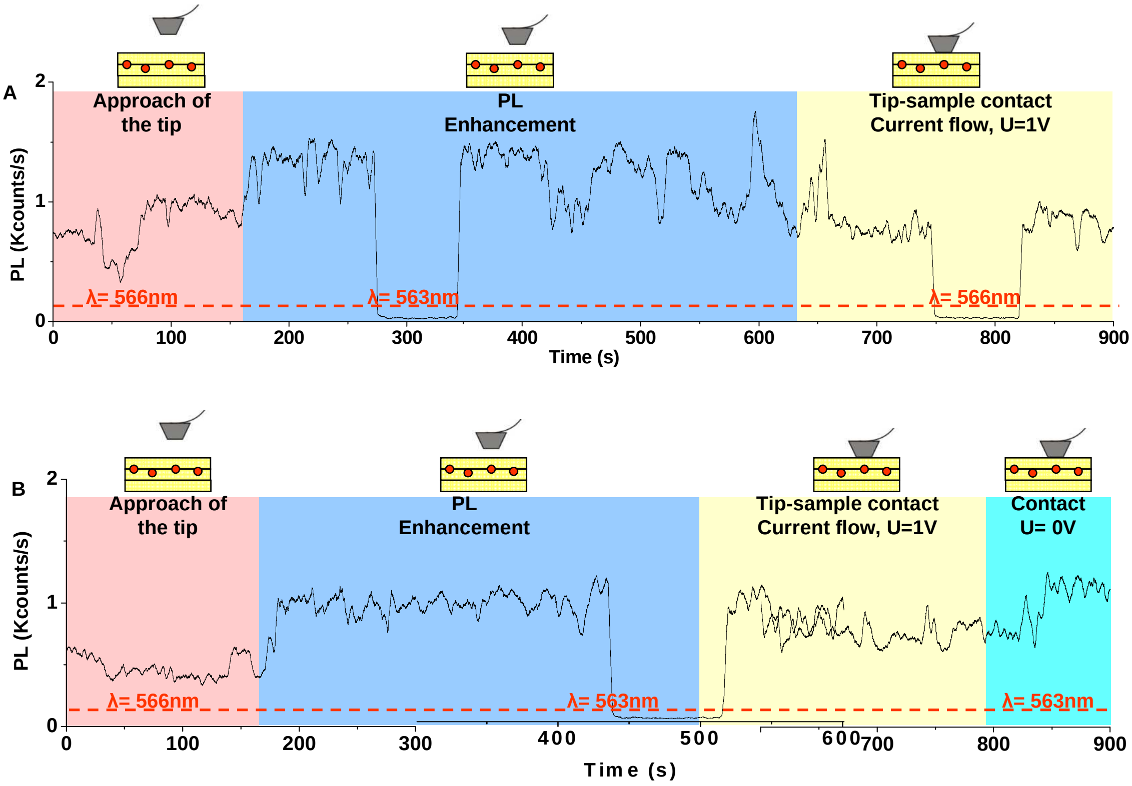

Figure 35: Nanomanipulation of single NCs in sandwiched PBD samples. A and B are taken on different single NCs. Different color codes are used to indicate changes in the PL. Sketches of the tip-sample relative position are given as guide to eye. The red dashed lines in the time traces indicate the background level. The emission spectra are acquired where the time traces are truncated.

In the example shown in figure 35, observation similar to those of figure 33 are made. There is a PL enhancement prior to the tip-sample contact. The magnitude of the enhancement is about 40% the initial PL intensity in the absence of the tip. When the tip-sample contact occurs in the presence of the voltage there is a PL quenching. The magnitude of the quenching is in this case also not uniform and varies between the experiments. In figure 35 C evidence of a PL recovery is shown, when the voltage is stopped and the tip is kept into contact with the sample (marked green). The stability of the NCs in sandwiched PBD samples allows the investigation of spectral changes during the nanomanipulation. The truncated parts of the time traces of figure 35 indicate the acquisition of spectra. There is a blue shift when the PL is enhanced and a red shift when it is quenched by the flow of current. Figure 35 B shows that the spectrum when the PL recovers while the tip is still in contact with the sample in the absence of voltage, is blue shifted in respected to the initial emission wavelength (in the absence of the tip influence). A control experiment on a NCs/PBD film (ensemble) is made to check the contribution of voltage and current flow in the observation reported above. This experiment could not be done with diluted sample with single NCs fluorescence because in this case a voltage is necessary to control the tip-sample contact.

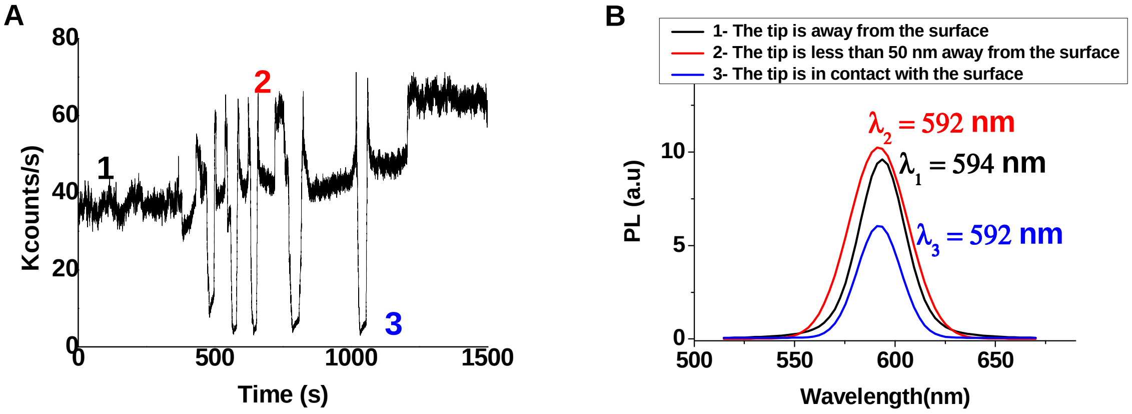

Figure 36: Enhancement and quenching of the PL by a non-biased metallic tip. A: Time trace of NCs/PBD film emission. B: Spectrum changes during the nanomanipulation.

Figure 36 shows an example of nanomanipulation on a NCs/PBD film without any voltage. Position 1 indicates the emission of the film in the absence of the tip. When the tip is close to the surface, there is a PL enhancement followed by a PL quenching when the tip is further pressed on the surface. Figure 36 A shows that the process is reversible indicating that minor destruction of the emitting film occurs. For each positions of figure 36 A, the experiment is repeated for the acquisition of spectral changes. Figure 36 B shows that there is a blue shift at the enhancement position (λ_2) which is kept at the quenching position (λ_3).

To understand the observations made during the nanomanipulation experiments, it is necessary to accounts previous reports on the effects of metallic surfaces in the proximity of single emitters. [96-100]. When an aluminized tip is placed close to a single NC, destructive and constructive interference of light with the tip acting as a mirror can be observed. Near field enhancement of the fluorescence and modification of radiative and non-radiative rates can occur. Mirror effects probably explain the reversible change of fluorescence shown in figure 36 when the tip is landed on an emitting NCS/PBD film. A clear understanding of the mechanism behind our observations implies an accurate control of the z-direction of the nanopositioner.

In the charging experiments on single NCs, there is a superposition of the general tip (mirror, near filed,…) effects mentioned above and the charging effects that are of interest in this work. There is a quenching due to the tip presence (mirror or near field effects), an irreversible quenching (sample destruction) and a quenching related to the electric current (charging effect). The PL recovery when the voltage is stopped (marked in green in figures 33E and 35B) is the evidence of a quenching due to charging. This recovery is low in single layer PBD samples probably because of the superposition of mechanical interactions between the tip and the NCs. The blue shift of the PL in figure 33 and 35 correlated to the recovery after charging can be explained by is accompanied by detrapping/trapping of charges at the surface of the NC or by the local cooling/heating occurring when the current stop/start to flow.

The major difficulty in the nanomanipulation experiment is the accurate control of the z-direction of the nanopositioner. A more elaborated experimental setup is currently being optimized. It consist of a close loop AFM (*Nanowizard, JPK*

Instruments) which correct thermal drifts, offer the possibility to biased the tip and improve the current detection sensitivity up to picoamperes resolution.

Summary and Conclusion

The aim of this thesis was the investigation of the blinking of single semiconductor nanocrystals. In the first chapter the difficulties in finding a common explanation for the blinking process are classified into three main parts: the controversies on the quantification of the blinking, on the physical reasons and on the theoretical model of the blinking. The threshold analysis method used to obtain the power law kinetics and a memory of the blinking of single semiconductor nanocrystals is described. The implications of the existence or the absence of truncated power law kinetics of ON events and the meaning of a memory are commented on the basis of the reports of Kuno et al.[24, 25], Shimizu et al. [26] and Stefani et al. [27]. Several experiments conducted to influence the fluorescence of single nanocrystals and understand the physical reasons behind the blinking are reviewed from the literature. It is shown that the “charging and blinking” picture is more complex than proposed in early times of the observation of the blinking of single NCs. Current pictures take into account the sign and the position of the charge and the interactions of NCs’ surface with the environment. At the end of the first chapter two main theoretical models proposed to explain the blinking are discussed. It is shown that despite of the accuracy of calculations made in these models, both fail to explain the controversies of the quantification and of the experimental manifestations of the blinking.

The synthesis of nanocrystals, the sample preparation and the experimental setup are described in the second chapter. Core shell CdSe/CdS/CdZnS/ZnS nanocrystals used in this work are synthesized using established methods. The preparation of NCs/matrix films and their characterization by AFM are described in the second section of the chapter. The experimental setup consisting of a laser scanning microscope on top of which an AFM or a nanopositioner are mounted is summarized. An original inexpensive procedure to flatten used AFM tips necessary to ease the nanomanipulation of single NCs is shown. It is shown that the flattening is a result of a heat assisted breakage.

The experimental results presented and discussed in the third chapter of the thesis start with the investigation of artifacts of threshold analysis. It is shown that the variation of the blinking statistic results with the chosen threshold are mainly due to intermediate ON levels in time traces of the fluorescence of single NCs. It follows that these low ON levels are also responsible for the truncation of the power law at long times reported in the literature [26]. In the second part of the chapter it is shown that electron and hole conducting materials differently interact with NCs. The PL of NCs is quenched in hole conducting material films whereas single NC emission is observed in electron conducting material films. Cyclic voltammetry experiments suggest that the quenching is due to a transfer of the photo-generated hole to the hole conducting materials. The blinking statistic of 38 single NCs in insulating material and 42 in electron conducting material shows that the is a power law exponents of OFF events and ON events are correlated. The strength of this correlation measured by linear correlation coefficients shows that this correlation is stronger in PBD than zeonex. The memory of the blinking shows also a dependence on the matrix. It is however suggested to take into accounts the artifacts inherent to threshold analysis and the high standard deviation of results shown in the investigation of the matrix's dependence. It is proposed to analyze the blinking with methods independent of the threshold separation between ON and OFF events. The results of the nanomanipulation are shown at the end of the chapter. It is shown that the experimental setup allows the detection of electroluminescence of areas of NCs/PBD films smaller than 1 µm^2. The mechanism of the electroluminescence is proposed to originate form a tunneling of charges in the films followed by a build up of electric field at the NCs-PBD interface. The attempt to charge single nanocrystals was difficult because of the lack of control of the last step of the nanopositioner. Examples of charging experiments are shown but no quantitative analysis is made because most of the single NCs investigated did not survive the experiment. In conclusions the findings reported in this thesis suggest the following:

- Intermediate ON levels are responsible of the artifacts of the threshold analysis and of the truncation of the power law. Temperature and experimental conditions as well as the complex interactions at the surface of NCs change the fluorescence intensity and explain variable truncation points observed for power law observed at truncation points. The truncation is therefore not necessary an information of the blinking kinetics but a measure of the fraction of intermediate ON states at the chosen threshold.
- The ON time and the OFF time power law exponents are correlated and there is a memory between consecutive ON, consecutive OFF and from ON to OFF events. This memory seems to depend on the matrix however the inaccuracy of threshold analysis suggests the necessity of a complementary analysis method to check this dependence. These results suggest that the blinking occurs near or at the surface of NCs. The mechanism is not clear however it should account fluctuations of tunneling barriers of traps states but this need to be refined to explain the correlation between the power law exponents and the memory observed.
- Electroluminescence of area as small as 1 μm^2 of simply spin coated NCs/PBD films can be measured with the home built experimental setup of this project. There is a great hope that the current improvement made by

using a close loop AFM will overcome the limits of the nanpositioner and allow the simultaneous investigation of charging and blinking of single NCs.

Literature

1. Henglein, A., *Photo-Degradation and Fluorescence of Colloidal-Cadmium Sulfide in Aqueous-Solution.* Berichte Der Bunsen-Gesellschaft-Physical Chemistry Chemical Physics, 1982. **86**(4): p. 301-305.
2. Rossetti, R. and L. Brus, *Electron-Hole Recombination Emission as a Probe of Surface-Chemistry in Aqueous Cds Colloids.* Journal of Physical Chemistry, 1982. **86**(23): p. 4470-4472.
3. Steigerwald, M.L. and L.E. Brus, *Synthesis, Stabilization, and Electronic-Structure of Quantum Semiconductor Nanoclusters.* Annual Review of Materials Science, 1989. **19**: p. 471-495.
4. Murray, C.B. and M.G. Bawendi, *Synthesis and Physical Characterization of Ii-Vi-Semiconductor Nanocrystallites (Quantum Dots).* Abstracts of Papers of the American Chemical Society, 1993. **205**: p. 136-PHYS.
5. Gaponik, N., et al., *Thiol-capping of CdTe nanocrystals: An alternative to organometallic synthetic routes.* Journal of Physical Chemistry B, 2002. **106**(29): p. 7177-7185.
6. Harrison, M.T., et al., *Wet chemical synthesis of highly luminescent HgTe/CdS core/shell nanocrystals.* Advanced Materials, 2000. **12**(2): p. 123-125.
7. Mekis, I., et al., *One-pot synthesis of highly luminescent CdSe/CdS core-shell nanocrystals via organometallic and "greener" chemical approaches.* Journal of Physical Chemistry B, 2003. **107**(30): p. 7454-7462.
8. Rogach, A.L., et al., *Thiol-stabilized CdSe and CdTe nanocrystals in the size quantization regime: Synthesis, optical and structural properties.* Macromolecular Symposia, 1998. **136**: p. 87-89.
9. Rogach, A.L., et al., *Colloidally prepared CdHgTe and HgTe quantum dots with strong near-infrared luminescence.* Physica Status Solidi B-Basic Research, 2001. **224**(1): p. 153-158.
10. Rogach, A.L., et al., *Synthesis and characterization of a size series of extremely small thiol-stabilized CdSe nanocrystals.* Journal of Physical Chemistry B, 1999. **103**(16): p. 3065-3069.
11. Talapin, D.V., et al., *A novel organometallic synthesis of highly luminescent CdTe nanocrystals.* Journal of Physical Chemistry B, 2001. **105**(12): p. 2260-2263.
12. Talapin, D.V., et al., *CdSe/CdS/ZnS and CdSe/ZnSe/ZnS core-shell-shell nanocrystals.* Journal of Physical Chemistry B, 2004. **108**(49): p. 18826-18831.
13. Talapin, D.V., et al., *Highly luminescent monodisperse CdSe and CdSe/ZnS nanocrystals synthesized in a hexadecylamine-trioctylphosphine oxide-trioctylphospine mixture.* Nano Letters, 2001. **1**(4): p. 207-211.
14. Talapin, D.V., et al., *Synthesis and surface modification of amino-stabilized CdSe, CdTe and InP nanocrystals.* Colloids and Surfaces a-Physicochemical and Engineering Aspects, 2002. **202**(2-3): p. 145-154.
15. Talapin, D.V., et al., *A new approach to crystallization of CdSe nanoparticles into ordered three-dimensional superlattices.* Advanced Materials, 2001. **13**(24): p. 1868-1871.
16. Xie, R.G., et al., *Synthesis and characterization of highly luminescent CdSe-Core CdS/Zn0.5Cd0.5S/ZnS multishell nanocrystals.* Journal of the American Chemical Society, 2005. **127**(20): p. 7480-7488.
17. Empedocles, S.A., D.J. Norris, and M.G. Bawendi, *Photoluminescence spectroscopy of single CdSe nanocrystallite quantum dots.* Physical Review Letters, 1996. **77**(18): p. 3873-3876.
18. Nirmal, M., et al., *Fluorescence intermittency in single cadmium selenide nanocrystals.* Nature, 1996. **383**(6603): p. 802-804.
19. Tittel, J., et al., *Fluorescence spectroscopy on single CdS nanocrystals.* Journal of Physical Chemistry B, 1997. **101**(16): p. 3013-3016.
20. Nagourney, W., J. Sandberg, and H. Dehmelt, *Observation of Quantum Jumps in a Single Barium Ion.* Journal of the Optical Society of America B-Optical Physics, 1986. **3**(8): p. 252-253.
21. Yip, W.T., et al., *Classifying the photophysical dynamics of single- and multiple-chromophoric molecules by single molecule spectroscopy.* Journal of Physical Chemistry A, 1998. **102**(39): p. 7564-7575.
22. Chepic, D.I., et al., *Auger Ionization of Semiconductor Quantum Drops in a Glass Matrix.* Journal of Luminescence, 1990. **47**(3): p. 113-127.
23. Efros, A.L. and M. Rosen, *Random telegraph signal in the photoluminescence intensity of a single quantum dot.* Physical Review Letters, 1997. **78**(6): p. 1110-1113.

24. Kuno, M., et al., *Nonexponential "blinking" kinetics of single CdSe quantum dots: A universal power law behavior.* Journal of Chemical Physics, 2000. **112**(7): p. 3117-3120.
25. Kuno, M., et al., *"On"/"off" fluorescence intermittency of single semiconductor quantum dots.* Journal of Chemical Physics, 2001. **115**(2): p. 1028-1040.
26. Shimizu, K.T., et al., *Blinking statistics in single semiconductor nanocrystal quantum dots.* Physical Review B, 2001. **6320**(20): artn. 205316
27. Stefani, F.D., et al., *Memory in quantum-dot photoluminescence blinking.* New Journal of Physics, 2005. **7**: article number 197.
28. Frantsuzov, P., et al., *Universal emission intermittency in quantum dots, nanorods and nanowires.* Nature Physics, 2008. **4**(7): p. 519-522.
29. Stefani, F.D., J.P. Hoogenboom, and E. Barkai, *Beyond quantum jumps: Blinking nanoscale light emitters.* Physics Today, 2009. **62**(2): p. 34-39.
30. Lee, S.F. and M.A. Osborne, *Brightening, Blinking, Bluing and Bleaching in the Life of a Quantum Dot: Friend or Foe?* Chemphyschem, 2009. **10**(13): p. 2174-2191.
31. Gomez, D.E., et al., *Blinking and surface chemistry of single CdSe nanocrystals.* Small, 2006. **2**(2): p. 204-208.
32. Li, S., M.L. Steigerwald, and L.E. Brus, *Surface States in the Photoionization of High-Quality CdSe Core/Shell Nanocrystals.* Acs Nano, 2009. **3**(5): p. 1267-1273.
33. Cherniavskaya, O., L.W. Chen, and L. Brus, *Imaging the photoionization of individual CdSe/CdS core-shell nanocrystals on n- and p-type silicon substrates with thin oxides.* Journal of Physical Chemistry B, 2004. **108**(16): p. 4946-4961.
34. Cherniavskaya, O., et al., *Photoionization of individual CdSe/CdS core/shell nanocrystals on silicon with 2-nm oxide depends on surface band bending.* Nano Letters, 2003. **3**(4): p. 497-501.
35. Krauss, T.D., S. O'Brien, and L.E. Brus, *Charge and photoionization properties of single semiconductor nanocrystals.* Journal of Physical Chemistry B, 2001. **105**(9): p. 1725-1733.
36. Krauss, T.D. and L.E. Brus, *Charge, polarizability, and photoionization of single semiconductor nanocrystals.* Physical Review Letters, 1999. **83**(23): p. 4840-4843.
37. Antelman, J., et al., *Suppression of Quantum Dot Blinking in DTT-Doped Polymer Films.* Journal of Physical Chemistry C, 2009. **113**(27): p. 11541-11545.
38. Zhang, Y.L., et al., *Photoluminescence Quenching of CdSe Core/Shell Quantum Dots by Hole Transporting Materials.* Journal of Physical Chemistry C, 2009. **113**(5): p. 1886-1890.
39. Chen, Y., et al., *"Giant" multishell CdSe nanocrystal quantum dots with suppressed blinking.* Journal of the American Chemical Society, 2008. **130**(15): p. 5026-5027.
40. Mahler, B., et al., *Towards non-blinking colloidal quantum dots.* Nature Materials, 2008. **7**(8): p. 659-664.
41. Frantsuzov, P.A., S. Volkan-Kacso, and B. Janko, *Model of Fluorescence Intermittency of Single Colloidal Semiconductor Quantum Dots Using Multiple Recombination Centers.* Physical Review Letters, 2009. **103**(20): artn.207402
42. Zhao, J., et al., *Challenge to the Charging Model of Semiconductor-Nanocrystal Fluorescence Intermittency from Off-State Quantum Yields and Multiexciton Blinking.* Physical Review Letters, 2010. **104**(15): p. -.
43. Brus, L.E., *A Simple-Model for the Ionization-Potential, Electron-Affinity, and Aqueous Redox Potentials of Small Semiconductor Crystallites.* Journal of Chemical Physics, 1983. **79**(11): p. 5566-5571.
44. Efros, A.L. and M. Rosen, *The electronic structure of semiconductor nanocrystals.* Annual Review of Materials Science, 2000. **30**: p. 475-521.
45. Efros, A.L. and A.L. Efros, *Interband Absorption of Light in a Semiconductor Sphere.* Soviet Physics Semiconductors-Ussr, 1982. **16**(7): p. 772-775.
46. Yoffe, A.D., *Low-dimensional systems: quantum size effects and electronic properties of semiconductor microcrystallites (zero-dimensional systems) and some quasi-two-dimensional systems.* Advances in Physics, 2002. **51**(2): p. 799-890.
47. Yoffe, A.D., *Semiconductor quantum dots and related systems: electronic, optical, luminescence and related properties of low dimensional systems.* Advances in Physics, 2001. **50**(1): p. 1-208.
48. Yoffe, A.D., *Low-Dimensional Systems - Quantum-Size Effects and Electronic-Properties of Semiconductor Microcrystallites (Zero-Dimensional Systems) and Some Quasi-2-Dimensional Systems.* Advances in Physics, 1993. **42**(2): p. 173-266.
49. Yaghini, E., A.M. Seifalian, and A.J. MacRobert, *Quantum dots and their potential biomedical applications in photosensitization for photodynamic therapy.* Nanomedicine, 2009. **4**(3): p. 353-363.

50. Spinicelli, P., et al., *Non-Blinking Semiconductor Colloidal Quantum Dots for Biology, Optoelectronics and Quantum Optics.* Chemphyschem, 2009. **10**(6): p. 879-882.
51. Minsky, M., *Memoir on Inventing the Confocal Scanning Microscope.* Scanning, 1988. **10**(4): p. 128-138.
52. Zhang, K., et al., *Continuous distribution of emission states from single CdSe/ZnS quantum dots.* Nano Letters, 2006. **6**(4): p. 843-847.
53. Marcus, R.A., *Interaction of theory and experiment: examples from single molecule studies of nanoparticles.* Philosophical Transactions of the Royal Society a-Mathematical Physical and Engineering Sciences, 2010. **368**(1914): p. 1109-1124.
54. Crouch, C.H., et al., *Excitation Energy Dependence of Fluorescence Intermittency in CdSe/ZnS Core-Shell Nanocrystals.* Journal of Physical Chemistry C, 2009. **113**(28): p. 12059-12066.
55. Catherine H. Crouch*†, O.S., Xiaohua Wu‡, Robert Purcell†, Claudia Querner§, Marija Drndic§ and Matthew Pelton‡, *Facts and Artifacts in the Blinking Statistics of Semiconductor Nanocrystals.* Nano Letters, 2010.
56. Schlegel, G., et al., *Fluorescence decay time of single semiconductor nanocrystals.* Physical Review Letters, 2002. **88**(13): p. -.
57. Fisher, B.R., et al., *Emission intensity dependence and single-exponential behavior in single colloidal quantum dot fluorescence lifetimes.* Journal of Physical Chemistry B, 2004. **108**(1): p. 143-148.
58. Sher, P.H., et al., *Power law carrier dynamics in semiconductor nanocrystals at nanosecond timescales.* Applied Physics Letters, 2008. **92**(10): Artn. 101111
59. Tachiya, M. and K. Seki, *Unified explanation of the fluorescence decay and blinking characteristics of semiconductor nanocrystals.* Applied Physics Letters, 2009. **94**(8): Artn. 019904.
60. Frantsuzov, P.A. and R.A. Marcus, *Explanation of quantum dot blinking without the long-lived trap hypothesis.* Physical Review B, 2005. **72**(15): Artn. 15321
61. Gooding, A.K., D.E. Gomez, and P. Mulvaney, *The effects of electron and hole injection on the photoluminescence of CdSe/CdS/ZnS nanocrystal monolayers.* Acs Nano, 2008. **2**(4): p. 669-676.
62. Bawendi, M.G., et al., *Luminescence Properties of Cdse Quantum Crystallites - Resonance between Interior and Surface Localized States.* Journal of Chemical Physics, 1992. **96**(2): p. 946-954.
63. Eychmuller, A., et al., *Fluorescence Mechanism of Highly Monodisperse Q-Sized Cds Colloids.* Journal of Luminescence, 1991. **48-9**: p. 745-749.
64. Malko, A.V., et al., *Interplay between optical gain and photoinduced absorption in CdSe nanocrystals.* Journal of Physical Chemistry B, 2004. **108**(17): p. 5250-5255.
65. Park, S.J., et al., *Effect of electric field on the photoluminescence intensity of single CdSe nanocrystals.* Chemical Physics, 2007. **341**(1-3): p. 169-174.
66. Htoon, H., et al., *Anomalous Circular Polarization of Photoluminescence Spectra of Individual CdSe Nanocrystals in an Applied Magnetic Field.* Physical Review Letters, 2009. **102**(1): Artn. 017402.
67. Goupalov, S.V., *Anomalous polarization of the photoluminescence from anisotropic colloidal CdSe nanocrystals subject to external magnetic fields.* Physical Review B, 2009. **79**(23): p. -.
68. Costi, R., et al., *Electrostatic Force Microscopy Study of Single Au-CdSe Hybrid Nanodumbbells: Evidence for Light-Induced Charge Separation.* Nano Letters, 2009. **9**(5): p. 2031-2039.
69. Wustholz, K.L., et al., *Memory and spectral diffusion in single-molecule emission.* Journal of Physical Chemistry C, 2008. **112**(21): p. 7877-7885.
70. Spinicelli, P., et al., *Bright and Grey States in CdSe-CdS Nanocrystals Exhibiting Strongly Reduced Blinking.* Physical Review Letters, 2009. **102**(13): p. -.
71. Gomez, D.E., et al., *Exciton-Trion Transitions in Single CdSe-CdS Core-Shell Nanocrystals.* Acs Nano, 2009. **3**(8): p. 2281-2287.
72. Jha, P.P. and P. Guyot-Sionnest, *Trion Decay in Colloidal Quantum Dots.* Acs Nano, 2009. **3**(4): p. 1011-1015.
73. Wang, X.Y., et al., *Non-blinking semiconductor nanocrystals.* Nature, 2009. **459**(7247): p. 686-689.
74. Qu, Y.Q., et al., *Effect of Hole Transporting Materials on Photoluminescence of CdSe Core/Shell Quantum Dots.* Spectroscopy and Spectral Analysis, 2009. **29**(12): p. 3204-3207.
75. Hohng, S. and T. Ha, *Near-complete suppression of quantum dot blinking in ambient conditions.* Journal of the American Chemical Society, 2004. **126**(5): p. 1324-1325.
76. Fomenko, V. and D.J. Nesbitt, *Solution control of radiative and nonradiative lifetimes: A novel contribution to quantum dot blinking suppression.* Nano Letters, 2008. **8**(1): p. 287-293.
77. Kim, Y., et al., *Ligand-dependent blinking of zinc-blende CdSe/ZnS core/shell nanocrystals.* Physical Chemistry Chemical Physics, 2009. **11**(18): p. 3497-3502.

78. Knappenberger, K.L., et al., *Expitation wavelength dependence of fluorescence intermittency in CdSe/ZnS core/shell quantum' dots.* Nano Letters, 2007. **7**(12): p. 3869-3874.
79. Ozasa, K., et al., *Excitation-wavelength-dependent photoluminescence evolution of CdSe/ZnS nanoparticles.* Journal of Applied Physics, 2007. **101**(10): Artn 103503
80. Koberling, F., A. Mews, and T. Basche, *Oxygen-induced blinking of single CdSe nanocrystals.* Advanced Materials, 2001. **13**(9): p. 672-676.
81. Margolin, G., et al., *Power-Law Blinking Quantum Dots: Stochastic and Physical Models.* Fractals, Diffusion, and Relaxation in Disordered Complex Systems, Part A, 2006. **133**: p. 327-356.
82. Neuhauser, R.G., et al., *Correlation between fluorescence intermittency and spectral diffusion in single semiconductor quantum dots.* Physical Review Letters, 2000. **85**(15): p. 3301-3304.
83. Tang, J. and R.A. Marcus, *Mechanisms of fluorescence blinking in semiconductor nanocrystal quantum dots.* Journal of Chemical Physics, 2005. **123**(5): Artn. 054704.
84. Verberk, R., A.M. van Oijen, and M. Orrit, *Simple model for the power-law blinking of single semiconductor nanocrystals.* Physical Review B, 2002. **66**(23): Artn. 233202
85. Issac, A., C. von Borczyskowski, and F. Cichos, *Correlation between photoluminescence intermittency of CdSe quantum dots and self-trapped states in dielectric media.* Physical Review B, 2005. **71**(16): Artn . 161302
86. Kuno, M., et al., *Modeling distributed kinetics in isolated semiconductor quantum dots.* Physical Review B, 2003. **67**(12): Artn. 125304
87. Zhou, X., *Synthesis and Surface Modification of CdSe and CdTe Nanocrystals*, in *Chemistry*. 2006, University Siegen:
88. Tchaya, M., *Combination of a Laser Scanning Confocal Microscope with an Atomic Force Microscope -Nanocrystal Spectroscopy and Microscopy-*, in *Chemistry*. 2005, University of Siegen. p. 62.
89. Zhao, J.L., et al., *Electroluminescence from isolated CdSe/ZnS quantum dots in multilayered light-emitting diodes.* Journal of Applied Physics, 2004. **96**(6): p. 3206-3210.
90. Kucur, E., W. Bucking, and T. Nann, *Electrochemical determination of mesoscopic phenomena, defect states in CdSe nanocrystals and charge carrier manipulability.* Microchimica Acta, 2008. **160**(3): p. 299-308.
91. Guyot-Sionnest, P., *Charging colloidal quantum dots by electrochemistry.* Microchimica Acta, 2008. **160**(3): p. 309-314.
92. Huang, H., et al., *Electrically driven light emission from single colloidal quantum dots at room temperature.* Applied Physics Letters, 2007. **90**(2): p. -.
93. Colvin, V.L., M.C. Schlamp, and A.P. Alivisatos, *Light-Emitting-Diodes Made from Cadmium Selenide Nanocrystals and a Semiconducting Polymer.* Nature, 1994. **370**(6488): p. 354-357.
94. Brown, A.R., et al., *Poly(P-Phenylenevinylene) Light-Emitting-Diodes - Enhanced Electroluminescent Efficiency through Charge Carrier Confinement.* Applied Physics Letters, 1992. **61**(23): p. 2793-2795.
95. Brown, A.R., et al., *Electroluminescence from Multilayer Conjugated Polymer Devices - Spatial Control of Exciton Formation and Emission.* Chemical Physics Letters, 1992. **200**(1-2): p. 46-54.
96. Ebenstein, Y., et al., *Interaction of scanning probes with semiconductor nanocrystals; physical mechanism and basis for near-field optical imaging.* Journal of Physical Chemistry A, 2006. **110**(27): p. 8297-8303.
97. Farahani, J.N., et al., *Single quantum dot coupled to a scanning optical antenna: A tunable superemitter.* Physical Review Letters, 2005. **95**(1): Artn. 017402
98. Becker, H., S.E. Burns, and R.H. Friend, *Effect of metal films on the photoluminescence and electroluminescence of conjugated polymers.* Physical Review B, 1997. **56**(4): p. 1893-1905.
99. Wu, X.H., Y.G. Sun, and M. Pelton, *Recombination rates for single colloidal quantum dots near a smooth metal film.* Physical Chemistry Chemical Physics, 2009. **11**(28): p. 5867-5870.
100. Yanpeng Zhang, V.K.K., Carl Rodriguez, and Min Xiao*, *Controlling fluorescence intermittency of a single colloidal CdSe/ZnS quantum dot in a half cavity.* Physical Review B, 2008. **78**.

Variation of the blinking statistic results with the threshold values.

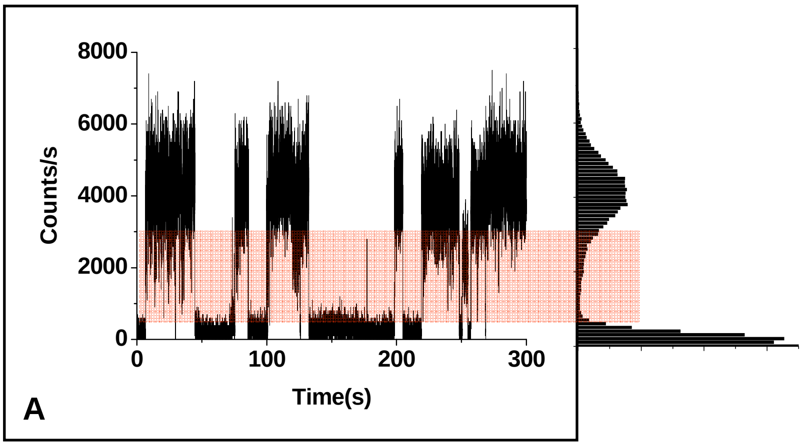

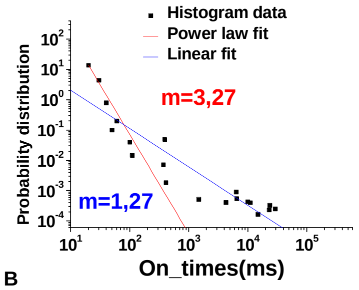

Threshold 500 Cts/s			
Correlation between consecutive events			
	On / next On	Off / next Off	On / next Off
R	0	0,17	0
R_{log}	0,15	0,24	-0,10

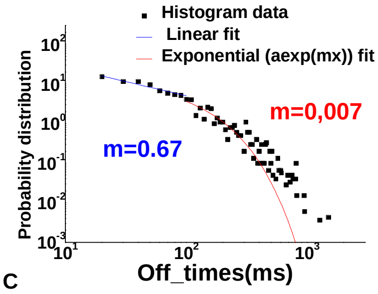

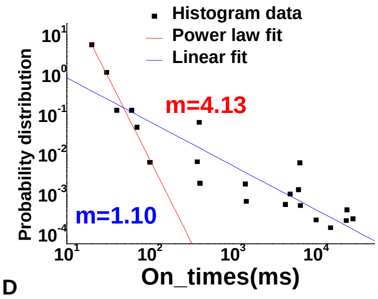

Threshold 600 Cts/s			
Correlation between consecutive events			
	On / next On	Off / next Off	On / next Off
R	0,03	0,38	-0,03
R_{log}	0,24	0,40	-0,12

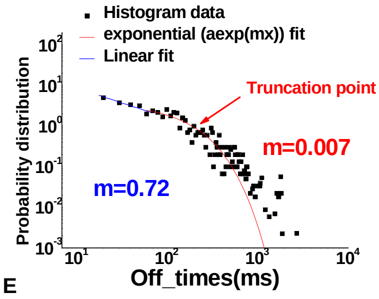

Annex 1: Variation of the blinking statistic results with the threshold values

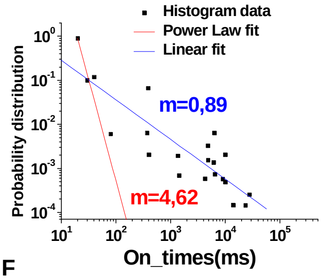

Threshold 790Cts/s			
Correlation between consecutive events			
	On / next On	Off / next Off	On / next Off
R	0,20	0,07	-0,04
R_{log}	0,50	0,41	-0,24

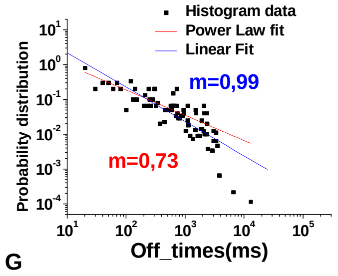

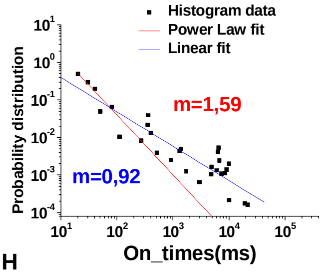

Threshold 990Cts/s			
Correlation between consecutive events			
	On / next On	Off / next Off	On / next Off
R	0,01	0,11	-0,16
R_{log}	0,26	0,32	-0,25

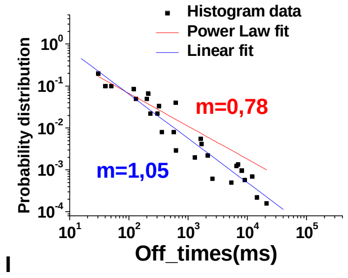

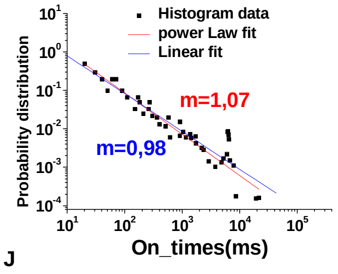

Threshold 1190Cts/s			
Correlation between consecutive events			
	On / next On	Off / next Off	On / next Off
R	0,06	0,29	-0,12
R_{log}	0,29	0,32	-0,15

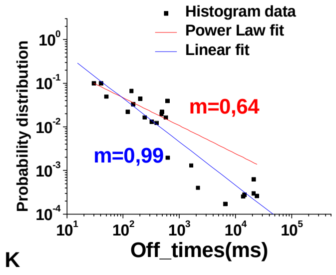

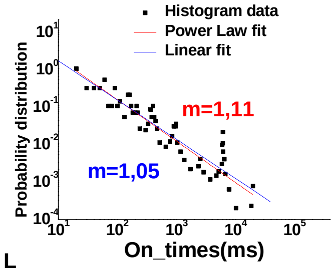

Threshold 1390Cts/s			
Correlation between consecutive events			
	On / next On	Off / next Off	On / next Off
R	0,06	0,22	-0,09
R_{log}	0,16	0,29	-0,14

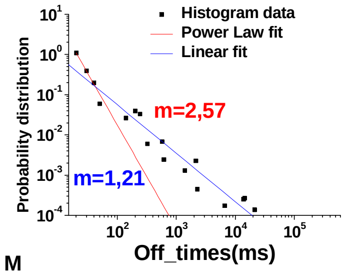

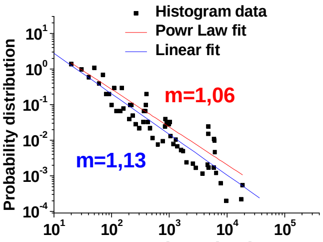

N

Threshold 1590Cts/s			
Correlation between consecutive events			
	On / next On	Off / next Off	On / next Off
R	0	0,24	-0,06
R_{log}	0,18	0,34	-0,09

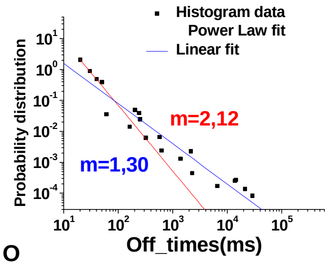

O

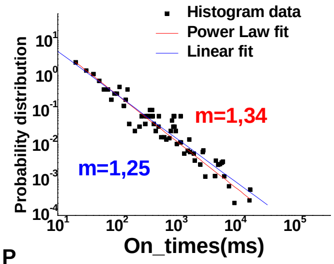

P

Threshold 1790Cts/s			
Correlation between consecutive events			
	On / next On	Off / next Off	On / next Off
R	0,03	0,25	-0,19
R_{log}	0,36	0,30	-0,11

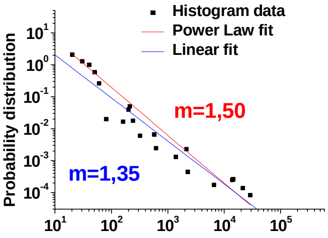

Q

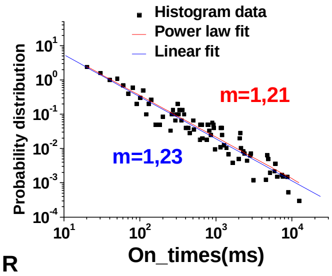

R

Threshold 2000 Cts/s			
Correlation between consecutive events			
	On / next On	Off / next Off	On / next Off
R	0,31	0,25	-0,05
R_{log}	0,47	0,27	-0,05

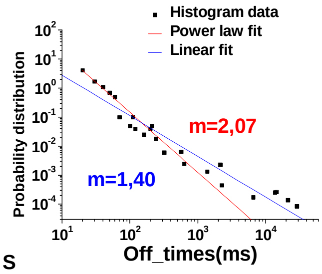

S

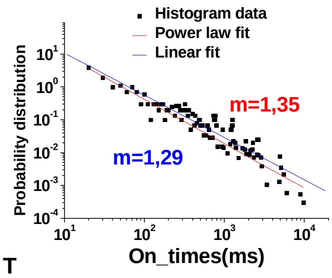

T

Threshold 2300 Cts/s			
Correlation between consecutive events			
	On / next On	Off / next Off	On / next Off
R	0,07	0,26	-0,03
R_{log}	0,42	0,26	-0,17

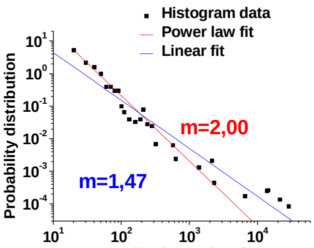

U

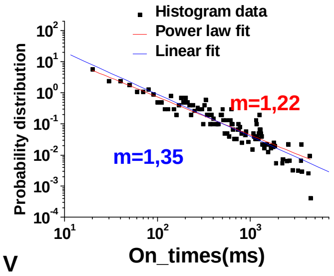

V

Threshold 2600 Cts/s			
Correlation between consecutive events			
	On / next On	Off / next Off	On / next Off
R	0,21	0,27	-0,03
R_{log}	0,38	0,31	-0,24

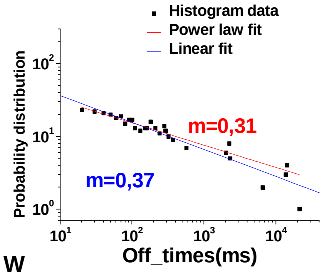

W

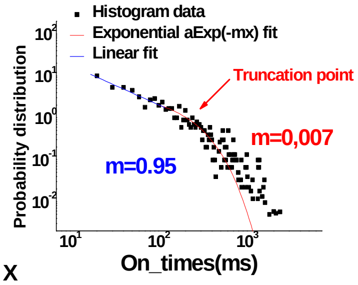

X

Threshold 3000 Cts/s			
Correlation between consecutive events			
	On / next On	Off / next Off	On / next Off
R	0,37	0	-0,01
R_{log}	0,36	0,23	-0,22

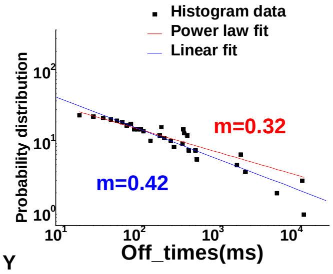

Y

Effect of the threshold on the blinking analysis results. Graph A is the time trace shown in figure 21. The red marked area indicates the intensity interval where the threshold was varied. The intensity histogram is shown close to the time trace. Graphs B to Y are the histograms of event durations plotted in double logarithmic scale. The tables in the middle show the memory coefficients obtained at different thresholds. The results obtained by fitting the histograms with a linear function and a power function are shown in blue and red respectively. The values obtained in this analysis are summarized in the table 3 in the third chapter of this thesis.

Chemicals

Solvents	Category of danger	R- Phrases	S- Phrases
Acetone	Xi, F	R: 11-36-66-67	S: 9-16-23
Chloroform	Xn	22-38-40-48/20/22	36/37
Ethanol	F	11	2-7-16
Hexane	F, Xn	11-38-48/20-51/53-62-65-67	9-16-29-33-36/37-61-62
Isopropanol	Xi, F	R: 11-36-67	S: 7-16-24/25-26
Methanol	F, T	11-23/24/25-39/23/24/25	1/2-7-16-36/37-45
Toluene	Xn	11-20	2-16-25-29-33

Cancer - causing, mutagen or reproduction-toxic substances

Substances	Category	Toxicity	Used
Chloroform	2	Cancer-causing	solvent
n-Hexane	2	Reproduction toxic	solvent
Toluene	2	Reproduction toxic	solvent

Hazard information

R-Phrases

R1 : Explosive when dry

R2 : Risk of explosion by shock, friction, fire or other source of ignition

R3 : Extreme risk of explosion by shock, friction, fire or other source of ignition

R4 : Forms very sensitive explosive metallic compounds

R5 : Heating may cause an explosion

R6 : Explosive with or without contact with air

R7 : May cause fire

R8 : Contact with combustible material may cause fire

R9 : Explosive when mixed with combustible material

R10: Flammable

R11: Highly flammable

R12: Extremely flammable

R13: Extremely flammable liquefied gas

R14: Reacts violently with water

R15: Contact with water liberates highly flammable gases

R16: Explosive when mixed with oxidizing substances

R17: Spontaneously flammable in air

R18: In use, may form flammable/explosive vapor-air mixture

R19: May form explosive peroxides

R20: Harmful by inhalation

R21: Harmful in contact with skin

R22: Harmful if swallowed

R23: Toxic by inhalation

R24: Toxic in contact with skin

R25: Toxic if swallowed

R26: Very toxic by inhalation

R27: Very toxic in contact with skin

R28: Very toxic if swallowed

R29: Contact with water liberates toxic gas

R30: Can become highly flammable in use

R31: Contact with acids liberates toxic gas

R32: Contact with acids liberates very toxic gas

R33: Danger of cumulative effects

R34: Causes burns

R35: Causes severe burns

R36: Irritating to eyes

R37: Irritating to respiratory system

R38: Irritating to skin

R39: Danger of very serious irreversible effects

R40: Possible risk of irreversible effects

R41: Risk of serious damage to eyes

R42: May cause sensitization by inhalation

R43: May cause sensitization by skin contact

R44: Risk of explosion if heated under confinement

R45: May cause cancer

R46: may cause heritable genetic damage

R47: May cause birth defects

R48: Danger of serious damage to health by prolonged exposure

R49: May cause cancer by inhalation

R50: Very toxic to aquatic organisms

R51: Toxic to aquatic organisms

R52: Harmful to aquatic organisms

R53: May cause long-term adverse effects in the aquatic environment

R54: Toxic to flora

R55: Toxic to fauna

R56: Toxic to soil organisms

R57: Toxic to bees

R58: May cause long-term adverse effects in the environment

R59: Dangerous to the ozone layer

R60: May impair fertility

R61: May cause harm to the unborn child

R62: Possible risk of impaired fertility

R63: Possible risk of harm to the unborn child

R64: May cause harm to breast-fed babies

R65 Harmful: may cause lung damage if swallowed

R66 Repeated exposure may cause skin dryness or cracking

R67 Vapors may cause drowsiness and dizziness

R68 May cause irreversible effects

Combinations of R-Phrases

R14/15: Reacts violently with water liberating highly flammable gases

R15/29: Contact with water liberates toxic, highly flammable gas

R20/21: Harmful by inhalation and in contact with the skin

R20/21/22: Harmful by inhalation, in contact with the skin and if swallowed

R20/22: Harmful by inhalation and if swallowed

R21/22: Harmful in contact with the skin and if swallowed

R23/24: Toxic by inhalation and in contact with the skin

R23/24/25: Toxic by inhalation, in contact with the skin and if swallowed

R23/25: Toxic by inhalation and if swallowed

R24/25: Toxic in contact with the skin and if swallowed

R26/27: Very toxic by inhalation and in contact with the skin

R26/27/28: Very toxic by inhalation, in contact with the skin and if swallowed

R26/28: Very toxic by inhalation and if swallowed

R27/28: Very toxic in contact with the skin and if swallowed

R36/37: Irritating to eyes and respiratory system

R36/37/38: Irritating to eyes, respiratory system and skin

R36/38: Irritating to eyes and skin

R37/38: Irritating to respiratory system and skin

R42/43: May cause sensitization by inhalation and skin contact

R48/20: Harmful: danger of serious damage to health by prolonged exposure through inhalation

R48/20/21: Harmful: danger of serious damage to health by prolonged exposure through inhalation and in contact with the skin

R48/20/21/22: Harmful: danger of serious damage to health by prolonged exposure through inhalation, in contact with the skin and if swallowed

R48/20/22: Harmful: danger of serious damage to health by prolonged exposure through inhalation and if swallowed

R48/21: Harmful: danger of serious damage to health by prolonged exposure in contact with skin

R48/21/22: Harmful: danger of serious damage to health by prolonged exposure in contact with skin and if swallowed

R48/22: Harmful: danger of serious damage to health by prolonged exposure if swallowed

R48/23: Toxic: danger of serious damage to health by prolonged exposure through inhalation

R48/23/24: Toxic: danger of serious damage to health by prolonged exposure through inhalation and in contact with the skin

R48/23/24/25: Toxic: danger of serious damage to health by prolonged exposure through inhalation, in contact with the skin and if swallowed

R48/23/25: Toxic: danger of serious damage to health by prolonged exposure through inhalation and if swallowed

R48/24: Toxic: danger of serious damage to health by prolonged exposure in contact with skin

R48/24/25: Toxic: danger of serious damage to health by prolonged exposure in contact with skin and if swallowed

R48/25: Toxic: danger of serious damage to health by prolonged exposure if swallowed

R50/53: Very toxic to aquatic organisms, may cause long term adverse effects in the aquatic environment

R51/53: Toxic to aquatic organisms, may cause long term adverse effects in the aquatic environment

R52/53: Harmful to aquatic organisms, may cause long term adverse effects in the aquatic environment

R68/20: May cause irreversible effects by inhalation

R68/21: May cause irreversible effects in contact with skin

R68/22: May cause irreversible effects if swallowed

R68/20/21: May cause irreversible effects by inhalation and in contact with skin

R68/20/22 May cause irreversible effects by inhalation and if swallowed

R68/21/22 May cause irreversible effects in contact with skin and if swallowed

R68/20/21/22 May cause irreversible effects by inhalation, in contact with skin and if swallowed

S-Phrases

S1 : Keep locked up
S2 : Keep out of reach of children
S3 : Keep in a cool place
S4 : Keep away from living quarters
S5 : Keep contents under.......(appropriate liquid to be specified by the manufacturer)
1 … water
2 … kerosene
3 … paraffin oil
S6 : Keep under.......(inert gas to be specified by the manufacturer)
1 … nitrogen
2 … argon
3 … carbon dioxide
S7 : Keep container tightly closed
S8 : Keep container dry
S9 : Keep container in a well ventilated place
S12: Do not keep the container sealed
S13: Keep away from food, drink and animal feedstuffs
S14: Keep away from..... (incompatible material to be indicated by the manufacturer)
1 … reducing agents, heavy metal compounds, acids, alkaline
2 … oxidizing and acidic substances and heavy metal compounds

3 … iron

4 … water and alkaline

5 … acids

6 … alkaline

7 … metals

8 … oxidizing and acidic substances

9 … flammable organic substances

10 .. acids, reducing agents and flammable materials

11 .. flammable substances

S15: Keep away from heat

S16: Keep away from sources of ignition - No Smoking!

S17: Keep away from combustible material

S18: Handle and open container with care

S20: When using do not eat or drink

S21: When using do not smoke

S22: Do not breathe dust

S23: Do not breathe gas/fumes/vapor/spray (appropriate wording to be specified by the manufacturer)

1 … gas

2 … vapor

3 … spray

4 … fumes

5 … vapor/spray

S24: Avoid contact with the skin

S25: Avoid contact with eyes

S26: In case of contact with eyes, rinse immediately with plenty of water and seek medical advice

S27: Take off immediately all contaminated clothing

S28: After contact with skin, wash immediately with plenty of......(to be specified by the manufacturer)

1 … water

2 … water and soap

3 … water, soap, and polyethylene glycol 400, if available

4 … polyethylene glycol 300 and ethanol (2:1), then water and soap

5 … polyethylene glycol 400

6 … polyethylene glycol 400, then cleaning with water

7 … water and acidic soap

S29: Do not empty into drains

S30: Never add water to this product

S33: Take precautionary measures against static discharges

S34: Avoid shock and friction

S35: This material and its container must be disposed of in a safe way

1 … through treatment with 2% sodium hydroxide

S36: Wear suitable protective clothing

S37: Wear suitable gloves

S38: In case of insufficient ventilation, wear suitable respiratory equipment

S39: Wear eye/face protection

S40: To clean the floor and all objects contaminated by this material use (to be specified by the manufacturer)

S41: In case of fire and/or explosion do not breath fumes

S42: During fumigation /spraying wear suitable respiratory equipment (appropriate wording to be specified by the manufacturer)

S43: In case of fire, use....(indicate in this space the precise type of fire fighting equipment. If water increases the risk, add "never use water")

1 … water

2 … water and powder extinguishing agent

3 … powder extinguishing agent, do not use water

4 … carbon dioxide, do not use water

6 … sand, do not use water

7 … metal extinguishing agent, do not use water

8 … sand, carbon dioxide, or powder extinguishing agent, do not use water

S44: If you feel unwell, seek medical advice (show the label where possible)

S45: In case of accident or if you feel unwell, seek medical advice immediately (show the label where possible)

S46: If swallowed, seek medical advice immediately and show the container or label

S47: Keep at temperature not exceeding .... ℃ (to be specified by the manufacturer)

S48: Keep wetted with .... (appropriate material to be specified by the manufacturer)

S49: Keep only in the original container

S50: Do not mix with... (to be specified by the manufacturer)

1 … acids

2 … alkaline

3 … strong acids, strong alkaline, heavy metals and their salts

S51: Use only in well ventilated areas

S52: Not recommended for interior use on large surface areas

S53: Avoid exposure - obtain special instructions before use

S54: Obtain the consent of pollution control authorities before discharging to waste-water treatment plants

S55: Treat using the best available techniques before discharge into drains or the aquatic environment

S56: Do not discharge into drains or the environment, dispose to an authorised waste collection point

S57: Use appropriate containment to avoid environmental contamination

S58: To be disposed of as hazardous waste

S59: Refer to manufacturer/supplier for information on recovery/recycling

S60: This material and/or its container must be disposed of as hazardous waste

S61: Avoid release to the environment. Refer to special instructions/ material safety data sheet

S62: If swallowed, do not induce vomiting: seek medical advice immediately and show the container or label

S63: In case of accident by inhalation: remove casualty to fresh air and keep at rest

S64: If swallowed, rinse mouth with water (only if the person is conscious)

Combinations of S-Phrases

S1/2: Keep locked up and out of reach of children

S3/9: Keep in a cool, well ventilated place

S3/7/9: Keep container tightly closed in a cool, well ventilated place

S3/14: Keep in a cool place away from...... (incompatible materials to be indicated by the manufacturer)

1 … reducing agents, heavy metal compounds, acids, alkaline

2 … oxidizing and acidic substances and heavy metal compounds

3 … iron

4 … water and alkaline

5 … acids

6 … alkaline

7 … metals

8 … oxidizing and acidic substances

S3/9/14: Keep in a cool, well ventilated place away from. ...... (incompatible materials to be indicated by the manufacturer)

1 … reducing agents, heavy metal compounds, acids, alkaline

2 … oxidizing and acidic substances and heavy metal compounds

3 … iron

4 … water and alkaline

5 … acids

6 … alkaline

7 … metals

8 … oxidizing and acidic substances

S3/9/49: Keep only in the original container in a cool, well ventilated place

S3/9/14/49: Keep only in the original container in a cool, well ventilated place away from. ......

(incompatible materials to be indicated by the manufacturer)

1 … reducing agents, heavy metal compounds, acids, alkaline

2 … oxidizing and acidic substances and heavy metal compounds

3 … iron

4 … water and alkaline

5 … acids

6 … alkaline

7 … metals

8 … oxidizing and acidic substances

S3/14: Keep in a cool place away from......(incompatible materials to be indicated by the manufacturer)

S7/8: Keep container tightly closed and dry

S7/9: Keep container tightly closed and in a well ventilated place

S7/47: Keep container tightly closed and at a temperature not exceeding ..... ℃ (to be specified by the manufacturer)

S20/21: When using do not eat, drink or smoke

S24/25: Avoid contact with skin and eyes

S27/28 Take off immediately all contaminated clothing. After contact with skin, wash immediately with plenty of ......(to be specified by the manufacturer)

S29/35 Do not empty into drains. This material and its container must be disposed of in a safe way.

S29/56: Do not empty into drains: dispose of this material and its container to hazardous or special waste collection point

S36/37: Wear suitable protective clothing and gloves

S36/37/39: Wear suitable protective clothing, gloves and eye/face protection

S36/39: Wear suitable protective clothing and eye/face protection

S37/39: Wear suitable gloves and eye/face protection

S47/49: Keep only in the original container at a temperature not exceeding ..... ℃ (to be specified by the manufacturer)

Talks and posters

11/05/2010:

Talk at the Physical Chemistry seminar, University of Hamburg

15 years of blinking nanocrystals: news and views

12/11/2009:

Talk at the group seminar of Prof. Dr. Meerholz in Cologne

Charging and blinking of single semiconductor nanocrystals

28/09/2009-30/09/2009:

Poster at the German Colloid Society conference in Hamburg

Charging and blinking of single semiconductor nanocrystals

19/07/2009-24/07/2009:

Poster at the Gordon Research Conference on Nanomaterials in Boston

Charging and blinking of single semiconductor nanocrystals

03/05/2008:

Talk at the “Bunsentagung” (Analysis, Manipulation and Simulation at the Nanoscale) in Saarbrücken

Charging and blinking of single semiconductor nanocrystals

08/10/2007: Talk at the Forschungszentrum Jülich GmbH during the International summer-school on “Advanced Spectroscopic Techniques in Life Science”

Charging and blinking of single semiconductor nanocrystals

CURRICULUM VITAE

PERSONAL DATA

Born on the: 6th May 1975 in Douala – Cameroon
Nationality: Cameroonian
Civil status: Married
E-mail: tchamax@yahoo.fr

EDUCATION

09/2008-Present **University of Hamburg,** Germany
PhD Chemistry (Due date 08/2009)
“Fluorescence spectroscopy and nanomanipulation of individual semiconductor nanocrystals”

11/2005 - 08/2008 **University of Siegen**, Germany
PhD Chemistry
“Fluorescence spectroscopy and nanomanipulation of individual semiconductor nanocrystals”

10/2003 - 10/2005 **University of Siegen**, Germany
MSc Chemistry (1.8-Very good)
“Combination of Atomic Force and Laser Scanning Microscope for single particles characterization.”

09/1993- 09/1999 **University of Yaoundé** I, Cameroon
BSc Chemistry (C, Satisfactory)

09/1986- 07/1993 **Lycee de New-Bell of Douala**, Cameroon
Baccalaureat “C” in Mathematics and Physical Sciences

RESEARCH AND WORK EXPERIENCE

09/2008 - Present	**Research and Teaching Assistant,** Institute of Physical Chemistry, University of Hamburg	Germany
11/2005- 08/2008	**Research and Teaching Assistant,** Institute of Physical Chemistry, University of Siegen	Germany
11/2006- 08/2008	**Language teacher (Freelancer)** Deutschen Angestellten-Akademie (DAA) Siegen	Germany
03/2005-10/2005	**Student Research Assistant,** Institute of Physical Chemistry, University of Siegen	Germany

LANGUAGES

French: Mother tongue
English: Academic level (language of education)
German: Intermediate communication skills

Ammersbek, 21th May 2010